hexagon:2611.00438v1

Electric-field hotspot packing and power channels in dielectric media

Daniel Wang
denialk391@gmail.com

AI-assisted research manuscript

13 November 2026

Abstract

We study quantified versions of two questions on field concentration and power channels posed by Miller and Monticone in OQ14. At a fixed driving frequency and under a common positive permittivity bound, we construct arbitrarily many simultaneous localized electric-field peaks in a single driven field, both in a two-dimensional invariant setting and in finite three-dimensional dielectrics. We also construct arbitrarily many localized peaks in a single normalized outgoing mode of a finite smooth dielectric, with prescribed real part of the complex resonance frequency and an arbitrarily high quality-factor target. The modal normalization is a reciprocal-residue normalization. Its relation to other possible interpretations of the original modal-volume question requires separate justification.

For a specified channel definition, we construct, for every finite N, an N-dimensional counted input space through the same square section at fixed frequency, material bounds, and thresholds. The construction applies when the permitted absolute-bypass threshold exceeds the required passage threshold and when the selected output is the complete outgoing scattering map, including reflection. Thus the corresponding unrestricted uniform finiteness assertion fails. The result does not decide stricter bypass conditions or receiving-only output formulations. These quantified results do not resolve every interpretation of the original OQ14. The formal verification and its scope are described in Appendix A.2.

Contents

1 Introduction: concentration and power channels **4**
- 1.1 Main results and their meaning . . . 5
- 1.2 How to read the argument . . . 5
- 1.3 Precise targets and conventions . . . 5
- 1.4 Relation to previous work . . . 7

2 Simultaneous driven hotspots in an invariant Maxwell geometry **8**
- 2.1 Physical reduction, normalization, and the exact target . . . 9
- 2.2 A local singular projection at positive frequency . . . 11
- 2.3 Outgoing well-posedness and global excitation . . . 13
- 2.4 Rounding without an assumed rounding power law . . . 15
- 2.5 Scope and limitations of the two-dimensional construction . . . 17

3 Finite three-dimensional driven hotspot packing **18**
- 3.1 A genuine conical point exponent . . . 19
- 3.2 An exact Maxwell coefficient functional at the conical point . . . 20
- 3.3 A uniform finite-device Maxwell inverse at fixed small contrast . . . 22
- 3.4 Physical illumination, total-field density, and rounding . . . 23
- 3.5 What an exact mode can mean in a finite dielectric device . . . 25

4 Excitation of conical points by one genuine resonance **26**
- 4.1 The angular branch through a homogeneous medium . . . 27
- 4.2 Nonvanishing from an annular pairing . . . 27
- 4.3 Conditional transfer to rounded modal peaks . . . 29

5 Spectral construction and normalization of the modal branch **30**
- 5.1 A compact analytic pencil and continuity under rounding . . . 30
- 5.2 A simple sphere resonance without a genericity assumption . . . 32
- 5.3 Reciprocal normalization of the resonant mode . . . 34
- 5.4 Modal hotspot theorem . . . 35

6 Channel bounds with an explicit field resource **37**
- 6.1 What the cited channel bounds actually control . . . 38
- 6.2 Exact operator reduction . . . 38
- 6.3 Local Maxwell hypotheses and a legitimate weighted flux . . . 39
- 6.4 Magnetic compactness and its quantitative cost . . . 40
- 6.5 Absolute bypass supplies the sharp-section bridge . . . 42
- 6.6 An explicit area scaling with its extra resource exposed . . . 44
- 6.7 The scope of the resource route . . . 45

7 Resonant amplification and candidate channel mechanisms **45**
- 7.1 An exact bounded-index Maxwell amplification obstruction . . . 45
- 7.2 Evanescent pairs can carry real power locally . . . 47
- 7.3 An exact feedback diagnostic independent of mode reduction . . . 48
- 7.4 Matched resonator pairs: energy, bandwidth, and errors . . . 48
- 7.5 Compression and coherent passage certification . . . 50
- 7.6 Physical realization attempts and their specific obstructions . . . 51

8 Coherent bypass and limits of local constructions **52**
- 8.1 A global power-budget restriction . . . 52
- 8.2 Arbitrarily many local fields with whole-plane coherent bypass control . . . 53
- 8.3 Why the local theorem is not the requested counterexample . . . 55
- 8.4 Matching theory and the global realization problem . . . 56

9 Radial channels: bypass, local synthesis, and gain limits **56**
9.1 Inversion parity and the threshold regime . . . 56
9.2 Both polarizations of a regular spherical partial wave . . . 57
9.3 An actual local inverse-synthesis step for mixed angular orders . . . 60

10 Growing radial support: simultaneous gain and its flux cancellation **64**
10.1 A vacuum flux trace estimate with physical normalization . . . 64
10.2 An explicit finite ordinary-dielectric stack . . . 65
10.3 What happens to physical passage in this entire finite band . . . 67

11 Global finite-order radial TE control with bounded positive index **69**
11.1 An identity loop with an amplified angular derivative . . . 69
11.2 A macroscopic angular shear in a thin distant annulus . . . 70
11.3 Finite-ensemble global transfer control . . . 71

12 Paired electric and magnetic radial control **73**
12.1 The same physical layers control a paired transfer graph . . . 73
12.2 Reflection parity and finite-band isolation . . . 75

13 Arbitrary physical passage dimension when bypass is omitted **76**

14 A flux-only count for globally propagating vacuum fields **78**
14.1 An explicit scalar observation estimate . . . 78
14.2 Finite positive trace from actual pointwise flux . . . 80
14.3 The limitation of moving controls to infinity . . . 81

15 A nonradial channel bound with small total material volume **82**
15.1 An exact real-frequency kernel estimate . . . 82
15.2 Physical incoming power and the full local field resource . . . 84
15.3 A genuine restricted channel theorem and its remaining limit . . . 85

16 Edge circulation and its physical completion **86**
16.1 Exact local profile and physical coherent jets . . . 86
16.2 Finite-rank diagonal edge circulation . . . 88
16.3 The precise physical estimate still required . . . 89

17 The small-inclusion limit for an explicit parity reaction kernel **90**
17.1 The exact kernel and elementary plane estimates . . . 91
17.2 Self-consistent inclusions and the complete plane remainder . . . 92

18 An actual radial Green limit with whole-plane flux convergence **94**
18.1 The common stack and its source coefficient . . . 95
18.2 Uniform angular tails at fixed gain . . . 96
18.3 The limiting Maxwell source kernel . . . 97
18.4 Source-normalized bounds throughout the remote layers . . . 98
18.5 The whole-plane physical limit . . . 99

19 Disproof of the unrestricted fixed-section channel bound **101**

A Verification, scope, and separate verdicts **104**
A.1 What was checked . . . 104
A.2 Lean verification and its precise boundary . . . 105
A.3 Stricter questions outside the quantified targets . . . 107
A.4 Separate scientific verdicts . . . 108
A.5 Build and provenance . . . 109

1 Introduction: concentration and power channels

Diffraction provides familiar scales for focusing and for the number of spatial patterns communicated through an aperture. Inhomogeneous dielectric media also support strong near fields and resonant energy storage. Motivated by OQ14 of Miller and Monticone [12, Section 5.6], we study two related questions: how many localized electric-field maxima can a single field produce, and how many independent inputs can carry power through a prescribed section? Both questions require explicit choices of normalization, geometric resources, and admissibility conditions.

For the *hotspot* question, we seek finitely many disjoint observation regions and one field with a large, localized electric-field maximum in each. A local singularity at a dielectric corner suggests a mechanism, but a packing theorem also requires a globally admissible field that excites all regions and retains the peaks after rounding. We distinguish driven fields, normalized by incoming power, from outgoing resonant modes, for which a different normalization is required. No fixed fraction of the total energy is required in each peak.

For the *channel* question, fix a square D in a plane and consider a linear space of incident fields. Every field in the space must satisfy three tests: a lower bound on power in selected outputs, a lower bound on signed power flux through D, and an upper bound on the integral of absolute flux over the rest of the plane. Requiring these inequalities for each basis vector alone would not control their coherent superpositions. The square is a measurement section and need not be the only topological route between input and output.

Figure 1 shows the measurement geometry and the distinction between flux through the square and flux elsewhere in its plane.

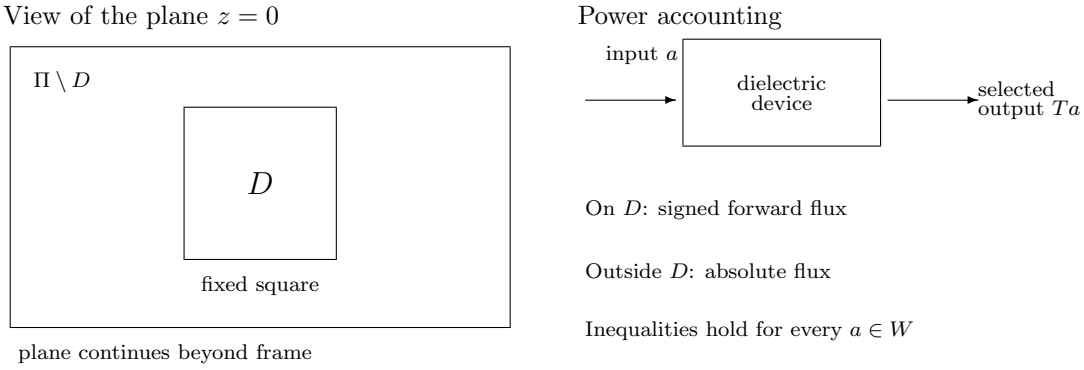


Figure 1: Schematic of the channel definition. The left panel is a view of the whole measurement plane, with a fixed square D; the outer frame only marks the drawing boundary. The right panel indicates input–output power accounting, not a prescribed one-way device geometry. Passage uses signed flux through D, whereas bypass measures the absolute flux on the rest of the plane. In the counterexample the selected output is the complete outgoing scattering map, including reflection.

Across each device family, the driving frequency or the real part of the resonance frequency, as appropriate, and the material bounds are fixed. For channels, the square and the thresholds are also fixed. The surrounding device may grow; the formulation imposes no positive lower bound on feature size and no uniform upper bound on quality factor, number of interfaces, or matching complexity. A bound depending on one of these additional resources addresses a more restricted

question. The precise admissibility and power conventions follow below.

1.1 Main results and their meaning

The following summary is informal; the linked statements give the exact hypotheses and conclusions.

- **Driven hotspots.** Theorem 2.2 gives simultaneous peaks in a two-dimensional invariant geometry, with incoming power normalized per unit invariant length. Theorem 3.1 gives a finite three-dimensional construction driven by one unit-power illumination. In that theorem the observation neighborhoods project into a prescribed planar patch; their maxima need not lie on the plane.

- **Modal hotspots.** Theorem 5.6 constructs arbitrarily many localized peaks in one normalized outgoing mode of a finite smooth dielectric. The real part of its resonance frequency, its quality-factor target and common material bounds can be prescribed. The norm is a reciprocal resonance-residue normalization, not an all-space positive-energy norm; the modal-volume conclusions are stated separately in Corollary 5.7. Equivalence to other possible interpretations of the original modal-volume question is not established.

- **Unrestricted channels.** Theorem 19.1 constructs an N-dimensional counted input subspace for every finite N, while the frequency, material interval, square and thresholds remain fixed. It applies when $0 < \eta < \delta$, with the complete outgoing scattering map selected. Thus the proposed uniform finite count, as quantified below over these allowed parameters, is false. This does not settle $\delta \leq \eta$, a specified receiving-only output, or fixed total device support. These results do not settle the original broad OQ14 for every possible interpretation of its undefined thresholds and outputs.

For intuition, the channel construction uses a distant radial dielectric stack to amplify independent local field patterns. Small dielectric inclusions turn those patterns into local flux circulation near the square's edge. The proof must control both the full self-consistent field and the absolute flux over the *whole* plane, uniformly over coherent inputs; a large local field by itself would not establish the conclusion.

1.2 How to read the argument

Sections 2 and 3 develop the driven hotspot constructions. Sections 4 and 5 treat excitation and normalization of a single resonant mode. Section 6 gives channel bounds that retain an explicit field resource; the intervening channel sections examine the passage, control and physical-construction issues. The unrestricted counterexample is stated and proved in Section 19. Appendix A separates mathematical results, formal checks and numerical diagnostics. A reader interested in the central conclusion can read this introduction and the theorem statements first, then return to the supporting estimates.

1.3 Precise targets and conventions

The source question does not fix every normalization, threshold, geometric resource, or interpretation of a mode. The definitions below make our choices explicit; they are not quotations of an already quantified theorem.

Assumption 1.1 (Ordinary dielectric class)**.** *Fix $\omega > 0$, $k_0 = \omega\sqrt{\varepsilon_0\mu_0}$, and $1 < \varepsilon_+ < \infty$. Use $e^{-i\omega t}$ and*

$$\nabla \times E = i\omega\mu_0 H, \qquad \nabla \times H = -i\omega\varepsilon_0\varepsilon_r E, \qquad 1 \le \varepsilon_r(x) \le \varepsilon_+. \tag{1}$$

The medium is real, scalar, reciprocal and nonmagnetic. There are no impressed interior sources, conductors, gain, or negative permittivities. Each geometry is piecewise smooth with finitely many pieces, but that number and all feature scales can vary. The exterior background is vacuum. Compactly supported three-dimensional dielectric perturbations form the default radiation class. Ideal leads and translationally invariant systems must instead be expressly labeled and supplied with their own exterior/port conventions.

The case $\varepsilon_+ = 1$ is homogeneous and is excluded only from hotspot constructions that need contrast. A broader positive class fixes the *same* $0 < \varepsilon_- \le \varepsilon_r \le \varepsilon_+$ for every member. Allowing $\varepsilon_- \to 0$ is a different target. Tensor permittivity requires separate statements. Losslessness here concerns one frequency; a nondispersive energy interpretation is an additional assumption.

Assumption 1.2 (Scattering and power)**.** *For each device specify a well-posed outgoing Maxwell scattering problem with incoming and selected outgoing Hilbert spaces $\mathcal{H}_{\mathrm{in}}, \mathcal{H}_{\mathrm{out}}$. Let $T : \mathcal{H}_{\mathrm{in}} \to \mathcal{H}_{\mathrm{out}}$ be the selected scattering map. The physical incoming power is $\|a\|^2$ and the selected output power is $\|Ta\|^2$. The total field depends linearly on a, belongs to $H_{\mathrm{loc}}(\mathrm{curl})$, and includes all feedback. The full scattering map includes reflected and unselected radiation. Thus $T^*T \le I$. At any exceptional frequency a finite, unique limiting-absorption field must be justified separately; adding a freely chosen trapped mode is forbidden.*

This assumption is an admissibility condition, not a theorem that arbitrary rough coefficients yield a scattering theory. Radiation channels can be normalized by incoming spherical-wave flux. An ideal waveguide uses its complete propagating-mode power form. Neither convention counts an infinite-power plane wave as a unit-power input.

Definition 1.3 (Counted subspaces through one physical section)**.** Fix the square $D = (-L/2, L/2)^2 \times \{0\}$, its orientation $+\hat{z}$, and $A = L^2$, together with a source-free neighborhood of $\overline{D}$. Fix $0 < \tau < 1$, $\eta > 0$ and $\delta \ge 0$. For the total fields (E_a, H_a) corresponding to $a \in \mathcal{H}_{\mathrm{in}}$, write $S_z(a) = \frac{1}{2}\,\mathrm{Re}(E_a \times \overline{H_a}) \cdot \hat{z}$ for the normal component of the time-averaged Poynting vector. A linear subspace $W \subset \mathcal{H}_{\mathrm{in}}$ is counted if *every* $a \in W$ satisfies

$$\|Ta\|^2 \ge \tau\|a\|^2, \tag{2}$$

$$P_D(a) := \tfrac{1}{2}\,\mathrm{Re}\int_D (E_a \times \overline{H_a}) \cdot \hat{z}\ \mathrm{d}A \ge \eta\|Ta\|^2, \tag{3}$$

$$\int_{\{z=0\}\setminus D} |S_z(a)|\ \mathrm{d}A \le \delta\|a\|^2. \tag{4}$$

These integrals require legitimate physical traces with integrable flux. Otherwise a specified regularized measurement must replace them, with its own target. No product of arbitrary distributional tangential traces is assumed defined. The passage interpretation is operational; D need not be a sole topological connection.

Using a square freezes shape. An extension to other fixed Lipschitz sections must list shape constants. In particular one cannot replace D with increasingly long thin sections of equal area while claiming a fixed-section counterexample.

Conjecture 1.4 (Primary channel target: DISPROVED as quantified)**.** *For fixed parameters in Definition 1.3 and Assumptions 1.1–1.2, there is a finite bound on* $\dim W$ *uniform over admissible devices. A stronger target for scaled copies of the same shape is*

$$\dim W \le C(\tau, \eta, \delta, \varepsilon_-/\varepsilon_+, \textit{declared shape data})(1 + k_0^2 \varepsilon_+ A). \tag{5}$$

Surrounding support, resonator quality factor, matching structures, port number, interface count and minimum feature size are not bounded resources of the area-only conjecture. A theorem depending on any of them must say so.

Finiteness precedes the scaling question; no optimal coefficient is requested. Theorem 19.1 disproves this assertion for every fixed $\delta > \eta > 0$ when all outgoing radiation is selected. It does not settle a modified assertion with $\delta \le \eta$ or specified receiving outputs. Fixing total support is also a different problem. Our flux-resource result additionally needs $\delta < \eta\tau$; other parameter values are not silently discarded from the target.

If $W_\tau = \operatorname{Ran} \mathbf{1}_{[\tau,1]}(T^*T)$ satisfies both passage conditions, a bound on counted subspaces bounds $\dim W_\tau$. Without that hypothesis there may be unrelated efficient channels bypassing D. Without compactness, the spectral projection is the definition; a discrete singular-value decomposition is not assumed. Nonzero coupling alone uses no positive threshold and answers a different question.

Definition 1.5 (Separate hotspot targets)**.** Fix contrast, frequency, a nonempty open patch $\mathcal{P}$, $N \in \mathbb{N}$, a localization length $\ell > 0$ (as small relative to $\lambda_0 = 2\pi/k_0$ as desired), and a peak target $M > 0$. The driven target seeks one admissible medium and one physical unit-power incident field with N disjoint observation neighborhoods in $\mathcal{P}$, each containing a peak exceeding M and having a controlled boundary below a fixed fraction of its peak. In a two-dimensional reduction power is per invariant length and localized regions are transverse, not finite three-dimensional points. A modal target instead requires a genuine mode and a defined modal normalization, for example the relevant electric-energy integral divided by local electric energy density. A driven monochromatic scattering field has infinite all-space energy and cannot be inserted into that formula.

No N-independent excitation coefficient or nonvanishing fraction of total energy per hotspot is required. Such conditions would define substantially stronger problems.

1.4 Relation to previous work

Table 1 summarizes relevant results and the hypotheses needed to compare them with the formulations above.

Table 1: Selected prior work and its relation to the present questions.

Source	Scope	Distinction from the present questions
Miller (2023), S2/S12 [11]	Uniform-medium channel counting motivates thickness estimates. S2 labels the nonuniform-index replacement conjectural; S12 distinguishes approximate aperture counting and design-specific Green operators.	A uniform estimate for actual structured interiors, including their total resonant response.

Source	Scope	Distinction from the present questions
Kuang et al. (2025), II/E [9]	Background Green operators between domains separable by a spherical surface; sizes and separations enter. Power normalization adds source/receiver response factors.	Their Eq. (1) retains the norms of those factors. Appendix E rejects general monotonicity of singular-value ratios and a step-shaped spectrum assumption.
Costabel et al. (1999) [3]	Piecewise constant positive coefficients on a bounded polyhedral partition; singular parts are linked to scalar transmission problems with stated boundary conditions.	Local singular structure alone does not prove global excitation, outgoing scattering, or simultaneous peaks.
Zhao et al. (2020) [21]	Mode-volume optimization with Maxwell constraints, refractive-index limits, minimum feature constraints and numerical dual bounds; polarization matters.	Numerical feature-size scaling is neither a packing proof nor a channel theorem. Driven fields need a different normalization.

Harrach, Lin, and Liu [8] establish field localization and a partial-boundary-data Runge approximation result for Maxwell equations in bounded domains. Their boundary-input setting differs from the present open-scattering constructions and their power normalization. Bille-Lauridsen and Mørk [2] analyze singularity regularization in dielectric bowtie geometries using electrostatic and quasinormal-mode calculations; their local scaling results do not imply simultaneous global hotspot packing.

The supplied 33-page report [20] proves a full-vector count with an explicit local field-norm resource, and identifies Bragg amplification, evanescent local flux, and resonant-feedback obstructions. We audit and retain these with their restrictions. Its ENZ slot construction varies both the lower permittivity bound and the section shape; that observation alone excludes it as a counterexample to Conjecture 1.4. We do not claim an independent recertification of every ENZ numerical result.

The supplied HTML notes [19] concern invariant slabs and fibers, scalar compact-support scattering, and finite-dimensional formal checks. Their fixed-propagation-constant magnetic variational form is monotone in ε^{-1} on a common divergence-free domain. Converting that count to a count of all propagation constants at fixed frequency needs additional spectral arguments; the notes themselves flag that step as numerically checked only. Neither a slab count nor such a fiber comparison is a full-device section theorem. The companion file named `optical_channel_bounds.pdf` was absent from the supplied Downloads location. No unprovided Lean or simulation archive was reconstructed or represented as verified.

A targeted search through 17 October 2026 also inspected primary recent work on metawaveguide microrings [7], singular dielectric cavities [10], and multi-plane communication-mode synthesis [5]. These concern specific confinement or wavefront-synthesis systems. None of the inspected material supplies the all-device fixed-section theorem with the quantifiers above. This is a limited search outcome, not a claim of exhaustive novelty or absence of a solution elsewhere.

2 Simultaneous driven hotspots in an invariant Maxwell geometry

Can one finite-power illumination produce many strong, sharply localized electric-field peaks at once? We first answer a cross-sectional version of this question. The dielectric pattern and the fields

are invariant along one direction, so each peak in the picture represents an infinitely long ridge. The three-dimensional construction in Section 3 removes that invariant direction by a separate argument.

The mechanism begins with two dielectric regions meeting at a sharp corner. At an excited corner, the field can grow without bound even though its local energy remains finite. A physical device in our construction has rounded, smooth interfaces: rounding cuts off this growth, leaving a finite peak. The proof chooses the rounding small enough that this peak is high while the field on a surrounding collar remains bounded. Figure 2 shows the local geometry; the full construction places finitely many such neighborhoods in one device and uses one incident field to excite them all.

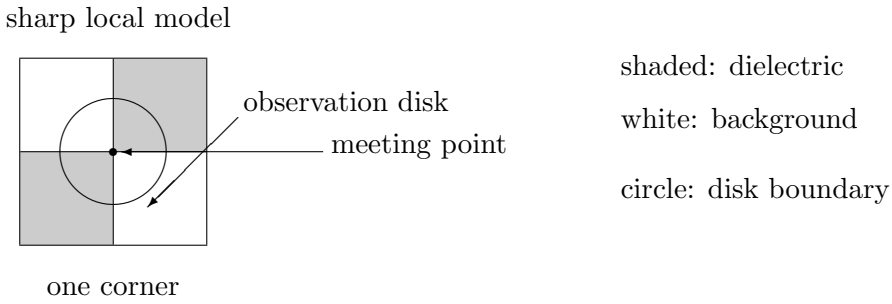


Figure 2: Schematic of one sharp two-dimensional checkerboard neighborhood. Two opposite dielectric sectors meet at a point; the other sectors are background. The circle indicates a fixed observation disk, not a material interface. In the proof finitely many disjoint copies are illuminated at once. The final interfaces are rounded and smooth; the sharp meeting point is used only as a reference for constructing their peaks.

Scope. Theorem 2.2 proves a driven, two-dimensional cross-sectional version of hotspot packing, with physical incoming power per unit invariant length. It uses ordinary binary dielectrics at one fixed positive frequency, one incident field, and smooth rounded interfaces. The proof includes local finite-frequency excitation, global illumination, and the rounding limit. It does not prove packing of finite-three-dimensional point hotspots or packing by a normalized resonator mode. Those distinctions are essential when comparing with the modal question in [12].

2.1 Physical reduction, normalization, and the exact target

Fix $k > 0$, $\omega = ck$, and $\varepsilon_+ > 1$. Set $b = \varepsilon_+^{-1} \in (0,1)$ and $Z_0 = \sqrt{\mu_0/\varepsilon_0}$. Every coefficient below is independent of z. Put $a = 1/\varepsilon_r$, so that $b \le a \le 1$, and consider

$$H = (0,0,u), \qquad E = \frac{ia}{\omega\varepsilon_0}(\partial_y u, -\partial_x u, 0), \qquad L_a u := \nabla\cdot(a\nabla u) + k^2 u = 0. \tag{6}$$

These are the full three-dimensional Maxwell equations restricted to z-invariant fields, rather than an electrostatic approximation. Indeed $\nabla\times H = -i\omega\varepsilon_0\varepsilon_r E$, and $\nabla\times E = i\omega\mu_0 H$ is exactly $L_a u = 0$. The weak scalar transmission conditions are $[u] = [a\partial_n u] = 0$. They give continuity of tangential H and E, and of normal displacement. The local electric energy is finite precisely when ∇u is locally square integrable, since

$$\int_Q \varepsilon_0\varepsilon_r|E|^2\,dx\,dy = \frac{1}{\omega^2\varepsilon_0}\int_Q a|\nabla u|^2\,dx\,dy. \tag{7}$$

The incident field is a smooth Herglotz wave

$$u_g^{\mathrm{in}}(x) = \left(\frac{k}{\pi Z_0}\right)^{1/2} \int_{S^1} g(d) e^{ikd\cdot x}\, ds(d), \qquad g \in C^\infty(S^1). \tag{8}$$

The scattered field satisfies the two-dimensional outgoing Sommerfeld condition. All material lies in a bounded cross section, and the exterior is vacuum. This convention specifies the incoming physical channels; no freely chosen homogeneous outgoing solution is added. Stationary phase, for $x = r\widehat{x}$, gives

$$u_g^{\mathrm{in}}(r\widehat{x}) = \left(\frac{2}{Z_0 r}\right)^{1/2} \left[e^{i(kr-\pi/4)} g(\widehat{x}) + e^{-i(kr-\pi/4)} g(-\widehat{x})\right] + O(r^{-3/2}). \tag{9}$$

An incoming radial wave has inward flux $Z_0|u|^2/2$; an outgoing one has outward flux $Z_0|u|^2/2$. Therefore

$$P_{\mathrm{in}} \text{ per unit } z \text{ length} = \|g\|^2_{L^2(S^1)}. \tag{10}$$

This is incoming, rather than net, power. The latter vanishes for a lossless scatterer after the outgoing power is included. A plane wave alone would not have this finite incoming-power normalization.

Definition 2.1 (Localized peaks used here)**.** For a smooth-interface, piecewise homogeneous configuration, let $E_*(x)$ equal $|E(x)|$ off interfaces and the maximum of the finitely many one-sided values at an interface. A collection of N localized peaks at length target $\ell > 0$ and amplitude target $M > 0$ means N pairwise disjoint closed disks Q_j, all of diameter below ℓ, such that

$$P_j := \max_{\overline{Q}_j,\, \text{one-sided}} |E| > M, \qquad \max_{\partial Q_j,\, \text{one-sided}} |E| < P_j/2. \tag{11}$$

We will in fact bound the field on an annular collar of each boundary. Consequently a connected component of the superlevel set $\{E_* > P_j/2\}$ containing a maximizing point stays in Q_j. Its diameter is below ℓ. The corresponding intensity half-maximum component is contained in it, since $P_j/\sqrt{2} > P_j/2$. No positive lower bound on the energy in each peak is stipulated.

Theorem 2.2 (Simultaneous rounded driven hotspot packing)**.** *For every fixed $k > 0$ and $\varepsilon_+ > 1$, every nonempty open patch $\mathcal{P} \subset \mathbb{R}^2$, every finite $N \geq 1$, and every $\ell, M > 0$, there exist $2N$ bounded dielectric inclusions with pairwise disjoint closures and C^∞ boundaries, all contained in $\mathcal{P}$, and one $g \in C^\infty(S^1)$ with $\|g\|_2 = 1$, such that:*

1. *$\varepsilon_r = \varepsilon_+$ inside the inclusions and $\varepsilon_r = 1$ outside them;*
2. *the unique outgoing scattering solution of (6) driven by (8) has N localized peaks in $\mathcal{P}$ satisfying Definition 2.1;*
3. *the same one incident field excites every peak, at the same frequency and with unit incoming power per unit z length.*

There is no uniform lower bound on the rounding radius, on any peak's integrated energy, or on any singular coefficient as N or the target parameters change. The physical construction is infinitely extruded in z and is not a finite-volume three-dimensional device.

The proof has four steps. First, a sharp checkerboard corner admits a finite-energy field with an electric singularity. Second, an outgoing scattering and approximation argument shows that an incident field can excite each prescribed corner. Linearity then lets us choose one field that excites all finitely many corners simultaneously. Third, the total fields converge as the corners are rounded.

Finally, the sharp field provides large values near each corner, while a uniform collar bound keeps the boundary of each observation disk low. This last comparison gives actual localized maxima in the smooth devices, not merely large values in an ideal singular geometry.

The strict contrast assumption matters: for $\varepsilon_+ = 1$ the material is vacuum. Cauchy–Schwarz in (8) then gives a finite pointwise electric-field bound at fixed unit incoming power and fixed k, so the arbitrary-amplitude conclusion cannot include that endpoint.

2.2 A local singular projection at positive frequency

Corner and edge singularities of positive-coefficient Maxwell transmission problems are established in [3]. Here we give the needed two-dimensional construction directly. In particular, we do not transfer a bounded-domain boundary condition from that paper into an unproved scattering claim.

The angular eigenvalue below controls the radial behavior near the corner. Its exponent lies between zero and one: the corresponding singular model term tends to zero like r^α, but its gradient, and hence the electric field, can grow like $r^{\alpha-1}$. The exponent also makes the squared gradient locally integrable. A nonzero coefficient of this angular pattern is essential; the existence of the pattern alone does not say that a particular illumination excites it.

Lemma 2.3 (A binary checkerboard angular exponent)**.** *Let $a(\theta)$ alternate between 1 and b in successive sectors of angle $\pi/2$. There is a nonzero real periodic $\phi \in H^1(S^1)$ such that*

$$-(a\phi')' = \alpha^2 a\phi, \qquad \alpha = \frac{4}{\pi}\arctan\sqrt{b} \in (0,1), \qquad \int_0^{2\pi} a\phi^2\,d\theta = 1. \tag{12}$$

Moreover $\int a\phi = 0$ and $\int a|\phi'|^2 = \alpha^2$.

Proof. In a sector with constant coefficient a_0, the state $(\phi, a_0\phi'/\alpha)^T$ propagates through angle L by

$$M_{a_0}(L) = \begin{pmatrix} \cos\alpha L & a_0^{-1}\sin\alpha L \\ -a_0\sin\alpha L & \cos\alpha L \end{pmatrix}. \tag{13}$$

Both state components are continuous at an interface. The half-turn matrix $B = M_b(\pi/2)M_1(\pi/2)$ has determinant one and trace $2\cos^2 t - (b + b^{-1})\sin^2 t$, where $t = \alpha\pi/2$. With $t = 2\arctan\sqrt{b}$ its trace is -2. Choose a nonzero eigenvector of B with eigenvalue -1. The resulting angular function is antiperiodic after a half turn and periodic after a full turn. It satisfies the stated weak eigenproblem. Integrating that equation and then testing it against ϕ proves the two identities. □

The coefficient in the next lemma identifies the part of the physical finite-frequency field associated with this angular profile. Its continuity in the local L^2 topology is needed later: an approximation of a locally excited field must preserve a nonzero singular coefficient.

Lemma 2.4 (Continuous finite-frequency singular coefficient)**.** *Suppose the checkerboard coefficient of Lemma 2.3 holds in $B_R(0)$ and $u \in H^1(B_R)$ weakly satisfies $L_a u = 0$ there. For almost every r, put*

$$U(r) = \int_0^{2\pi} a(\theta)u(r,\theta)\phi(\theta)\,d\theta, \qquad F(r) = \int_0^{2\pi} u(r,\theta)\phi(\theta)\,d\theta. \tag{14}$$

There is a complex number $c(u)$, linear in u, such that

$$\begin{aligned} U(r) &= c(u)r^\alpha + p(r), \\ p(r) &= -\frac{k^2}{2\alpha}\left[r^\alpha\int_0^r s^{1-\alpha}F(s)\,ds - r^{-\alpha}\int_0^r s^{1+\alpha}F(s)\,ds\right]. \end{aligned} \tag{15}$$

In particular,

$$|p(r)| \le C_{b,\phi,\alpha} k^2 r \|u\|_{L^2(B_r)}, \qquad |c(u)| \le C_{R,k,b,\phi} \|u\|_{L^2(B_R)}. \tag{16}$$

Thus c is continuous even for the local L^2 topology on the space of solutions. If $c(u) \neq 0$, ordinary points strictly inside the homogeneous sectors have arbitrarily large $|E|$ as they approach the origin.

Proof. Testing the weak equation with a product of a radial test function and ϕ gives the distributional ordinary differential equation

$$(rU')' - \frac{\alpha^2}{r} U = -k^2 r F. \tag{17}$$

Variation of constants gives the particular solution in (15). The two integrals converge because $F \in L^2((0,R), r\,dr)$ and $\alpha < 1$. For example,

$$\int_0^r s^{1-\alpha} |F(s)|\, ds \le \left(\int_0^r s |F(s)|^2\, ds \right)^{1/2} \frac{r^{1-\alpha}}{\sqrt{2-2\alpha}}. \tag{18}$$

The second integral is bounded in the same way, with exponent $1+\alpha$ and denominator $\sqrt{2+2\alpha}$. These estimates prove the first bound in (16). With $I_\mp(r) = \int_0^r s^{1\mp\alpha} F(s)\, ds$, differentiation gives

$$p'(r) = -\frac{k^2}{2} \left[r^{\alpha-1} I_-(r) + r^{-\alpha-1} I_+(r) \right], \qquad |p'(r)| \le C k^2 \|u\|_{L^2(B_r)}. \tag{19}$$

Thus p' is locally square integrable with radial measure. The general remaining homogeneous term is $cr^\alpha + dr^{-\alpha}$. Since $u \in H^1$, U' is square integrable with measure $r\,dr$, which excludes $d \neq 0$.

To avoid any assumption about point evaluation of an H^1 function, solve (15) for c and average over $r \in (R/2, R)$ with the probability measure $2\,dr/R$. The resulting formula is

$$c(u) = \frac{2}{R} \int_{R/2}^R \left\{ r^{-\alpha} U(r) + \frac{k^2}{2\alpha} \left[\int_0^r s^{1-\alpha} F(s)\, ds - r^{-2\alpha} \int_0^r s^{1+\alpha} F(s)\, ds \right] \right\} dr. \tag{20}$$

Cauchy–Schwarz and (18) bound this expression by $C\|u\|_{L^2(B_R)}$. This proves continuity without invoking a weighted corner-expansion theorem.

For almost every radius, angular integration by parts and (12) yield

$$\alpha |U(r)| \le \left(\int_0^{2\pi} a |\partial_\theta u(r,\theta)|^2\, d\theta \right)^{1/2}. \tag{21}$$

Since $p(r) = o(r)$ and $\alpha < 1$, $c \neq 0$ implies $|U(r)| \ge |c| r^\alpha / 2$ for sufficiently small radii. Consequently the essential supremum of $|\nabla u|$ on each such circle is at least $\alpha |c| r^{\alpha-1} / (2\sqrt{2\pi})$. Here $a \le 1$ was used. Interior analyticity in each constant-coefficient sector permits the large values to be selected at ordinary points, off the interfaces. Formula (6) gives $|E| \ge b|\nabla u|/(\omega \varepsilon_0)$ there. □

Remark 2.5 (Energy and what has actually been expanded)**.** The static singular scalar field $u_0 = r^\alpha \phi$ has

$$\int_{B_R} a |\nabla u_0|^2\, dx\, dy = \alpha R^{2\alpha}. \tag{22}$$

Its electric-field exponent is $\alpha - 1$, and its energy is integrable. The finite-frequency fields above have finite local energy by membership in H^1. Formula (15) is an exact singular *angular projection*; no unproved pointwise expansion of all vector components is needed for the lower-bound argument. In particular, finite local energy does not bound the peak electric field.

Lemma 2.6 (A local finite-frequency solution with $c \neq 0$)**.** *For every fixed $k > 0$ there is $R_* > 0$, depending on k and b, such that for $0 < R < R_*$ the checkerboard equation in B_R has an H^1 solution with nonzero coefficient in Lemma 2.4.*

Proof. Scale $x = Ry$ and set $\kappa = kR$. In the unit disk solve $\nabla \cdot (a\nabla v) + \kappa^2 v = 0$ with Dirichlet trace ϕ. The static extension $v_0 = |y|^\alpha \phi$ belongs to H^1 and has that trace. Write $v = v_0 + w$, $w \in H_0^1(B_1)$. Its equation is

$$\int_{B_1} a\nabla w \cdot \nabla\overline{\psi} - \kappa^2 w\overline{\psi} = \kappa^2 \int_{B_1} v_0\overline{\psi}, \qquad \psi \in H_0^1(B_1). \tag{23}$$

If C_P is the unit-disk Poincare constant, choose $\kappa^2 C_P^2 < b/2$. The left form is coercive; Lax–Milgram gives $\|w\|_{H^1} \le C_b\kappa^2\|v_0\|_2$ and hence a uniform bound on $\|v\|_2$ for these small κ. Because the boundary trace has $U(1) = \int a\phi^2 = 1$, (15) at $r = 1$ gives

$$c(v) = 1 + \frac{\kappa^2}{2\alpha}\left[\int_0^1 s^{1-\alpha}F_v(s)\,ds - \int_0^1 s^{1+\alpha}F_v(s)\,ds\right] = 1 + O_b(\kappa^2). \tag{24}$$

The integral estimates already proved justify the last bound. Reduce R_* until $|c(v) - 1| < 1/2$. For $u(x) = v(x/R)$ the physical coefficient is $R^{-\alpha}c(v)$, which is nonzero. The frequency remained the prescribed positive k; only the local matching disk was made small. □

2.3 Outgoing well-posedness and global excitation

We spell out the scalar scattering and Runge arguments because density of free-space Herglotz waves alone would not establish excitation of the total field in a material. General Herglotz approximation results such as [16] motivate the method, but are not substituted for the following transmission argument.

The approximation is applied to *total* fields in the dielectric, including the scattered response. For each corner it gives an incident field whose singular coefficient is nonzero. The fields chosen for different corners may differ; Proposition 2.9 then combines them into one field. Because only finitely many coefficients must be kept nonzero, no uniform lower bound on their magnitudes is needed.

Lemma 2.7 (Scattering for the finite polygonal geometry)**.** *Let a be real, take values in $[b, 1]$, equal one outside a disk, and be constant on a finite polygonal partition. The outgoing scattering problem for (6) has a unique H^1_{loc} total field for each incident Herglotz wave. The map from $g \in L^2(S^1)$ to u_g in H^1 on any fixed bounded disk is continuous. An outgoing solution also exists uniquely for any compactly supported L^2 forcing.*

Proof. Choose B_L enclosing the material with a vacuum collar. Let $\Lambda_L : H^{1/2}(\partial B_L) \to H^{-1/2}(\partial B_L)$ be the exact exterior outgoing Dirichlet-to-Neumann map. Its Fourier multiplier on angular mode $m \in \mathbb{Z}$ is

$$\lambda_m = k\frac{(H^{(1)}_{|m|})'(kL)}{H^{(1)}_{|m|}(kL)}. \tag{25}$$

The Hankel denominator is nonzero on the positive real axis, since the real Bessel functions J_m, Y_m have nonzero Wronskian. Their large-order asymptotics give $\lambda_m = -|m|/L + O((1 + |m|)^{-1})$ as $|m| \to \infty$. Thus the form

$$B_a(v, w) = \int_{B_L} \left(a\nabla v \cdot \nabla\overline{w} - k^2 v\overline{w}\right) - \langle \Lambda_L v, w\rangle_{\partial B_L} \tag{26}$$

satisfies, by the trace inequality,

$$\operatorname{Re} B_a(v,v) + C\|v\|^2_{L^2(B_L)} \geq c\|v\|^2_{H^1(B_L)}. \tag{27}$$

The constants can be chosen using only b, k, L, not the positions or curvatures of the interfaces: a finite upper bound for the real parts of the multipliers suffices, and $\|v\|^2_{L^2(\partial B_L)} \leq \epsilon\|v\|^2_{H^1(B_L)} + C_\epsilon\|v\|^2_2$ absorbs it. The compact embedding $H^1(B_L) \hookrightarrow L^2(B_L)$ makes this a Fredholm form of index zero.

For the homogeneous outgoing problem, take the imaginary part of Green's identity. The far-field outgoing power is nonnegative and must vanish. Equivalently, an exterior Hankel expansion and its Wronskians show that all outgoing coefficients vanish. The solution is zero in the exterior vacuum. It continues as zero across every open polygon edge: its value and its conormal derivative are zero on that edge, so extension by zero to the other side solves that side's constant-coefficient Helmholtz equation in a small ball. Interior analytic uniqueness forces it to vanish there too. A path can avoid the finitely many vertices, and cross only open edges. Propagation along such paths proves that the solution is zero everywhere. This argument also proves unique continuation through this particular partition in any connected open subset. Fredholm alternative gives existence and a bounded inverse.

For scattering, the right-hand side of (26) is the boundary functional with density $\partial_n u_g^{\text{in}} - \Lambda_L u_g^{\text{in}}$. For a volume source $L_a w = f$, it is $-\int f\overline{v}$. Both are continuous functionals. The incident field and all its derivatives on bounded sets are bounded by $C\|g\|_2$, directly from (8). The bounded inverse gives the asserted continuity. □

The density result is used only after a locally excited field has been constructed. It turns that local field into the restriction of an outgoing scattering solution to the chosen accuracy; the coefficient estimate above then preserves excitation.

Lemma 2.8 (Local Runge approximation by total scattering fields)**.** *Under Lemma 2.7, let Q be a closed disk whose complement is connected. A solution of $L_a v = 0$ in an open neighborhood of Q can be approximated in $L^2(Q)$ by restrictions of total fields u_g, with $g \in C^\infty(S^1)$. The disk may cross material interfaces and contain a checkerboard vertex. The same statement holds for a finite disjoint union of disks if its complement is connected.*

Proof. We use complex bilinear pairings, with conjugation absorbed into the annihilating function. Suppose $f \in L^2(Q)$ satisfies $\int_Q f u_g = 0$ for all smooth g. Extend f by zero and solve $L_a w = f$ outgoing. For a plane-wave incidence $e^{ikd\cdot x}$, write $u_d = e^{ikd\cdot x} + u_d^{\text{sc}}$ for its total field. Linearity of scattering and Fubini imply $\int_Q f u_d = 0$ for all $d \in S^1$: the quantity is continuous in d and its pairing with every smooth density vanishes.

Green's second identity on a sufficiently large circle gives

$$\int_Q f u_d = \int_{\partial B_R} (\partial_n w\, u_d - w\, \partial_n u_d)\, ds. \tag{28}$$

The part pairing w with u_d^{sc} is zero. For example, expand both in outgoing Hankel modes; bilinear angular orthogonality pairs m with $-m$, whose equal radial Hankel functions have zero Wronskian. The remaining part is the free-space incident wave paired with w. The exterior Green representation with the fundamental solution $(i/4)H_0^{(1)}(k|x-y|)$ identifies this as a nonzero constant times $w_\infty(-d)$. This can also be checked by the Jacobi–Anger expansion of $e^{ikd\cdot x}$ and the $J_m, H_m^{(1)}$ Wronskian. Hence $w_\infty = 0$. The outgoing Hankel expansion gives $w = 0$ outside a sufficiently large circle.

Now $L_a w = 0$ in $\mathbb{R}^2 \setminus Q$. That set is connected, and the edgewise continuation proved in Lemma 2.7 implies $w = 0$ throughout it. Thus $w \in H_0^1(Q)$ and both its Dirichlet and conormal

traces on ∂Q vanish. The latter statement is in the weak $H^{-1/2}$ sense: the global equation has only the volume source f, and no surface distribution. Applying weak Green's identity to any local solution v gives

$$\int_Q fv = \int_Q (L_a w)v = \int_Q w(L_a v) = 0. \tag{29}$$

For a union of disks apply the same identity on each component. The Hahn–Banach annihilator characterization of a closed subspace of $L^2(Q)$ now proves the density assertion. No interior transmission-eigenvalue exception was introduced: the argument used the invertible outgoing source problem, not an inverse of an interior transmission operator. □

Nonvanishing at each corner separately is insufficient for simultaneous packing. The following proposition obtains all nonvanishing coefficients from a single incident density. Its finite-dimensional polynomial argument does not assert a uniform lower bound on those coefficients.

Proposition 2.9 (One incident field excites every selected corner)**.** *In a fixed finite polygonal geometry with N disjoint checkerboard disks of the same contrast, each local coefficient $c_j(u_g)$ is a nonzero continuous linear functional of g. There exists one $g \in C^\infty(S^1)$ with $\|g\|_2 = 1$ for which $c_j(u_g) \neq 0$ for every j.*

Proof. Continuity follows from Lemmas 2.4 and 2.7. Inside corner j choose a sufficiently small disk, and then a concentric disk twice its radius still within the checkerboard region. Lemma 2.6 on the larger disk supplies a local finite-frequency solution with $c_j \neq 0$. Lemma 2.8 approximates it on the smaller disk by total scattering fields. The L^2 continuity of c_j shows that at least one smooth density g_j has $c_j(u_{g_j}) \neq 0$.

Let $g(t) = \sum_{m=1}^{N} t^{m-1} g_m$. For each fixed j, $c_j(u_{g(t)})$ is a polynomial in t with nonzero coefficient of t^{j-1}. It has only finitely many zeros. Choose a real t outside the union of these finite root sets. Then $g(t) \neq 0$ and all the coefficients are nonzero. Dividing by $\|g(t)\|_2$ preserves that property and enforces (10). This finite-union argument requires no uniform quantitative lower bound on the coefficients and uses exactly one illumination. □

2.4 Rounding without an assumed rounding power law

The sharp corner is a device for proving the existence of large fields, not the final geometry. We first fix the illumination and observation disks, then round all the corners. Convergence on bounded regions lets us retain large fields at selected points away from the original tips; regularity away from those tips supplies a bound on each disk's collar. We do not need to predict the peak as an explicit function of the rounding radius.

Lemma 2.10 (Outgoing solutions converge under local rounding)**.** *Let a be as in Lemma 2.7. Let a_ρ equal one in a common exterior collar, satisfy $b \le a_\rho \le 1$, and converge to a almost everywhere. Assume each a_ρ defines a well-posed outgoing problem, as do the finite disjoint smooth binary inclusions used below. For a fixed incident field,*

$$u_\rho \longrightarrow u \quad \text{strongly in } H^1(B_L). \tag{30}$$

If $a_\rho = a$ in a fixed neighborhood of a compact observation set away from polygon vertices, convergence there is C^1 on each closed material side. The compact set may cross a straight interface. Thus both ordinary field values and one-sided field bounds on fixed observation circles converge.

Proof. All forms B_{a_ρ} satisfy the same Gårding estimate (27). Their inverse norms on $H^1(B_L)^* \to H^1(B_L)$ are uniformly bounded for sufficiently small ρ. Otherwise there would exist v_ρ with $\|v_\rho\|_{H^1} = 1$ and $\|B_{a_\rho} v_\rho\|_{H^{1*}} \to 0$. Pass to a weakly convergent H^1 subsequence, strongly convergent in L^2. For every fixed test z, dominated convergence gives $(a_\rho - a)\nabla z \to 0$ in L^2, so the limit v solves $B_a v = 0$. Lemma 2.7 implies $v = 0$. Estimate (27) then forces $\|v_\rho\|_{H^1} \to 0$, a contradiction.

Subtracting the equations with the same boundary forcing gives

$$B_{a_\rho}(u_\rho - u, z) = \int_{B_L} (a - a_\rho)\nabla u \cdot \nabla \overline{z}. \tag{31}$$

The right-hand functional tends to zero in H^{1*} because $(a - a_\rho)\nabla u \to 0$ in L^2 by dominated convergence. The uniform inverse bound proves (30).

For completeness, the additional local regularity needed here does not rely on estimates uniform near the rounded tips. In a ball with constant coefficient, interior elliptic estimates applied to $u_\rho - u$ give convergence of all derivatives on smaller balls. In a ball meeting one unchanged straight interface, tangential difference quotients preserve both transmission conditions. Caccioppoli estimates for these quotients, iterated to each order, bound tangential derivatives by the H^1 norm on a larger ball. On each side the equation $\partial_n^2 v = -\partial_t^2 v - (k^2/a_\pm)v$ then bounds the second normal derivative. Differentiating this identity on each material side inductively bounds derivatives with two or more normal factors by the tangential derivatives already controlled and lower-order derivatives. This yields, for each integer m and fixed nested interface balls, a piecewise H^m estimate with a constant depending on those balls, b, k, m. Sobolev embedding with $m \geq 3$ in two dimensions gives the claimed one-sided C^1 convergence. A finite cover handles the compact observation set. None of these balls contains a moving rounded tip.

The well-posedness assertion for the smooth inclusions follows by the same Fredholm and radiation argument. For uniqueness, zero exterior Cauchy data extend by zero across a smooth material boundary as a weak solution of that inclusion's constant-coefficient Helmholtz equation, so interior analyticity again applies. Standard flattening and the same transmission regularity argument show that each fixed rounded solution has bounded, continuous one-sided gradients up to its smooth interfaces. These last bounds may depend arbitrarily badly on ρ; the proof never assumes otherwise. □

Proof of Theorem 2.2. Choose distinct points $p_1, \ldots, p_N$ in $\mathcal{P}$ and small pairwise disjoint closed squares $p_j + [-s_j, s_j]^2$ contained there. For the sharp reference configuration, put dielectric material in the two opposite open squares

$$p_j + (0, s_j)^2, \qquad p_j + (-s_j, 0)^2, \tag{32}$$

and vacuum elsewhere. The coefficient near p_j is the required four-sector checkerboard. The two material squares initially touch only at p_j. There is no source at this touching point; the problem is the global uniformly elliptic weak equation.

Choose concentric observation disks $Q_j = B_{r_j}(p_j)$ with $2r_j < \ell$, their closures inside these reference blocks, and small fixed annular collars that avoid every polygon vertex. Proposition 2.9 supplies one smooth unit-norm g for which every $c_j(u_g)$ is nonzero. Keep this g fixed from now on. The sharp solution is piecewise smooth on the collars; let $B < \infty$ bound all one-sided values of $|E|$ on them. Choose an electric-field threshold $S > \max\{M, 2B\}$. By Lemma 2.4, for every j one can choose an ordinary point $x_j \in Q_j$, strictly off the interfaces, with

$$|E(x_j)| > 4S. \tag{33}$$

All these choices precede rounding.

Round every vertex of every material square *inwards* within a distance ρ, leaving all edge portions outside the vertex balls unchanged. A smooth curve joining the shortened straight edges with all endpoint derivatives matched gives C^∞ boundaries. For $\rho > 0$ the two opposite inclusions have disjoint closures. The resulting binary coefficient a_ρ differs from a only in the union of finitely many shrinking vertex balls, so $a_\rho \to a$ almost everywhere and retains exactly the original material bounds and exterior background.

Choose one sufficiently small ρ so that no changed vertex ball meets any selected point or collar. Lemma 2.10 and finiteness of N then permit a further decrease of this same ρ until simultaneously

$$|E_\rho(x_j)| > 3S \quad (1 \le j \le N), \qquad \sup_{\text{all collars, one-sided}} |E_\rho| < S. \tag{34}$$

For each fixed rounded geometry the one-sided field is bounded and continuous on the closure of each smooth material subdomain. Hence its maximum P_j on $\overline{Q}_j$ is finite and attained on at least one side, with $P_j > 3S > M$. The collar values are below $S < P_j/2$. Each maximum is therefore inside its disk, and its half-amplitude superlevel component cannot cross the collar. This is (11), with distinct components in distinct disks. The inclusions remain entirely in $\mathcal{P}$, and the fixed g still has the same unit incoming power. This proves the theorem. □

2.5 Scope and limitations of the two-dimensional construction

The order of choices in the proof is

$$(N, \mathcal{P}, \ell, k, b) \ ; \ \text{sharp geometry} \ ; \ g \ ; \ (S, x_1, \dots, x_N) \ ; \ \rho. \tag{35}$$

No interchange of the $N \to \infty$ and $\rho \to 0$ limits occurs. Runge approximation can have arbitrarily large illumination norms before normalization; after normalization the nonzero coefficients can be arbitrarily small. This costs a smaller rounding radius, which is permitted. The proof supplies no effective rate or manufacturable feature-size estimate. It also supplies no lower bound on the energy fraction in a peak, no independence of different peaks as communication channels, and no finite spectral bandwidth. All square dimensions can be chosen inside the given patch, so even the total *cross-sectional* material support is small.

Proposition 2.11 (Bounded-region energy-to-peak ratios)**.** *For the fixed sharp geometry and one illumination used above, along the rounded sequence the electromagnetic energy on any fixed bounded cross-sectional disk remains bounded, whereas the electric-field maximum in every selected corner disk tends to infinity in the sense that its lower limit is infinite. Thus the ratio of that bounded-region energy to the maximum electric energy density in any one selected disk tends to zero.*

Proof. Strong H^1 convergence and (7) bound the electric energy; $H = (0, 0, u)$ bounds the magnetic energy by L^2 convergence. For each arbitrary threshold, choose the finitely many high ordinary points in the limiting sharp field first. Pointwise convergence at those fixed points then puts all sufficiently small rounding radii above that threshold. The weighted density $\varepsilon_0 \varepsilon_r |E|^2$ differs from $|E|^2$ by uniformly bounded positive factors. This proves the ratio statement. □

This ratio is deliberately not called a modal volume. A nonzero monochromatic scattering field has infinite all-space energy. A fixed bounded integration region is a different normalization from the all-space energy of a mode. The bounds and examples in [21] concern dielectric-resonator mode volumes with their specified confinement and feature constraints; they cannot replace the separate modal argument in Sections 4 and 5.

Remark 2.12 (Scope: finite extrusion and modal packing)**.** Two specific bridges remain unproved by this section. First, truncating the z-invariant construction to a finite height changes the exact scalar reduction and introduces end radiation. A proof of finite-three-dimensional packing would need a vector Maxwell local singular coefficient, a corresponding physical illumination density argument, and stability of that coefficient under finite-height realization and simultaneous rounding. Our two-dimensional proof does not supply a uniform estimate that permits this truncation. Second, a modal theorem would need an actual mode or a stated open-resonator normalization and a proof that the same normalized mode retains all the selected singular coefficients through the geometry and rounding limits. The freely selected Herglotz illumination cannot be substituted for such a mode. The finite-extrusion route remains unproved by this section. Section 3 supplies a different finite three-dimensional driven construction with conical point tips and explicit projection constraints. The separate modal bridge is closed by Theorem 5.6. These are additional statements, not assumptions hidden in Theorem 2.2.

Remark 2.13 (Scope of material extensions)**.** The construction is an ordinary, reciprocal, nonmagnetic, scalar, lossless dielectric example. It therefore also belongs to any larger material class that contains 1 and some fixed $\varepsilon_h > 1$ within its admissible bounds, by replacing ε_+ with ε_h. The theorem needs neither near-zero permittivity nor anisotropy. A positive-definite tensor class containing these scalar tensors inherits this existence example, but no anisotropic Runge or corner theorem is claimed.

3 Finite three-dimensional driven hotspot packing

This section constructs finite inclusions with conical *point* tips. Small positive contrast supplies a convenient uniform scattering inverse; it does not remove the point singularity. The material bounds and frequency remain fixed. The modal question is separated at the end.

The two-dimensional construction suggests a mechanism, but truncating its invariant direction would introduce new boundaries and radiation. Here each sharp reference point instead has two opposite dielectric cones meeting at their tips. The resulting high-field region is localized in all three spatial directions. We again first prove excitation of the sharp points by one physical illumination and then round the tips.

Theorem 3.1 (Finite three-dimensional driven point localization)**.** *Fix $k > 0$ and an upper bound $\varepsilon_+ > 1$. There is a number $\varepsilon_h \in (1, \varepsilon_+]$ that can be kept fixed in the following construction. Given any nonempty open patch $\mathcal{P}$ in a plane, any finite N, and any $\ell, M > 0$, there exist a compactly supported binary dielectric $\varepsilon_r \in \{1, \varepsilon_h\}$ with $2N$ disjoint smooth inclusions and one unit-incoming-power Maxwell illumination at frequency k such that there are N pairwise disjoint three-dimensional balls Q_j, of diameter less than ℓ, satisfying*

$$\max_{\overline{Q}_j,\ \textit{one-sided}} |E| > M, \qquad \sup_{\textit{a collar of } \partial Q_j,\ \textit{one-sided}} |E| < \tfrac{1}{2} \max_{\overline{Q}_j,\ \textit{one-sided}} |E|. \tag{36}$$

The centers of the balls lie in $\mathcal{P}$, and the orthogonal projections of the balls and of the material support are contained in $\mathcal{P}$. In particular the selected superlevel components are localized in all three spatial dimensions. The maximizing points after rounding need not lie exactly in the original plane. There is no invariant infinite direction, no internal impressed source, and no conducting boundary in the physical device.

The prescribed patch is therefore a projection constraint, while the localized neighborhoods themselves are three-dimensional. In particular, the theorem concerns finite point neighborhoods

rather than invariant ridges. As before, no minimum energy fraction in an individual peak is required.

The proof follows the same logic as the cross-sectional case, but each step is a three-dimensional Maxwell statement. A spherical angular problem supplies a conical exponent below one; a coefficient functional detects whether the corresponding electric singularity is present. A scattering inverse and total-field approximation provide an illumination with a nonzero coefficient at every chosen point. Finally, convergence under rounding retains high values inside each ball, and bounds on its collar separate the resulting maximum from the boundary. The small contrast is selected once within the prescribed material bound; the number and size of the peaks may then be chosen as stated in the theorem.

3.1 A genuine conical point exponent

The two caps in (37) describe the directions occupied by the opposing cones. The angular eigenfunction determines the shape of a potential $r^\lambda \phi$ near their common tip. Because $0 < \lambda < 1$, its gradient is unbounded at the tip but has finite local energy. This electrostatic calculation identifies the candidate singularity; the following subsection is needed to establish its role in the finite-frequency Maxwell field.

Lemma 3.2 (Strict positive contrast gives a conical exponent below one)**.** *Choose $t \in (1/\sqrt{3}, 1)$ and set, on the unit sphere,*

$$q(\widehat{x}) = 1 + d\,\mathbf{1}_{\{|\widehat{x}\cdot e_3| > t\}}, \qquad d > 0. \tag{37}$$

There are a real $\phi \in H^1(S^2)$ and $\lambda \in (0,1)$ satisfying

$$-\operatorname{div}_{S^2}(q\nabla_{S^2}\phi) = \nu q\phi, \qquad \nu = \lambda(\lambda+1), \qquad \int_{S^2} q\phi^2 = 1, \quad \int_{S^2} q\phi = 0. \tag{38}$$

The electrostatic field $E_0 = \nabla(r^\lambda\phi)$ is curl free, satisfies $\operatorname{div}(qE_0) = 0$ weakly in a ball, and obeys

$$\int_{B_R} q|E_0|^2\,dx = \lambda R^{2\lambda+1}. \tag{39}$$

Proof. The weighted Rayleigh quotient on the subspace orthogonal to constants has a positive minimum by the compact embedding $H^1(S^2) \hookrightarrow L^2(S^2)$ and the sphere Poincare inequality. Use the trial function $z = \widehat{x}\cdot e_3$, whose weighted mean vanishes by reflection symmetry. Since $|\nabla_{S^2} z|^2 = 1 - z^2$,

$$\int_{S^2} q(|\nabla_{S^2} z|^2 - 2z^2) = d\int_{|z|>t} (1 - 3z^2) < 0. \tag{40}$$

Explicitly, the trial quotient is

$$\mathcal{Q}(z) = \frac{2 + d(2 - 3t + t^3)}{1 + d(1 - t^3)}, \qquad \mathcal{Q}(z) - 2 = -\frac{3dt(1-t^2)}{1 + d(1-t^3)} < 0. \tag{41}$$

Thus the first positive eigenvalue ν is less than two; its positive indicial root satisfies $0 < \lambda < 1$. Separation in spherical coordinates proves the weak electrostatic equation. The interface conditions are exactly those in the angular weak problem. The flux through a small sphere is of order $r^{\lambda+1}$, so there is no point source at the origin. Finally $\int q|\nabla_{S^2}\phi|^2 = \nu$ gives $(\lambda^2 + \nu)\int_0^R r^{2\lambda}\,dr = \lambda R^{2\lambda+1}$. □

3.2 An exact Maxwell coefficient functional at the conical point

At positive frequency the Maxwell field is not simply the electrostatic field just described. The decomposition below separates a gradient part, which can contain the conical singularity, from a more regular remainder. Projecting the gradient part onto the angular eigenfunction then defines a coefficient that can be tested for the actual total field. This is the bridge from the local model to a physical scattering solution.

We use one standard regularity theorem in a precise local form. On a ball there is a bounded linear regularized Poincare lifting

$$\mathcal{R} : H^1(B)^3 \cap \ker \operatorname{div} \longrightarrow H^2(B)^3, \qquad \operatorname{curl} \mathcal{R} f = f. \tag{42}$$

This is the regularized curl-potential operator of Costabel and McIntosh [4]; their homotopy identity and order-minus-one mapping theorem apply to a ball. Only this established local Sobolev mapping is imported. It is not a scattering, corner-excitation, or rounding theorem.

Use normalized units $\operatorname{curl} E = ikH$, $\operatorname{curl} H = -ikqE$ in the local arguments; the magnetic field here is the physical magnetic field multiplied by Z_0.

Lemma 3.3 (Local regular decomposition with controlled remainder)**.** *Suppose E, H solve the source-free Maxwell system with $1 \le q \le \varepsilon_h$ on B_{3R} and have finite local energy. On B_R one can write*

$$E = \nabla v + W, \qquad v \in H^1(B_R), \quad W \in H^2(B_R)^3, \quad \|v\|_{H^1} + \|W\|_{H^2} \le C\|E\|_{L^2(B_{3R})}, \tag{43}$$

after fixing the additive constant of v. The maps can be chosen linear. The constant depends on the displayed radii, frequency and material bounds, not on derivatives of q.

Proof. Testing $\operatorname{curl}\operatorname{curl} E = k^2 qE$ against $\chi^2 E$, for a compactly supported cutoff, and applying Young's inequality gives $\|\operatorname{curl} E\|_{L^2(B_{5R/2})} \le C\|E\|_{L^2(B_{3R})}$. Since $\operatorname{div} H = 0$ and $\operatorname{curl} H = -ikqE$, the Fourier curl/div identity applied to a cutoff of H gives $\|H\|_{H^1(B_{2R})} \le C\|E\|_{L^2(B_{3R})}$. This is the same constant-permeability interior mechanism as Lemma 6.6. Apply (42) on B_{2R} to $\operatorname{curl} E = ikH$, which is divergence free, and restrict the resulting W to B_R. The curl-free difference $E - W$ is a gradient on the simply connected ball. Its potential with zero mean satisfies the stated bound by the ordinary Poincare inequality. All operations are bounded and linear. □

The local decomposition separates the singular potential from a bounded remainder. The coefficient below is defined by an angular projection; its independence of the chosen lifting makes it a property of the field, rather than of the decomposition.

Lemma 3.4 (Intrinsic conical singular coefficient)**.** *In the conical material of Lemma 3.2, every local Maxwell solution as above has a linear coefficient $c(E)$, continuous for the $L^2(B_{3R})$ topology on its solution space. If $c(E) \neq 0$, then $|E|$ is unbounded at ordinary points approaching the conical vertex from the homogeneous regions. Its local energy remains finite.*

Proof. Use $E = \nabla v + W$ from Lemma 3.3. Since $H^2(B_R) \hookrightarrow C^{0,\gamma}(\overline{B}_R)$ for $0 < \gamma < 1/2$, W is bounded. Define

$$U(r) = \int_{S^2} qv(r, \widehat{x})\phi, \qquad A(r) = \int_{S^2} qW_r(r, \widehat{x})\phi, \qquad B(r) = \int_{S^2} qW_t(r, \widehat{x}) \cdot \nabla_{S^2}\phi. \tag{44}$$

The subscripts denote radial and tangential components. Projecting $\operatorname{div}(q(\nabla v + W)) = 0$ gives

$$(r^2 U')' - \lambda(\lambda + 1)U = -(r^2 A)' + rB. \tag{45}$$

The exact solution with finite H^1 energy is

$$U(r) = c(E)r^\lambda + p(r),$$
$$p(r) = \frac{1}{2\lambda+1}\left[r^\lambda \int_0^r s^{-\lambda}\{B(s) - (\lambda+1)A(s)\}\,ds \right.$$
$$\left. -r^{-\lambda-1}\int_0^r s^{\lambda+1}\{B(s) + \lambda A(s)\}\,ds\right]. \tag{46}$$

To verify this formula, variation of constants for the two homogeneous solutions $r^\lambda, r^{-\lambda-1}$ first gives integrals of $-A' - 2A/r + B/r$. Integrating the A' terms by parts cancels their endpoint contributions and gives (46). The integrals converge because A, B are bounded and $\lambda < 1$. They show

$$|p(r)| \le Cr\|W\|_\infty, \qquad |p'(r)| \le C\|W\|_\infty. \tag{47}$$

For the second inequality, differentiation produces the additional term $-A(r)$ and two bounded integral terms. Finite H^1 energy excludes the other homogeneous term $r^{-\lambda-1}$.

Average $r^{-\lambda}(U(r) - p(r))$ on $R/2 < r < R$ to define $c(E)$. This is a bounded functional of v in L^2 and W in L^∞; Lemma 3.3 proves the required continuity. It is independent of the chosen lifting. Indeed, two liftings differ by a bounded curl-free vector field; the corresponding potentials differ by a Lipschitz function. Its angular projection is $O(r)$ after subtracting its constant value, and the weighted mean of ϕ is zero. Such a difference has coefficient zero.

Angular integration by parts gives

$$\sqrt{\nu}|U(r)| \le \left(\int_{S^2} q|\nabla_{S^2} v(r,\widehat{x})|^2\right)^{1/2}. \tag{48}$$

If $c(E) \neq 0$, then $|U(r)| \ge |c(E)|r^\lambda/2$ at all sufficiently small admissible radii, since $p = O(r)$. Consequently the essential supremum of $|\nabla v|$ on these spheres is at least a positive constant times $r^{\lambda-1}$. Subtracting the bounded W cannot remove the divergence of $|E|$. Inside each constant-coefficient region the Maxwell field is analytic; the large values can be selected away from interfaces. Its energy is finite by the starting local L^2 assumption. □

The local coefficient alone does not determine whether a prescribed illumination excites the singularity. We next construct a local finite-frequency solution with a nonzero coefficient; the subsequent Runge argument supplies a physical illumination.

Lemma 3.5 (Local positive-frequency excitation of the point coefficient)**.** *For the conical coefficient q, at every fixed $k > 0$ there are local source-free Maxwell solutions on a sufficiently small ball with $c(E) \neq 0$.*

Proof. Scale a physical ball to B_1 and write $\kappa = kR$. Let $E_0 = \nabla(r^\lambda\phi)$ and consider

$$X_q = \{w \in H_0(\mathrm{curl}, B_1) : \mathrm{div}(qw) = 0\}. \tag{49}$$

There is a finite constant C_q with $\|w\|_2 \le C_q\|\operatorname{curl} w\|_2$ on X_q. Here is a reduction to the ordinary ball estimate, which avoids an unproved smoothness assumption on q. Decompose $w = w_T + \nabla p$ with $p \in H_0^1$ and $\operatorname{div} w_T = 0$, $w_T \in H_0(\mathrm{curl})$. Weighted divergence yields $\int q\nabla p\cdot\nabla\overline{\psi} = -\int(q-1)w_T\cdot\nabla\overline{\psi}$, so $\|\nabla p\|_2 \le d\|w_T\|_2$. For a ball the usual Maxwell estimate is $\|w_T\|_2 \le C\|\operatorname{curl} w_T\|_2$. For clarity, H^1 membership in this assertion is not assumed. The order-minus-one lifting also maps L^2 to H^1; lift $\operatorname{curl} w_T$ to $V \in H^1$. The difference $w_T - V = \nabla p_0$ has $\Delta p_0 = -\operatorname{div} V$ and tangential boundary

gradient $-V_t$. The latter is in $H^{1/2}(S^2)$, so the boundary trace of p_0, modulo a constant, is in $H^{3/2}(S^2)$. This follows by the scalar sphere Laplacian estimate applied to its tangential gradient. Dirichlet regularity on the smooth ball gives $p_0 \in H^2$, hence $w_T \in H^1$. One can now use the Gaffney identity for tangential-zero fields,

$$\|\operatorname{curl} w_T\|_2^2 + \|\operatorname{div} w_T\|_2^2 = \|\nabla w_T\|_2^2 + 2\|w_T \cdot n\|_{L^2(S^2)}^2, \tag{50}$$

initially for smooth fields and then by trace-preserving approximation on the smooth ball. Poincare's inequality with the tangential trace condition excludes constant vectors and bounds the L^2 norm. Thus $C_q \le (1+d)C$ is sufficient.

Solve on X_q

$$\int \operatorname{curl} w \cdot \operatorname{curl} \overline{z} - \kappa^2 q w \cdot \overline{z} = \kappa^2 \int q E_0 \cdot \overline{z}. \tag{51}$$

For $\kappa^2 \varepsilon_h C_q^2 < 1/2$ this is coercive and gives $\|w\|_{H(\mathrm{curl})} \le C\kappa^2 \|E_0\|_2$. It is also the equation for every test in $H_0(\mathrm{curl})$: the weighted Helmholtz decomposition splits such a test into an X_q part and a gradient from H_0^1, and both sides vanish on the gradient part. Hence $E = E_0 + w$ satisfies $\operatorname{curl}\operatorname{curl} E = \kappa^2 q E$ and $H = (i\kappa)^{-1} \operatorname{curl} E$ completes the exact Maxwell solution.

On an interior ball, cutoff curl/div regularity gives

$$\|\operatorname{curl} w\|_{H^1(B_{1/2})} \le C\left(\|\operatorname{curl} w\|_2 + \kappa^2 \|q(E_0 + w)\|_2\right) = O(\kappa^2). \tag{52}$$

Apply the lifting to $\operatorname{curl} w$. Its W has H^2 norm $O(\kappa^2)$; the potential in $E = \nabla v + W$ differs from $r^\lambda \phi$, up to a constant, by $O(\kappa^2)$ in H^1. The averaged formula in Lemma 3.4 therefore gives $c(E) = 1 + O(\kappa^2)$. This proves nontriviality for small positive κ. The local tangential boundary data used to construct this solution are a mathematical matching device. The physical construction below uses global incoming waves and has no PEC boundary. □

3.3 A uniform finite-device Maxwell inverse at fixed small contrast

The following inverse controls the complete response of the finite dielectric, including multiple scattering among the inclusions. Small contrast makes the volume operator invertible uniformly over the family used for rounding. It is a device for controlling the global problem; the local conical exponent remains below one at every positive contrast.

Lemma 3.6 (Uniform volume-integral inverse)**.** *Fix a ball B_L and $k > 0$. There is $C_{kL} < \infty$ such that the electric volume operator*

$$\mathcal{K}_k f = (k^2 I + \nabla\nabla)\Phi_k * f, \qquad \Phi_k(x) = \frac{e^{ik|x|}}{4\pi|x|}, \tag{53}$$

restricted to B_L, with f zero extended, has L^2 norm at most C_{kL}. For $0 < d < (2C_{kL})^{-1}$ and any measurable $0 \le \chi \le d$ supported in B_L,

$$E = E^{\mathrm{in}} + \mathcal{K}_k(\chi E) \tag{54}$$

has a unique solution and $\|(I - \mathcal{K}_k\chi)^{-1}\| \le 2$. It is the unique outgoing Maxwell scattering field for $\varepsilon_r = 1 + \chi$. An outgoing electric source problem with compact L^2 forcing is likewise well posed.

Proof. Split $\mathcal{K}_k = \nabla\nabla\Phi_0 * + [k^2 I\Phi_k + \nabla\nabla(\Phi_k - \Phi_0)]*$. The first operator has Fourier multiplier $-\xi\xi^T/|\xi|^2$, of norm at most one on all-space L^2; this includes its distributional diagonal term. The

bracketed matrix kernel is locally integrable: the expansion $\Phi_k - \Phi_0 = ik/(4\pi) - k^2|x|/(8\pi) + O(k^3|x|^2)$ shows a Hessian of order $1/|x|$. Away from zero it is smooth. Young's inequality after cutting the kernel off at $|x| = 2L$ therefore bounds the remainder by its finite matrix L^1 norm. Rescaling x by L shows that the resulting constant depends only on kL. This proves the operator estimate.

The Neumann series proves the inverse bound, uniformly over all the admitted geometries. The dyadic kernel $k^{-2}\mathcal{K}_k$ is the outgoing fundamental solution of $\operatorname{curl}\operatorname{curl} - k^2$. Consequently (54) gives the Maxwell equations and radiation condition in distributions. Conversely, subtracting that representation from an outgoing solution gives an entire outgoing vacuum solution, which is zero by the spherical-wave expansion. This proves uniqueness and equivalence, including for discontinuous χ. An electric forcing $f \in L^2_c$ replaces E^{in} by $k^{-2}\mathcal{K}_k f$ on a ball enclosing its support; the same inverse applies when that support is in B_L. Only this latter case is needed below. □

For the theorem choose $L = 1/k$ and fix once and for all

$$0 < d < \min\{\varepsilon_+ - 1, (2C_1)^{-1}\}, \qquad \varepsilon_h = 1 + d. \tag{55}$$

Every finite collection of tips and inclusions can be placed in a much smaller ball whose projected closure lies in $\mathcal{P}$. The containing comparison ball of radius $1/k$ is only used for the inverse; it is not extra material.

3.4 Physical illumination, total-field density, and rounding

The incoming field is a superposition of plane waves with a square integrable angular density. Its incoming power is finite and can be normalized to one. The density result below concerns the resulting *total* fields in the actual dielectric, not just the incident waves. It connects the local conical solutions to one globally admissible source.

We now restore physical units: E is the physical electric field and H is the physical magnetic field, without the local Z_0 rescaling used above. For a smooth tangential density $g : S^2 \to \mathbb{C}^3$, $d \cdot g(d) = 0$, use the physical electric incident field

$$E_g^{\mathrm{in}}(x) = \frac{k\sqrt{Z_0}}{\sqrt{2}\,\pi} \int_{S^2} g(d) e^{ikd\cdot x}\, dS(d), \qquad H_g^{\mathrm{in}}(x) = \frac{k}{\sqrt{2Z_0}\,\pi} \int_{S^2} d \times g(d) e^{ikd\cdot x}\, dS(d). \tag{56}$$

Stationary phase on the sphere gives an incoming electric amplitude $\sqrt{2Z_0}\, g(-\widehat{x})/r$, up to a phase of unit modulus. The radial incoming flux is $|E^{\mathrm{in}}_{\mathrm{incoming}}|^2/(2Z_0)$, so the total incoming power is exactly $\|g\|^2_{L^2(S^2)}$. This is finite total power, rather than power per invariant length.

Lemma 3.7 (Total-field Maxwell Runge approximation for these devices)**.** *Let the small-contrast coefficient be piecewise constant, with finitely many smooth interface pieces and finitely many conical vertices and joining curves. Let Q be a closed ball, or a finite disjoint union of closed balls, compactly contained in the comparison ball B_L and with connected complement. A source-free Maxwell electric field defined on a neighborhood of Q can be approximated in $L^2(Q)^3$ by total electric fields from (56).*

Proof. Take $f \in L^2(Q)^3$ annihilating all such total fields under the complex bilinear pairing, and solve $(\operatorname{curl}\operatorname{curl} - k^2\varepsilon_r)W = f$ outgoing by Lemma 3.6. Orthogonality to every smooth tangential density says $\int_Q f \cdot E_{d,p} = 0$ for all incident plane waves $pe^{ikd\cdot x}$ with $p \cdot d = 0$. Continuity in d, p justifies passing from integrated illuminations to individual plane waves. Maxwell Green's identity, without complex conjugation, equates this integral to a nonzero constant times $p \cdot W_\infty(-d)$. One may obtain the identity directly by inserting the dyadic outgoing representation; the pairing of two outgoing solutions has zero boundary Wronskian. Since the electric far field is tangential, testing all

$p \perp d$ proves $W_\infty = 0$. The vacuum vector spherical-wave expansion then gives $W = 0$ outside a sufficiently large sphere.

The exterior of Q is connected. Unique continuation here is elementary within each material: the electric and magnetic fields satisfy constant-coefficient Helmholtz equations. Zero extends across an open smooth interface because both tangential electric and magnetic traces are zero; extending by zero gives a weak constant-coefficient Maxwell solution on a ball crossing that interface, hence an analytic one. Paths avoid the finitely many vertices and joining curves and cross only open interface pieces. Thus $W = 0$ outside Q. Both W and $\operatorname{curl} W$ are in local $H(\operatorname{curl})$, and have zero tangential traces on ∂Q. For every local homogeneous solution V, Green's identity consequently gives $\int_Q f \cdot V = \int_Q W \cdot (\operatorname{curl}\operatorname{curl} - k^2\varepsilon_r)V = 0$. The annihilator characterization of the L^2 closure proves density. This is density of total fields in the actual material, not an assumed free-space approximation inside it. □

The rounding estimate has two distinct roles: L^2 convergence transfers large values from the sharp reference field, while the collar bound confines the resulting peaks. The latter depends on regularity estimates in fixed smooth-interface charts away from the shrinking tips; convergence in L^2 alone does not supply a pointwise bound on the collars.

Lemma 3.8 (Finite-device rounding continuity)**.** *Let χ_ρ, χ be supported in the common comparison ball, $0 \le \chi_\rho, \chi \le d$, with $\chi_\rho \to \chi$ almost everywhere. For one fixed incident field, their total electric fields satisfy $E_\rho \to E$ in $L^2(B_L)^3$. For the smooth rounded conical family used here, suppose in addition that the coefficients agree exactly with one fixed smooth reference body on a neighborhood of each prescribed sphere collar, for every sufficiently small rounding parameter. The collars avoid all vertices and joining curves. Then the continuous electric fields on both closed material sides have one common finite bound on those collars. This includes collars intersecting smooth conical interfaces.*

Proof. Subtract the volume equations:

$$E_\rho - E = (I - \mathcal{K}_k\chi_\rho)^{-1}\mathcal{K}_k((\chi_\rho - \chi)E). \tag{57}$$

Dominated convergence makes the last multiplication tend to zero in L^2, and Lemma 3.6 bounds both operators uniformly. This proves the first claim.

For the collar bound, write the actual total field as $E_\rho = \nabla v_\rho + W_\rho$, retaining the same fixed smooth incident field. The convergent volume unknowns have bounded source norms; the compact scalar Green operators give bounded local scalar potential and gradient norms, and bounded H^2 correction norms. Choose a fixed smooth rounded reference body that agrees with every later body near the collar. Its regular interfaces supply fixed signed graph charts; homogeneous neighborhoods complete the cover.

In each chart the actual scalar transmission equation is localized with nested smooth cutoffs. A regional difference-quotient energy estimate first derives the mixed derivative entering the differentiated forcing. Thus no second derivative of the original potential on an outer cutoff annulus is assumed. Two tangential iterations and the normal-flux equation then give continuous tangential and flux representatives with bounds depending only on the original scalar and forcing norms and the fixed chart data. Reconstructing the physical gradient gives uniformly bounded actual electric branches on both closed material sides. A finite cover of the compact sphere gives one bound on an open collar, chosen before the rounding index. The same local regularity argument, without a uniform constant, gives continuous one-sided branches for every fixed smooth rounded device. No estimate uniform at a shrinking tip is used. □

Proof of Theorem 3.1. Select distinct centers p_j in the planar patch and sufficiently small disjoint balls about them. Put two opposite dielectric cones at each center, with opening angle from (37). They agree exactly with the homogeneous conical geometry on a smaller ball, and are smoothly capped farther away, all within the selected neighborhood. Their closures touch only at the center in this sharp reference geometry. The projections of all these neighborhoods lie in $\mathcal{P}$, and their total support fits in a ball of radius $1/k$.

For each selected vertex, Lemma 3.5 constructs a local finite-frequency field with nonzero coefficient. Lemma 3.7 approximates it on a slightly larger ball than that used to measure the coefficient. Lemma 3.4 then shows that the coefficient $c_j(E_g)$ is a nonzero continuous linear functional of the smooth tangential incident density g. Choose one density outside the finite union of its kernels, exactly as in Proposition 2.9, and divide by its $L^2(S^2)$ norm. All coefficients remain nonzero, and the incoming power is one.

Fix disjoint observation balls Q_j of diameter less than ℓ inside the exact conical regions, and round all tips inward while leaving their collars unchanged. The result has $2N$ disjoint smooth inclusions and the same two material values. The changed sets shrink to the finite vertex set. Lemma 3.8 gives a common bound B for both actual material-side traces on all fixed collars, uniformly for sufficiently small rounding parameters.

Choose $S > \max\{M, 2B\}$. Each nonzero conical coefficient supplies a positive-volume superlevel $|E| > 2S$ inside its observation ball. Local L^2 convergence preserves a positive-volume superlevel $|E_\rho| > S$ in every ball for all sufficiently small ρ. The continuous one-sided branches attain their joint maximum on the compact ball. Each maximum exceeds S and twice the collar bound. The collar is therefore a strict low barrier for its half-amplitude superlevel set. Its full connected component is compact and stays strictly inside the observation ball, proving (36). All choices of illumination precede rounding; the same normalized input is used for every rounded field. □

Corollary 3.9 (Finite-region volume-to-peak ratios in three dimensions)**.** *Along the rounded sequence for one fixed sharp configuration and one normalized input, electromagnetic energy in a fixed bounded region stays bounded, while the electric maximum in every selected ball tends to infinity. Each resulting finite-region energy-to-peak ratio tends to zero. This is a driven local-energy statement, not an all-space modal normalization.*

Proof. The electric L^2 norms are uniformly bounded by the volume inverse. The magnetic fields are bounded on fixed bounded regions by the Maxwell equations, the local curl estimate, and exterior vacuum regularity; a slightly larger comparison ball may be used for the cutoffs. For every finite amplitude threshold, the sharp field has a positive-volume superlevel in every selected ball. Local L^2 convergence preserves a smaller superlevel for every sufficiently late rounded device. The attained one-sided maxima therefore diverge along the same family. The material factors are bounded above and below. □

3.5 What an exact mode can mean in a finite dielectric device

Proposition 3.10 (Absence of real-frequency finite-energy modes)**.** *Let the real positive scalar permittivity be constant on finitely many material pieces with piecewise smooth interfaces, and equal one outside a bounded set. At a fixed real $\omega > 0$, a source-free Maxwell field with finite all-space electromagnetic energy is zero. The same conclusion holds for an outgoing source-free field, without a finite-energy assumption.*

Proof. In the exterior vacuum every Cartesian component satisfies the scalar Helmholtz equation. A spherical harmonic expansion of an L^2 exterior solution has radial terms proportional to incoming

and outgoing spherical Hankel functions. Each nonzero radial combination has nondecaying mean radial L^2 mass, because its leading amplitude is a nonzero combination of e^{ikr} and e^{-ikr} divided by r. It cannot be square integrable on (R, ∞) with volume weight r^2. Orthogonality of spherical harmonics excludes cancellation between different angular terms. Thus a finite-energy field is zero in the exterior. For an outgoing source-free field, the real part of the complex Poynting identity instead sets its nonnegative far-field radiation power to zero, giving the same exterior conclusion. Tangential electric and magnetic continuity then propagates zero across each open smooth material interface by the constant-coefficient extension argument used in Lemma 3.7. Paths can avoid the finite lower-dimensional interface singular sets. Hence the field is zero everywhere. □

This proposition diagnoses an inappropriate literal interpretation of the modal numerator; it does *not* refute the tutorial's high-Q or quasinormal-mode interpretation. A finite radiating resonator has complex-frequency poles. Their outgoing fields grow at spatial infinity and require a specified regularized mode norm, or a justified high-Q approximation, instead of the ordinary positive all-space energy integral. The tutorial explicitly notes open-cavity generalizations of its mode-volume definition.

Remark 3.11 (The driven proof and the separate modal construction)**.** Theorem 3.1 establishes the finite-device *driven* point-localization statement given above. It does not turn the chosen illumination into a resonator mode. A possible modal route starts with a simple isolated dielectric resonance, inserts finitely many small conical inclusions where its electric field is nonzero, and then rounds their tips. To complete that route one must prove that a single continued resonance has nonzero conical coefficients at every selected vertex, and that the chosen resonance normalization stays finite and nonzero under insertion and rounding. These are not consequences of Runge approximation: Runge varies external illumination, whereas a pole's eigenfield is fixed by its homogeneous outgoing eigenproblem. Strong local field convergence without a coefficient topology also does not prove nonzero singular coefficients. Sections 4 and 5 establish these conditions for the particular modal family considered there. Eventual nonzero excitation is proved by a strict annular pairing in Theorem 4.2, without requiring continuation of the intrinsic coefficient through zero contrast; a simple pole, its genuine reciprocal normalization and its rounded continuation are proved in Lemmas 5.3–5.5. The resulting closed modal statement is Theorem 5.6. It does not rely on varying a driven illumination or on a divergent all-space positive energy integral.

4 Excitation of conical points by one genuine resonance

This section proves a local bridge that the driven-field construction does not provide: a single analytically continued Maxwell resonance retains a nonzero electric singular coefficient at every member of a finite family of newly inserted conical points. The contrast of the insertions may depend on that finite family; the bounds $1 \le \varepsilon_r \le \varepsilon_+$ do not change. A resonance here has a complex frequency and satisfies the analytically continued outgoing condition. It is not a real-frequency driven solution.

The issue is not merely whether each cone *can* support a singular field. A resonator mode is selected by the global source-free problem, so we cannot tune an independent illumination at each tip. We start with one mode that is nonzero at the proposed insertion points, add small positive-contrast cones, and show that the resulting *same* continued mode excites each tip. This section proves the local excitation step; Section 5 constructs and normalizes the global mode.

4.1 The angular branch through a homogeneous medium

The two spherical caps below encode opposite conical sectors. As their contrast tends to zero, the angular eigenfunction approaches a linear potential along the cone axis. Its electric field approaches a constant axial vector. At every positive contrast in the family the exponent is less than one, so a nonzero coefficient produces an unbounded field at the sharp tip. The limiting constant field tells us which component of the original mode can excite this singularity.

Fix an axis $e \in S^2$, a number $t \in (1/\sqrt{3}, 1)$, and put

$$a(\widehat{x}) = \mathbf{1}_{\{|\widehat{x}\cdot e|>t\}}, \qquad q_\eta(\widehat{x}) = 1 + \eta a(\widehat{x}). \tag{58}$$

The physical permittivity near a selected point is $\varepsilon_b q_\eta$, where $1 < \varepsilon_b < \varepsilon_+$ is the permittivity of its initially homogeneous host. The contrast parameter is real and positive. We need a convergent real angular family; analytic continuation of its singular coefficient or of its angular eigenfunction is not required.

Lemma 4.1 (A positive-contrast angular family)**.** *Fix $1/2 \le t < 1$ and any sequence $\eta_j > 0$ tending to zero. There are real, axisymmetric, odd angular eigenfunctions ϕ_j and numbers $0 < \lambda_j < 1$, $\nu_j = \lambda_j(\lambda_j + 1)$, satisfying*

$$-\operatorname{div}_{S^2}(q_{\eta_j}\nabla_{S^2}\phi_j) = \nu_j q_{\eta_j}\phi_j, \qquad \int_{S^2} q_{\eta_j}\phi_j \, dS = 0. \tag{59}$$

They may be normalized so that $\nu_j \to 2$, $\lambda_j \to 1$, $\phi_j(\widehat{x}) \to \widehat{x}\cdot e$, and, almost everywhere on the sphere, the corresponding angular electric vector $\lambda_j\phi_j\widehat{x} + \nabla_{S^2}\phi_j$ tends to e. The angular bounds needed for dominated convergence are uniform along this family. The construction below uses $t = 3/4$.

Proof. Use the regular polar and odd equatorial Legendre solutions of the angular equation, and impose potential continuity and weighted normal flux continuity at the cap boundary. Their matching determinant $D(\eta, t, \nu)$ is continuous for $0 \le \nu \le 2$. It is negative at zero and equals $\eta t > 0$ at two, so it has a root $\nu_j \in (0, 2)$ for each positive contrast. The associated piecewise profile and its weighted flux satisfy the full weak angular equation; odd symmetry gives the zero weighted mean.

At zero contrast the only determinant root in $[0, 2]$ is two. Indeed, test its weak angular equation against $\widehat{x}\cdot e$ and test the weak tangential gradient identity against the constant axial vector. These give, for the same strictly positive profile-axis pairing I, the identity $2I = \nu I$. Positivity follows from the polar and odd equatorial profiles for $t \ge 1/2$. Every subsequential limit of the roots is a zero-contrast root by continuity of the determinant. Compactness therefore gives $\nu_j \to 2$ and $\lambda_j = (-1 + \sqrt{1 + 4\nu_j})/2 \to 1$. The convergent Legendre series and their first derivatives give the stated normalized profile and electric-vector limits, together with the uniform angular majorants. This supplies the real family used in the annular pairing argument. □

4.2 Nonvanishing from an annular pairing

We use only positive real contrasts in the following excitation step. The singular coefficient need not be continued analytically, or even shown to converge, as the contrast tends to zero.

The proof tests each mode against a localized angular pattern on an annulus around the tip. The key estimate is uniform as the contrast tends to zero: if the singular coefficient vanished, the pairing would be small compared with the annulus size. The same pairing converges to a nonzero multiple of the original mode's axial field. Choosing the annulus sufficiently close to the tip makes these conclusions incompatible. The uniform estimate depends on cancellation of the constant part of the regular correction; simple L^2 convergence alone cannot provide it.

Theorem 4.2 (Eventual excitation by a convergent mode family)**.** *Let $\eta_j > 0$ tend to zero and let E_j be actual outgoing volume-response Maxwell fields in a fixed conical ball $B_b(p)$ with material $\varepsilon_b q_{\eta_j}$ as in (58). Assume their frequencies are nonzero and bounded, their compactly supported volume sources have uniformly bounded L^2 norms in one fixed containing ball, and $E_j \to E_0$ in $L^2(B_b(p))^3$. Suppose E_0 has a continuous representative near p and $E_0(p) \cdot e \neq 0$. Then the intrinsic conical coefficients of E_j are nonzero for all sufficiently large j.*

Proof. The real angular eigenpairs in Lemma 4.1 have $\nu_j \to 2$, $\lambda_j \to 1$, and $\lambda_j < 1$ for all sufficiently large j. The actual compact-source volume representation supplies the decomposition used in Lemma 3.4. Its regular correction W_j has a common bound

$$|W_j(x) - W_j(p)| \le M|x-p|^\alpha \qquad (x \in B_b(p)), \tag{60}$$

for some $M < \infty$ and $\alpha > 0$. Indeed, on the fixed source ball the difference of two scalar outgoing Green rows has squared L^2 norm $O(|x-p|)$: split the source ball into a near part and its complement and use the $1/r$ kernel and its $1/r^2$ derivative. Cauchy–Schwarz and the uniform source and frequency bounds give (60), with $\alpha = 1/2$.

Let $P_j(\zeta)$ be the electric field's angularly projected pairing with a smooth nonnegative radial test ζ supported in $(0, b)$. Subtracting the constant $W_j(p)$ before solving the projected radial equation removes the apparent $1/(1-\lambda_j)$ singularity. The angular eigenvalue identity cancels the constant correction exactly. The remaining forcing is $O(r^\alpha)$, and the regular particular solution is $O(r^{1+\alpha})$ uniformly as $\lambda_j \uparrow 1$. Finite local energy excludes the singular homogeneous solution. Consequently, if the intrinsic coefficient is zero, there is a constant C independent of j such that

$$|P_j(\zeta)| \le CM \int_0^b r^{2+\alpha} |\zeta(r)|\, dr. \tag{61}$$

This is the zero-coefficient consequence of the same radial projection and coefficient formula used in Lemma 3.4.

For each fixed ζ, the L^2 convergence of the actual fields and convergence of the real angular projections give $P_j(\zeta) \to P_0(\zeta)$. The limiting pairing has the form

$$P_0(\zeta) = c_t \int_0^b r^2 \zeta(r) A(r)\, dr, \qquad c_t > 0, \quad A(r) \longrightarrow E_0(p) \cdot e \quad (r \downarrow 0), \tag{62}$$

where A is the corresponding spherical average of the continuous limiting field. Choose a nonzero nonnegative bump supported in a sufficiently small annulus. Continuity and $A(0) \neq 0$ give a strict lower bound on $|P_0(\zeta)|$ proportional to $\int r^2 \zeta$, whereas the right side of (61) has the extra factor r^α. Thus the latter is strictly smaller than $|P_0(\zeta)|$. The convergence of P_j contradicts zero coefficient for every sufficiently large j. The conclusion uses the actual fields and their local L^2 limit; it does not infer nonvanishing merely from L^2 closeness without this quantitative projection estimate. □

Corollary 4.3 (Simultaneous excitation by one mode)**.** *Suppose one family of actual resonant fields satisfies the theorem at each of finitely many disjoint conical balls, with the same positive contrasts $\eta_j \downarrow 0$, and that its limiting field has a nonzero axial component at each center. Then one sufficiently large index j gives one resonance whose intrinsic coefficient is nonzero at every selected vertex. The contrast can also be chosen below any prescribed positive ceiling, including that required by $\varepsilon_b(1+\eta_j) \le \varepsilon_+$.*

Proof. Apply the theorem at each center and take the maximum of the finitely many resulting indices. The selected coefficients belong to the same actual eigenfield and the same complex resonance. □

4.3 Conditional transfer to rounded modal peaks

The next proposition isolates the global spectral assumptions needed by the local argument: one continuing resonance, a stable nonzero normalization, and control of the rounded fields on collars. It is a conditional transfer statement; the next section verifies its hypotheses for an explicit sphere-based family.

Proposition 4.4 (Transfer from a simple resonance to rounded modal peaks)**.** *Assume a finite homogeneous dielectric sphere with permittivity $\varepsilon_b \in (1, \varepsilon_+)$ has a simple resonance in the axisymmetric TM sector, whose axial electric component is nonzero on an open interval of its symmetry axis. Assume furthermore:*

1. *This sector's eigenpair has a holomorphic continuation under the finite axisymmetric cone insertions in Corollary 4.3.*
2. *An explicitly specified genuine QNM normalization is finite, nonzero and continuous along that branch and under the rounded approximations below.*
3. *Rounding the conical vertices while retaining the same material values gives a nearby resonance and normalized eigenfield converging locally in L^2, with uniformly bounded one-sided fields on fixed smooth-interface collars away from the vertices.*

Then, for every finite N and every $M, \ell > 0$, one normalized resonance of a finite smooth dielectric has N disjoint three-dimensional peak balls of diameter less than ℓ, each with one-sided maximum larger than M and a collar maximum smaller than half its peak. Their centers may be placed on a line in a prescribed open plane patch, and their projections may be contained in that patch, provided that the chosen nonzero axial interval is positioned to meet the patch. If the symmetry axis lies in that plane and the rounding remains axisymmetric, a maximizing point in each ball can itself be selected in the plane patch. The surrounding resonator need not project into the patch. A maximum off the symmetry axis may belong to a rotational ring inside its small ball; no nondegeneracy or uniqueness of a maximum is asserted.

Proof. Choose N distinct axial centers in a sufficiently short nonzero subinterval and choose disjoint balls and insertions as small as necessary. Axisymmetric insertions preserve the indicated sector. Choose one small positive contrast from Corollary 4.3. Its one normalized sharp resonance is unbounded at every tip. The uniform collar hypothesis gives one bound for all sufficiently late rounded modes on the chosen collars. In each ball, essential unboundedness gives a positive-volume superlevel above twice that common collar bound and the target M, with strict margins. Local L^2 convergence preserves a positive-volume superlevel above these thresholds at every sufficiently small rounding scale. The eventual collar bound and finiteness of the collection let one choose a common scale. Smooth-interface regularity makes the one-sided maxima on the closed balls finite and attained; each peak lies inside its ball because of the collar inequality. This is the same final compactness step as the driven construction, but it is applied to a homogeneous resonance branch with its stated QNM normalization.

For the last placement assertion, an axisymmetric vector field obeys $E(\mathcal{R}x) = \mathcal{R}E(x)$ under rotations about its axis, and therefore $|E|$ is invariant. The same is true for its one-sided material traces. A ball centered on that axis is rotation invariant. Rotate any maximizing point into the specified plane through the axis; it stays in the same ball and retains its maximal value. The projection constraint puts this representative in the prescribed patch. □

This proposition is a proved implication with explicit global hypotheses. Lemmas 5.3, 5.2, 5.4, and 5.5 supply those hypotheses for the finite-device construction in Theorem 5.6. Theorem 4.2 and Corollary 4.3 establish its local excitation bridge. No resonance is inferred from a driven field, and no radiating mode is normalized by a divergent all-space positive energy integral. A real dilation fixes the real part of the nonzero resonance frequency; its negative imaginary part remains part of the QNM statement.

5 Spectral construction and normalization of the modal branch

This section supplies the global hypotheses used by Proposition 4.4. Frequencies in this section are complex vacuum wavenumbers. An outgoing resonance means the analytic continuation of the vacuum outgoing Green function from $\operatorname{Im} k > 0$; no decay at real spatial infinity is imposed when $\operatorname{Im} k < 0$. The material is still real, positive, scalar, nondispersive, and equal to vacuum outside a bounded set. The normalization below is a reciprocal Green-function residue norm. It is not a positive all-space energy integral.

The construction starts with a dielectric sphere whose selected electric resonance has a nonzero axial field. A sequence of radial dipole resonances provides arbitrarily high quality factor. Small conical insertions preserve one simple resonance in a specified symmetry sector; the preceding section shows that the continued field excites all their tips. Rounding then yields a smooth finite device with large, localized peaks in that same mode. Finally, a spatial dilation restores the exact target real frequency without changing the quality factor.

There are two distinct reasons for the spectral machinery. The pole must survive changes of the material and remain a genuine outgoing Maxwell solution; separately, the amplitude of its eigenfield must be fixed by a nonzero normalization that also survives those changes. The following subsections establish those properties before combining them in Theorem 5.6.

5.1 A compact analytic pencil and continuity under rounding

An eigenfield can be multiplied by any nonzero constant, so convergence of modes requires a choice of scale. The operator pencil below first locates resonances as values of k at which the source-free volume equation has a nonzero solution. Splitting off the static part leaves a compact analytic problem. This form also controls changes in the material that converge almost everywhere, as happens when tips are rounded; pointwise material convergence alone would not generally give operator-norm convergence of the original multiplication operator.

Let B be a ball containing all material changes, let $X = L^2(B;\mathbb{C}^3)$, and extend its elements by zero when applying whole-space operators. Write $\chi = \varepsilon_r - 1$. With $\Phi_k(x) = e^{ik|x|}/(4\pi|x|)$, put

$$K(k)f = (k^2 I + \nabla\nabla)\Phi_k * f\big|_B, \qquad L_\chi(k) = I - K(k)\chi. \tag{63}$$

Multiplication by χ is included in the last expression. The static longitudinal Fourier projection, compressed to B, is denoted by P. It satisfies $P = P^*$ and $0 \le P \le I$. The distributional identity

$$K(k) = -P + R(k), \qquad R(k) = k^2\Phi_k I + \nabla\nabla(\Phi_k - \Phi_0), \qquad R(0) = 0 \tag{64}$$

holds as an identity of bounded operators on X.

Lemma 5.1 (Analytic Fredholm reduction with a fixed material bound)**.** *For every measurable $0 \le \chi \le C$ supported in B,*

$$L_\chi(k) = A_\chi F_\chi(k), \quad A_\chi = I + P\chi, \quad F_\chi(k) = I - A_\chi^{-1} R(k)\chi \tag{65}$$

has A_χ invertible with $\|A_\chi^{-1}\| \le 1 + C$. The operator $R(k)$ is an entire Hilbert–Schmidt family, and F_χ is an analytic identity-minus-compact pencil with $F_\chi(0) = I$. Its noninvertible values are isolated, of finite algebraic multiplicity. At $k \neq 0$, its kernel is exactly the restriction to B of the finite local-energy Maxwell resonances for this material, with exterior field given by (63).

If $0 \le \chi_j \le C$ and $\chi_j \to \chi$ almost everywhere in this same ball, then $F_{\chi_j}(k) \to F_\chi(k)$ in operator norm, locally uniformly in k, as do all k derivatives.

Proof. The Fourier symbol of $\nabla\nabla\Phi_0$ is $-\xi\xi^T/|\xi|^2$, including its distributional local term. Taylor expansion of e^{ikr} shows that each entry of the remaining kernel in (64) is $O(1/r)$ as $r \downarrow 0$, uniformly for k in compact subsets of $\mathbb{C}$. The constant term $ik/(4\pi)$ in $\Phi_k - \Phi_0$ has zero Hessian. The squared kernel is locally integrable in three dimensions; on bounded $B \times B$ it is integrable. Its parameter power series and derivatives have the same local majorants on compact parameter sets. This proves the entire Hilbert–Schmidt assertion.

Put $s = \sqrt{\chi}$. The positive selfadjoint operator $I + sPs$ has inverse of norm at most one, and direct multiplication gives

$$A_\chi^{-1} = I - Ps(I + sPs)^{-1}s. \tag{66}$$

This proves the stated bound and factorization. Analytic Fredholm theory applies, with the invertible value at zero fixing its nontrivial alternative. This application needs no small contrast, smooth boundary, or uniform feature size.

For completeness, the volume representation is an exact Maxwell equation. In distributions, $(\operatorname{curl}\operatorname{curl} - k^2)K(k)f = k^2 f$. Consequently a kernel vector extended by $E = K(k)(\chi E)$ satisfies $\operatorname{curl}\operatorname{curl} E = k^2(1+\chi)E$. Its curl is locally square integrable, by the first-derivative Newton-potential estimate; equivalently this follows from local cutoff testing. Set $H = (ik)^{-1}\operatorname{curl} E$ in units with vacuum impedance one. This gives the two first-order Maxwell equations and the outgoing continued representation. Conversely, subtracting this volume field from any such resonance leaves an entire vacuum Maxwell field regular at the origin and outgoing outside a ball. In each vector spherical harmonic its regular radial function and outgoing radial function have nonzero Wronskian for $k \neq 0$, so all coefficients vanish. Thus the restriction is a kernel vector. A zero restriction gives the zero global field.

Almost-everywhere convergence and the common bound give strong convergence of the multiplication operators. The resolvent identity and (66) give strong convergence of $A_{\chi_j}^{-1}$ with a uniform bound. Dominated convergence of the integral kernels gives $R(k)\chi_j \to R(k)\chi$ in Hilbert–Schmidt norm. A uniformly bounded strongly convergent operator sequence converges in norm after composition on the right with a fixed compact operator: approximate that compact operator by finite-rank operators. Apply this observation to $A_{\chi_j}^{-1}R(k)\chi$ and add the Hilbert–Schmidt difference. Compactness in the parameter k makes the convergence locally uniform; Cauchy's formula gives the same claim for derivatives. □

All these arguments also hold on a fixed closed symmetry sector preserved by P, $R(k)$, and the material multiplication. We use the axisymmetric electric sector: E has only meridional components and H only the azimuthal component in cylindrical coordinates. Rotationally invariant scalar material preserves this sector. It is closed in L^2 and orthogonal to the axisymmetric magnetic sector, both for the Hermitian pairing and for the unconjugated bilinear pairing. At the coordinate axis these statements are understood in the distributional and almost-everywhere sense.

Lemma 5.2 (Persistence of a simple resonance)**.** *Suppose the restriction of F_χ to such a fixed sector has an isolated characteristic value k_* of algebraic multiplicity one. An analytic L^∞ material perturbation has a locally holomorphic continued wavenumber k_η and nonzero eigenfield $E_\eta \in X$.*

Their values at zero are k_* and a prescribed nonzero eigenfield. If instead bounded nonnegative materials χ_j converge almost everywhere to χ, and preserve this sector, they have unique nearby simple characteristic values $k_j \to k_*$ and eigenfields $E_j \to E$ in X, after one fixed nonzero linear functional fixes their scale.

Proof. Choose closed complements of the one-dimensional kernel and cokernel of $F_\chi(k_*)$. The block between those complements is invertible, and remains so in a small operator-norm neighborhood. Block elimination reduces the kernel equation to a single scalar analytic function $f(k)$, multiplied by invertible analytic block operators. Algebraic multiplicity one is exactly $f(k_*) = 0$, $f'(k_*) \neq 0$. For an analytic material perturbation, A_χ^{-1} continues analytically by a Neumann series near the base material, so every block is jointly analytic. The scalar analytic implicit-function theorem supplies k_η; back substitution supplies E_η. For almost-everywhere material convergence, Lemma 5.1 gives uniform convergence of the blocks and scalar functions on a small closed disk. Rouché's theorem gives exactly one zero, counting multiplicity. It tends to k_* and is simple. Back substitution and a linear functional nonzero on E give the stated field convergence. This reduction must use F for the almost-everywhere convergence claim: the leading multiplication in L need not converge in operator norm. Multiplication by A is analytic and invertible and does not alter a characteristic value's multiplicity or its right kernel. □

5.2 A simple sphere resonance without a genericity assumption

We use a sphere because its modes can be separated into angular and radial factors and its resonance condition can be written explicitly. The selected dipole-like mode has nonzero axial electric field near the center, providing places for the cone tips. Simplicity is required only within the invariant sector used for the construction; the familiar degeneracy among other azimuthal directions is not asserted to disappear.

Choose an algebraic real refractive index $1 < n < \sqrt{\varepsilon_+}$, leaving a positive margin for the subsequent insertions. Rational numbers already provide this choice for every $\varepsilon_+ > 1$. In a sphere of radius a and permittivity n^2, write $z = ka$ and $\psi_l(z) = z j_l(z)$, $\xi_l(z) = z h_l^{(1)}(z)$. Matching the tangential electric and magnetic fields of the regular interior electric multipole and the outgoing exterior multipole gives, for $l \geq 1$, the determinant

$$D_l(z) = n\psi_l(nz)\xi_l'(z) - \xi_l(z)\psi_l'(nz). \tag{67}$$

Primes mean derivatives with respect to the displayed argument. For example the interior tangential electric component is proportional to $\psi_l'(nz)/(nz)$, and its tangential magnetic component to $n\psi_l(nz)/(nz)$; their exterior analogues are $\xi_l'(z)/z$ and $\xi_l(z)/z$. Eliminating their two amplitudes gives (67).

Lemma 5.3 (Simplicity and separation of electric sphere poles)**.** *For algebraic $n > 1$, every nonzero zero of D_l is simple, and D_l and D_j have no common nonzero zero if $l \neq j$. In the axisymmetric electric sector each such zero is therefore a simple Maxwell characteristic value. There are $l = 1$ poles*

$$z_m = \frac{\pi(m + 1/2)}{n} - \frac{i}{2n} \log \frac{n+1}{n-1} + O(m^{-1}), \qquad m \longrightarrow \infty. \tag{68}$$

Their real parts are positive, imaginary parts negative, and $\operatorname{Re} z_m/(-2 \operatorname{Im} z_m) \to \infty$. The $l = 1, m_{\mathrm{az}} = 0$ interior electric field has a nonzero axial component at the center and on a sufficiently short axial interval.

Proof. The exact finite spherical-Hankel expansions[15] are

$$\xi_l(z) = (-i)^{l+1} e^{iz} p_l(z), \qquad zh_l^{(2)}(z) = i^{l+1} e^{-iz} \widetilde{p}_l(z), \tag{69}$$

$$p_l(z) = \sum_{s=0}^{l} \frac{i^s (l+s)!}{2^s s!(l-s)! z^s}, \qquad \widetilde{p}_l(z) = \sum_{s=0}^{l} \frac{(-i)^s (l+s)!}{2^s s!(l-s)! z^s}. \tag{70}$$

Using $\psi_l = (\xi_l + zh_l^{(2)})/2$, the determinant, up to a nonzero factor independent of its zero condition, is

$$C_{l,+}(z) e^{inz} + C_{l,-}(z) e^{-inz}, \tag{71}$$

where, with $p = p_l$, $\widetilde{p} = \widetilde{p}_l$,

$$C_{l,+} = (-i)^{l+1} \{ i(n-1) p(z) p(nz) + np(nz) p'(z) - p(z) p'(nz) \}, \tag{72}$$

$$C_{l,-} = i^{l+1} \{ i(n+1) p(z) \widetilde{p}(nz) + n\widetilde{p}(nz) p'(z) - p(z) \widetilde{p}'(nz) \}. \tag{73}$$

These are rational functions with algebraic coefficients. They cannot vanish together at $z \neq 0$: the two corresponding equations would annihilate both independent interior Riccati–Hankel solutions. Their nonzero Wronskian would then force both $\xi_l(z)$ and $\xi_l'(z)$ to vanish, contradicting uniqueness for their second-order radial equation. Thus at any zero of D_l both coefficients are nonzero and the equation is equivalently

$$e^{2inz} = R_l(z) := -C_{l,-}(z)/C_{l,+}(z). \tag{74}$$

The expansion $p_l(z) = 1 + il(l+1)/(2z) + O(z^{-2})$ gives

$$R_l(z) = (-1)^l \frac{n+1}{n-1} \left(1 - \frac{il(l+1)}{nz} + O(z^{-2}) \right). \tag{75}$$

For different parity the leading constants differ; for the same parity and distinct l the coefficients of $1/z$ differ. Hence $R_l - R_j$ is never identically zero when $l \neq j$.

The Lindemann–Weierstrass theorem implies that e^α is transcendental for every nonzero algebraic complex α[1]. If D_l and D_j had a common nonzero zero z, the nontrivial rational equation $R_l(z) = R_j(z)$ would make z algebraic. Equation (74) would make e^{2inz} algebraic, a contradiction. If D_l had a multiple nonzero zero, differentiation of (74) would give $R_l'(z) = 2inR_l(z)$. This too is a nontrivial rational equation: $R_l'/R_l \to 0$ at infinity, whereas $2in \neq 0$. It again makes z algebraic and yields the same contradiction. No division by a zero coefficient was used at a pole.

Separation of variables decomposes the axisymmetric electric sector into the degrees $l = 1, 2, \ldots$, with one azimuthal mode at each degree. Regularity at the origin and the outgoing condition leave one radial amplitude on each side of the sphere. Locally in $k \neq 0$, solving the inhomogeneous radial equations and matching them reduces each block, by analytic invertible elimination, to its two-by-two tangential matching matrix. Its determinant is (67) times a nonzero analytic factor. Thus a simple zero is a one-dimensional simple characteristic value of that block. Lemma 5.1 excludes accumulation at a finite nonzero k; the other angular blocks are invertible near the selected zero. The proved separation across l gives algebraic multiplicity one in the whole selected sector. The familiar degeneracy across the other azimuthal indices in the full sphere is irrelevant to this invariant-sector statement.

For $l = 1$ let $r_\infty = -(n+1)/(n-1)$ and choose the centers z_m^0 equal to the two leading terms in (68). They obey $e^{2inz_m^0} = r_\infty$. On the circle $|z - z_m^0| = C/m$, the modulus of $e^{2inz} - r_\infty$ is at least cC/m for large m, with $c > 0$ independent of m. The rational correction $R_1(z) - r_\infty$ is at most C_0/m there. Taking C large enough, Rouché's theorem gives exactly one zero in this disk.

This proves (68). Finally $\psi_1(u) = u^2/3 + O(u^4)$. The regular electric dipole vector spherical wave therefore tends to a nonzero constant axial vector at the center, for a nonzero radial amplitude. The amplitude cannot vanish without making the whole matched eigenfield zero. Analyticity in the homogeneous core preserves the nonzero component on a short axial interval. □

5.3 Reciprocal normalization of the resonant mode

An outgoing mode at a complex resonance frequency grows at real spatial infinity, so its ordinary positive all-space energy is not a finite normalization. Instead, we use the coefficient of the Green operator's pole. A simple pole has a nonzero derivative pairing, and this pairing sets the scale of the mode. The definition below is bilinear and may be complex; setting it to one is a choice of mode amplitude, not a claim that it equals positive stored energy.

The bilinear pairing in the remainder of this section has no complex conjugation. Reciprocity gives $K(k)^T = K(k)$ on X. For a simple characteristic value in the selected sector, define

$$d(E, k, \chi) = -\int_B \chi E \cdot K'(k)(\chi E)\, dx, \qquad \mathcal{N}(E) = -\frac{k}{2} d(E, k, \chi). \tag{76}$$

The derivative kernel is a bounded compact operator; these are finite integrals of locally square-integrable fields. Their values are independent of which containing ball is used.

Lemma 5.4 (Nonzero residue norm and its stability)**.** *At a simple nonzero Maxwell pole in the selected sector, $\mathcal{N}(E) \neq 0$. Scaling E by $a \in \mathbb{C}$ scales $\mathcal{N}$ by a^2. The reciprocal electric Green operator for* $\operatorname{curl}\operatorname{curl} - k^2\varepsilon_r$*, with both the source and output restricted to this sector, has residue*

$$\operatorname*{Res}_{k=k_*} G(k; x, y) = -\frac{E(x) \otimes E(y)}{2k_* \mathcal{N}(E)}. \tag{77}$$

The norm is continuous along the almost-everywhere material and eigenfield convergence of Lemma 5.2, and holomorphic along its analytic branches. A local nonzero analytic choice of scale makes $\mathcal{N} = 1$.

Proof. The functional $\ell_E(v) = \int_B \chi E \cdot v$ is nonzero: if $\chi E = 0$, the volume equation makes $E = 0$. It lies in the left kernel of $L_\chi(k_*)$, since $\ell_E L_\chi = \langle \chi E, \cdot \rangle - \langle K(k_*)\chi E, \chi \cdot \rangle = 0$. It is a nonzero functional also on the chosen sector, because that sector is closed under complex conjugation and multiplication by the real rotationally invariant χ. Its derivative pairing $\ell_E L'_\chi(k_*)E$ is exactly d. The scalar Schur reduction in Lemma 5.2 shows that this pairing is nonzero at a simple characteristic value; otherwise the scalar zero would have multiplicity at least two. The residue of L_χ^{-1} is therefore $E \otimes \ell_E/d$.

The vacuum electric resolvent is $G_0(k) = k^{-2}K(k)$, with its natural restriction when the source is supported in B. The full electric field for a compact source is $L_\chi(k)^{-1}G_0(k)f$ in B. At the pole, reciprocity and $K(k_*)\chi E = E$ give

$$\ell_E G_0(k_*) f = k_*^{-2} \int E(y) \cdot f(y)\, dy. \tag{78}$$

For an arbitrary compact source, first project it onto the selected sector. The same identity for sources outside B follows from the global volume representation and the symmetric kernel. Since E lies in the sector, the projection can be removed from its bilinear pairing with E; the Maxwell source itself remains the projected source. Multiplying the two residue factors yields $E \otimes E/(k_*^2 d)$, which is (77). This is a genuine pole normalization of a quasinormal mode, consistent with reciprocal Green-residue normalizations[13]; the sign reflects the displayed choice of Maxwell operator. For a

degenerate full-space pole the formula describes the selected symmetry block, not a claim that the entire Green residue has rank one.

Under rounding, $\chi_j E_j \to \chi E$ in L^2: split the difference into the uniformly bounded multiplier times $E_j - E$ and dominated convergence applied to $(\chi_j - \chi)E$. Operator-norm continuity of $K'(k)$ proves convergence of d and $\mathcal{N}$. Holomorphy and quadratic scaling follow from the formulas. A nonzero analytic square root of $\mathcal{N}$ on a sufficiently small parameter disk normalizes the field. □

Lemma 5.5 (Normalized resonance convergence and fixed-collar bounds)**.** *Fix the finite axisymmetric conical construction and a simple sector pole with $\mathcal{N} = 1$. Round all its vertices axisymmetrically within balls of radius ρ, leaving the material values and all other interfaces fixed. For sufficiently small ρ, there is a simple sector pole $k_\rho \to k_*$ and eigenfield with $\mathcal{N}(E_\rho) = 1$ converging to E locally in L^2. On the fixed collars around the selected tips, contained in their conical neighborhoods and separated from the vertices, the one-sided fields have a common finite bound independent of the sufficiently small rounding radius.*

Proof. The rounded coefficients converge almost everywhere with fixed support and the same positive material bound. Apply Lemmas 5.1–5.4 and choose the square-root scale converging to the sharp field's scale. The volume representation supplies local L^2 convergence also on any larger fixed ball, by the same static and compact estimates. For the collar estimate, the convergent normalized volume unknowns give uniformly bounded compact L^2 sources and frequencies. The scalar Green representation writes the actual electric field as $E_\rho = \nabla v_\rho + W_\rho$, with $W_\rho = k_\rho^2 \Phi_{k_\rho} * (\chi_\rho E_\rho)$. On a fixed containing ball the scalar Green operator, its gradient, and the dynamic-minus-static Hessian have uniform operator bounds. The static Hessian is controlled by the Fourier Newton projection. After multiplication by a fixed smooth cutoff, W_ρ therefore has uniformly bounded first and second weak derivatives. The localized scalar potential and its first gradient are uniformly bounded in L^2 as well.

Choose a smooth reference rounding before the final family index. Every sufficiently late rounded body agrees exactly with it on the fixed collars. Cover those collars by finitely many fixed signed C^4 graph charts, including constant-material charts at points away from the interfaces. The scalar Gauss equation becomes a positive binary transmission equation in each flattened chart. A regional difference-quotient estimate supplies the mixed scalar derivative needed in the outer-cutoff forcing. Product rules then bound both tangential derivatives of that forcing from the original data and fixed cutoff constants. Thus the subsequent localized iterations do not assume extra scalar regularity on the outer cutoff annulus.

Two tangential iterations bound the tangential gradient components. The divergence equation gives the corresponding bounds for the normal flux. The local Sobolev estimates for these derivative arrays yield continuous bounded representatives. On the inner cutoff plateau they are the original tangential gradient and physical flux; the positive material values reconstruct the actual one-sided electric components. Taking a finite cover gives a single collar bound chosen before the rounding index and the peak threshold. □

5.4 Modal hotspot theorem

The theorem assembles the local excitation and global continuation steps. All peaks belong to the same mode; the construction does not require a separate mode for each observation region. The target frequency is the real part of the complex resonance frequency, and the norm is the reciprocal residue normalization defined above. The theorem allows the support and fine feature scales to vary with the requested number and strength of peaks.

Theorem 5.6 (Arbitrarily many peaks in one normalized finite-device mode)**.** *Fix $\varepsilon_+ > 1$, a real target wavenumber $k_0 > 0$, a nonempty open patch $\mathcal{P}$ of a plane, a positive integer N, and numbers $\ell, M, Q_0 > 0$. There is a finite smooth piecewise-constant dielectric with vacuum exterior and $1 \le \varepsilon_r \le \varepsilon_+$, and one nonzero outgoing Maxwell quasinormal mode (E, H, k_*), such that*

$$\operatorname{Re} k_* = k_0, \qquad \operatorname{Im} k_* < 0, \qquad \frac{\operatorname{Re} k_*}{-2 \operatorname{Im} k_*} > Q_0, \qquad \mathcal{N}(E) = 1. \tag{79}$$

There are N disjoint three-dimensional observation balls of diameter less than ℓ, centered in $\mathcal{P}$ and with orthogonal projections contained in $\mathcal{P}$. In each ball the one-sided electric-field maximum exceeds M and is more than twice a uniform bound for both material-side fields on an open collar of its boundary. A point attaining each maximum can be chosen in $\mathcal{P}$. Thus each peak's half-amplitude connected region stays in its small ball. No uniform support-size bound, minimum feature size, nondegeneracy of the maximum, or positive energy fraction per peak is asserted. The insertion contrast may depend on N; the common material bounds do not.

Proof. Take an algebraic index n strictly between one and $\sqrt{\varepsilon_+}$. Lemma 5.3 gives a simple axisymmetric electric dipole pole with quality factor strictly greater than Q_0. Scale the sphere initially to make the real part of its wavenumber k_0. Put its symmetry axis in the target plane and its center in the open patch. Choose N distinct points on a sufficiently short axial interval where the background axial component is nonzero, with ample clearance from the patch boundary. Choose disjoint arbitrarily small conical neighborhoods and close their material insertions smoothly away from their vertices, inside the homogeneous sphere.

Axisymmetry preserves the electric sector. Lemma 5.2 gives one holomorphic pole and eigenfield under simultaneous positive cone contrast η. Theorem 4.2 and Corollary 4.3 give nonzero singular coefficients at all N vertices for one sufficiently small $\eta > 0$. Choose it also so that $n^2(1+\eta) < \varepsilon_+$, the pole remains simple, its imaginary part remains negative, and its quality factor remains strictly above Q_0. Lemma 5.4 fixes its genuine norm to one. Lemma 5.5 supplies every rounding and normalization hypothesis of Proposition 4.4. Its high-point and collar argument now proves all the simultaneous strict peak inequalities for sufficiently small rounding radius. The same axisymmetric rotation argument puts an actual maximizing point of each ball in the specified plane.

There is one final harmless adjustment because the real pole frequency has shifted. About a point in the interior of the patch, dilate space by $s = \operatorname{Re} k_*/k_0 > 0$. Maxwell scaling sends the wavenumber to k_*/s, keeps the quality factor and material values unchanged, and tends to the identity as the insertion contrast tends to zero. A normalized field scales as $E_s(x) = s^{-3/2} E(x/s)$: indeed (76) and the scaled kernel give $\mathcal{N}(E(x/s)) = s^3 \mathcal{N}(E)$. Choose all observation-ball diameters with strict margins below ℓ, their projections with strict interior clearance, and their pre-scaling peak targets larger than $s^{3/2} M$ for every s in a fixed small neighborhood of one. These choices can be made before the final rounding. The dilation therefore preserves every desired inequality and sets the exact real frequency. □

Corollary 5.7 (Vanishing residue-normalized localization ratios)**.** *For one fixed sharp modal construction with N tips, its rounded normalized modes, with the frequency-adjusting dilations and corresponding observation balls, have reciprocal norm one, and the maximum in each selected ball tends to infinity. Consequently*

$$\frac{|\mathcal{N}(E_\rho)|}{\max\limits_{x \text{ in ball } j} \varepsilon_\rho(x) |E_\rho(x)|^2} \longrightarrow 0 \quad (1 \le j \le N). \tag{80}$$

These are positive intensity ratios formed from the genuine reciprocal norm. The displayed maximum is over both continuous material-side traces on the closed observation ball; at an interface, each trace

is weighted by the permittivity of that same side. The same representatives are defined continuously on the phase closures in a strictly larger ball and agree almost everywhere there with the actual field. Thus their values on the observation ball are intrinsic, including at tangential contact between its sphere and an interface. A directional complex mode volume uses $\mathcal{N}/[\varepsilon(u \cdot E)^2]$ instead; selecting a Cartesian component of size at least $|E|/\sqrt{3}$ gives the same vanishing magnitude along a subsequence with a fixed component. No divergent all-space positive energy is substituted for $\mathcal{N}$.

Proof. For every finite amplitude threshold, essential unboundedness of the fixed sharp eigenfield gives a positive-volume superlevel in each selected ball. Local L^2 convergence preserves a positive-volume superlevel above any smaller threshold for every sufficiently late rounded field. Its attained one-sided maximum is at least that threshold. This proves divergence of every maximum along the fixed rounded family. For the maximum selection, first construct the two continuous phase representatives on a larger closed ball and then restrict these same functions to the smaller observation ball. Two such representatives agree on the open phase by continuity and almost-everywhere equality; taking phase limits proves equality on its closure in the smaller ball. This argument also handles tangencies, where continuity and almost-everywhere equality on the smaller ball alone would not suffice. The normalized numerator is one, and the positive permittivities have a common lower bound. There are only three Cartesian components, so the indicated subsequence exists for a directional volume. The finite-frequency dilation has a finite nonzero limit and leaves the vanishing-ratio conclusion unchanged. □

6 Channel bounds: complete operators and a resource-dependent Maxwell theorem

An efficient channel is an input pattern whose selected output retains a specified fraction of its incident power. The question here is more restrictive: every coherent combination of the counted inputs must also carry positive power through the *same* section, while the absolute flux outside it stays small. Counting individual basis fields is not enough, because interference changes their flux. Nor does a count of modes of an empty aperture automatically control the fields inside an arbitrary device.

The route in this section makes explicit the missing physical resource. A bound on the field in a box around the section limits how many independent inputs can each produce a prescribed through-flux. The argument first replaces the sharp section by a smooth window, then controls that window's flux by the local magnetic field. Maxwell's equations provide a derivative bound on that field, allowing a finite-dimensional approximation in the box. The resulting count depends on the local field resource; a resonator can make that resource large even when its incident power is fixed. Thus the estimate is useful when the resource is separately controlled, but it is not an area-only bound for the unrestricted class.

The unrestricted fixed-section assertion is disproved later in Theorem 19.1 for $\delta > \eta$. The stronger small-bypass regime of the resource bounds below remains a separate question. This section proves three usable conclusions: an exact finite-rank reduction, a local full-vector field-resource estimate, and a bridge from the prescribed absolute-bypass condition to that estimate. The local estimates reproduce the argument in the supplied report and make its assumptions explicit [20, Section 3]. The outer-window construction below avoids that report's extra conserved-collar assumption for a sharp section. None of these results bounds resonant amplification by external passivity.

6.1 What the cited channel bounds actually control

Miller's Supplement S2 explicitly treats the maximum-index substitution as a conjecture; S12 distinguishes homogeneous-background SVD estimates from a design-specific calculation of the complete Green function. These are useful diagnostics, without a uniform theorem for every structured interior [11, Supplements S2 and S12].

Kuang, Miller, and Miller first identify the physically normalized map as $R_R^{1/2} T_R G T_S R_S^{-1/2}$. Their Eq. (1) retains the product of the two endpoint operator norms when bounding its singular values by those of G. Their explicit domain bounds concern the background Green operator, with source/receiver size and separation data and spherical separation; their relative-channel thresholds use a sum-rule normalization. Appendix E rejects the older largest-singular-value normalization as a general monotonic bound [9, Section II and Appendix E]. In particular, neither the endpoint norms nor these geometric data are determined by the area of the internal section. A continuum use additionally needs bounded endpoint maps: invertibility of a finite resistance matrix does not prove a uniformly bounded inverse in an infinite-dimensional current space.

6.2 Exact operator reduction

We begin with a simple observation about the complete input-to-output map. Suppose it can be approximated, uniformly on the candidate input space, by a map with only M output directions. If there were more than M independent efficient inputs, some nonzero combination would disappear under the approximating map. The approximation error would then have to carry its entire output, contradicting the efficiency threshold. The following lemma states this argument without assuming that the full map is compact.

Throughout, norms in the incident and delivered channel spaces are physical power norms. Let $T : \mathcal{H}_{\mathrm{in}} \to \mathcal{H}_{\mathrm{out}}$ be a bounded operator, and fix $0 < \tau < 1$. A counted linear subspace W satisfies

$$\|Ta\|^2 \geq \tau \|a\|^2 \qquad (a \in W). \tag{81}$$

The other passage requirements are imposed separately below.

Lemma 6.1 (Finite-rank obstruction)**.** *If a linear map $R : W \to \mathcal{H}_{\mathrm{out}}$ has rank at most M and $\|T|_W - R\| < \sqrt{\tau}$, then $\dim W \leq M$.*

Proof. If $\dim W > M$, choose $M+1$ linearly independent vectors in W. The restriction of R to their span has a nonzero kernel vector a. Then $\|Ta\| = \|(T-R)a\| < \sqrt{\tau}\|a\|$, contradicting (81). This proof also covers an infinite-dimensional W. The strict inequality is indispensable: on $\mathbb{C}^{M+1}$, $T = \sqrt{\tau} I$ and $R = 0$ attain equality in the norm estimate. □

Definition 6.2 (Approximation number)**.** For a bounded operator U between Hilbert spaces, define

$$a_{M+1}(U) = \inf_{\operatorname{rank} R \leq M} \|U - R\|. \tag{82}$$

No compactness is required for this definition. Thus $a_{M+1}(T|_W) < \sqrt{\tau}$ is sufficient in Lemma 6.1.

Proposition 6.3 (Factorization with every amplification factor retained)**.** *Suppose $T = AGB + E$, where all maps are bounded between their stated Hilbert spaces and $\|E\| \leq e$. If $\operatorname{rank} G_M \leq M$, then*

$$\operatorname{rank}(AG_MB) \leq M, \qquad \|T - AG_MB\| \leq \|A\|\,\|B\|\,\|G - G_M\| + e. \tag{83}$$

Consequently $\dim W \leq M$ if the right side is less than $\sqrt{\tau}$. If G is compact, one may replace $\|G - G_M\|$ by its $(M+1)$st singular value using the truncated singular-value expansion.

Proof. The image of AG_MB is contained in the image under A of the at-most-M-dimensional image of G_M. Submultiplicativity and the triangle inequality prove (83). Apply Lemma 6.1. For compact G, its singular expansion is an orthogonal expansion and the norm of its discarded tail is exactly its next singular value. □

Remark 6.4 (Algebraic examples; no Maxwell realization)**.** For $G_N = \operatorname{diag}(1, 2^{-1}, \dots, N^{-1})$ and $A_N = \operatorname{diag}(1, 2, \dots, N)$, the full map $A_N G_N = I_N$ is passive and has N unit transmission singular values. Passivity controls the product, not $\|A_N\| = N$. Likewise, the finite-rank orthogonal projections onto the first N coordinates of ℓ^2 are individually compact contractions, although their counts above any fixed threshold below one grow without bound. Finally, compressing $\operatorname{diag}(100, 1, 1)$ to the last two coordinates decreases every singular value, but increases the ratio of the second to the first from $1/100$ to 1. These exact examples identify invalid operator inferences. They supply no dielectric realization and no section or bypass certificate.

6.3 Local Maxwell hypotheses and a legitimate weighted flux

To apply a finite-dimensional argument to passage through a section, we need a measurement that is defined for the actual fields and can be estimated by volume norms. The smooth weight ψ below measures flux through a window on the section plane; it is a mathematical aid, not a change in the physical square. A cutoff in the longitudinal direction turns this weighted plane measurement into a volume integral. The term involving the transverse gradient of ψ records power crossing the side of that window, so conservation does not require us to assume that this lateral flux vanishes.

Let $B \subset \mathbb{R}^3$ be an open rectangular box with side lengths L_1, L_2, L_3 and volume V_B. The physical dielectric extends beyond B; no physical boundary condition is imposed on its faces. A fixed well-posed scattering problem supplies fields depending linearly on the input a. Write

$$e_a = \sqrt{\varepsilon_0} E_a, \qquad h_a = \sqrt{\mu_0} H_a, \qquad c_0 = (\varepsilon_0 \mu_0)^{-1/2}, \qquad k_0 = \omega / c_0. \tag{84}$$

Assume on B, in distributions,

$$\nabla \times e_a = i k_0 h_a, \qquad \nabla \times h_a = -i k_0 \varepsilon_r e_a, \qquad 0 < \varepsilon_- \le \varepsilon_r(x) \le \varepsilon_+ < \infty. \tag{85}$$

The real scalar coefficient may be merely measurable. Define the local weighted field resource

$$\mathcal{E}_B(a) = \int_B (\varepsilon_r |e_a|^2 + |h_a|^2)\, dx. \tag{86}$$

Each field has finite resource. A uniform bound relative to incident power will be an *additional* assumption. For nondispersive material this integral is four times the time-averaged local electromagnetic energy. In dispersive material a physical stored-energy formula requires frequency derivatives of the constitutive law, absent from these hypotheses.

Choose a real $\psi \in W^{1,\infty}_c(\mathbb{R}^2)$ with $0 \le \psi \le 1$, and $\ell > 0$, so that B contains a neighborhood of $\operatorname{supp}\psi \times [0, \ell]$, including a negative-$z$ collar. Let $\chi \in W^{1,\infty}(0, \ell)$ be real, with $\chi(0) = 1$, $\chi(\ell) = 0$. Set

$$g(x, y, z) = \begin{cases} (\chi(z) \nabla_\perp \psi(x, y), \chi'(z) \psi(x, y)), & 0 < z < \ell, \\ 0, & \text{otherwise}, \end{cases} \qquad G = \|g\|_\infty. \tag{87}$$

Select real cutoffs $0 \le \zeta, \rho \le 1$ in $W^{1,\infty}_c(B)$, with $\zeta = 1$ on $\operatorname{supp} g$ and $\rho = 1$ on $\operatorname{supp}\zeta$. Introduce explicit constants

$$\begin{aligned} d_1 &= \|\nabla \rho\|_\infty, \qquad d_2 = \|\nabla \zeta\|_\infty, \\ C_H &= k_0^2 \varepsilon_+ + d_1^2, \qquad C_E = \left(2 + \frac{4 d_2^2}{k_0^2 \varepsilon_-}\right)^{1/2}, \qquad K = \frac{c_0 G C_E}{2\sqrt{\varepsilon_-}}. \end{aligned} \tag{88}$$

Lemma 6.5 (Canonical weak flux)**.** *Define the Hermitian cross-Poynting vector*

$$p(a,b) = \frac{c_0}{4}\left(e_a \times \overline{h_b} + \overline{e_b} \times h_a\right). \tag{89}$$

For almost every z near $[0,\ell]$, put $F_{ab}(z) = \int_{\mathbb{R}^2} \psi p_z(a,b)\,dx\,dy$. This is a $W^{1,1}$ function of z, with its unique continuous representative satisfying

$$F'_{ab}(z) = \int_{\mathbb{R}^2} \nabla_\perp \psi \cdot p_\perp(a,b)\,dx\,dy, \qquad q_\psi(a,b) := F_{ab}(0) = -\int_B g \cdot p(a,b)\,dx. \tag{90}$$

The diagonal $p(a,a)$ is the physical real time-averaged Poynting vector.

Proof. Both fields are locally in $H(\mathrm{curl})$ by (85); their cross products belong to L^1. For such fields the identity $\operatorname{div}(u \times v) = v \cdot \operatorname{curl} u - u \cdot \operatorname{curl} v$ holds in distributions. To justify it, mollify both fields in a relatively compact neighborhood of the test function; the fields and their curls converge in L^2, and every product converges in L^1. For the first cross product in (89) its divergence is $ik_0(h_a \cdot \overline{h_b} - \varepsilon_r e_a \cdot \overline{e_b})$. The second has the opposite divergence, since ε_r is real. Thus $\operatorname{div} p(a,b) = 0$. Testing this with $\psi(x,y)\theta(z)$ and using Fubini proves the derivative formula in (90). Both terms are integrable in z, establishing $W^{1,1}$ membership. Finally integrate $(\chi F_{ab})'$ between zero and ℓ and use the endpoint values of χ. This gives the volume formula, including its transverse-gradient contribution. □

The transverse-gradient contribution accounts for lateral collar flux. Dropping it would assert an unproved conservation law for the individual aperture. This construction requires no L^2 tangential trace of a rough Maxwell field.

6.4 Magnetic compactness and its quantitative cost

The counting step uses the magnetic field because its curl and divergence give a local first-derivative estimate even when the dielectric coefficient is only measurable. The cutoff ρ localizes the field inside the box. We first bound its gradient by the local field resource, then show that its L^2 norm controls the weighted flux. Together, these estimates prevent an input with substantial passage and bounded resource from living entirely in arbitrarily fine box eigenfunctions.

Lemma 6.6 (Uniform magnetic regularity)**.** *The zero extension of ρh_a is in $H_0^1(B)^3$, and*

$$\|\nabla(\rho h_a)\|_2^2 \le C_H \mathcal{E}_B(a). \tag{91}$$

Proof. Taking divergence of $\operatorname{curl} e_a = ik_0 h_a$ gives $\operatorname{div} h_a = 0$. The compactly supported zero extension $v = \rho h_a$ has curl and divergence in L^2. The Fourier identity $|\xi|^2|\widehat{v}|^2 = |\xi \times \widehat{v}|^2 + |\xi \cdot \widehat{v}|^2$ gives

$$\|\nabla v\|_2^2 = \|\operatorname{curl} v\|_2^2 + \|\operatorname{div} v\|_2^2. \tag{92}$$

It proves H^1 membership; compact support supplies zero boundary trace. Let $X^2 = \int_B \varepsilon_r |e_a|^2$ and $Y^2 = \int_B |h_a|^2$. Minkowski's inequality in the direct sum of the curl and divergence spaces, and $|u \times v|^2 + |u \cdot v|^2 = |u|^2|v|^2$ for real u, give

$$\|\nabla(\rho h_a)\|_2 \le k_0\sqrt{\varepsilon_+}X + d_1 Y \le \sqrt{C_H}\sqrt{X^2 + Y^2}. \tag{93}$$

No derivative of ε_r occurs. □

Lemma 6.7 (Caccioppoli and flux domination)**.** *The complete physical fields obey*

$$\int_{\operatorname{supp} g} \varepsilon_r |e_a|^2 \le C_E^2 \int_{\operatorname{supp} \zeta} |h_a|^2, \qquad |q_\psi(a,a)| \le K \|\rho h_a\|_2^2. \tag{94}$$

Proof. Eliminating e_a gives the distributional equation

$$\operatorname{curl}(\varepsilon_r^{-1} \operatorname{curl} h_a) = k_0^2 h_a. \tag{95}$$

Test with $\zeta^2 h_a$, permissible by compactly supported $H(\operatorname{curl})$ approximation. Write $A_0 = \int_B \zeta^2 \varepsilon_r^{-1} |\operatorname{curl} h_a|^2$ and $J_0 = \int_B \varepsilon_r^{-1} |\nabla\zeta \times h_a|^2$. Taking real parts and applying Young's inequality gives

$$A_0 \le k_0^2 \int_B \zeta^2 |h_a|^2 + 2\sqrt{A_0 J_0} \le k_0^2 \int_B \zeta^2 |h_a|^2 + \tfrac{1}{2} A_0 + 2J_0. \tag{96}$$

Use $\varepsilon_r^{-1} \le \varepsilon_-^{-1}$ and $\varepsilon_r |e_a|^2 = k_0^{-2} \varepsilon_r^{-1} |\operatorname{curl} h_a|^2$ to obtain the first estimate in (94). The volume representation and Cauchy–Schwarz then give

$$|q_\psi(a,a)| \le \frac{c_0 G}{2} \|e_a\|_{L^2(\operatorname{supp} g)} \|h_a\|_{L^2(\operatorname{supp} g)} \le \frac{c_0 G C_E}{2\sqrt{\varepsilon_-}} \|h_a\|^2_{L^2(\operatorname{supp} \zeta)} \le K \|\rho h_a\|_2^2. \tag{97}$$

This is a vector Maxwell estimate, including the actual reflected and evanescent fields, not a scalar reduction or a propagating-wave cutoff. □

The next theorem implements that idea. If the input space had more dimensions than the retained box eigenfunctions, a nonzero combination would have no component in any of those low-frequency directions. Its gradient bound would make its remaining magnetic field too small to carry the required flux. The count is therefore finite at fixed B_W, with an explicit cost when B_W increases.

Theorem 6.8 (Through-flux resource bound)**.** *Let W have finite dimension N, and suppose $q_\psi(a,a) \ge p\|a\|^2$ for every $a \in W$, where $p > 0$. Define*

$$B_W = \sup_{a \in W,\, \|a\|=1} \mathcal{E}_B(a), \qquad \Lambda = K C_H B_W / p. \tag{98}$$

Then, with $N_{D,B}(\Lambda)$ the scalar Dirichlet eigenvalue count of the comparison box,

$$N \le 3 N_{D,B}(\Lambda) \le \frac{V_B}{2\pi^2} \left(\frac{K C_H B_W}{p} \right)^{3/2}. \tag{99}$$

Here B_W is finite for a finite-dimensional W, but it is not uniformly bounded by the fixed physical class.

Proof. Let Π_Λ project onto vector Dirichlet eigenfunctions with scalar eigenvalue at most Λ. Its rank is $3N_{D,B}(\Lambda)$. If N exceeds that rank, there is a unit $a \in W$ with $\Pi_\Lambda(\rho h_a) = 0$. Writing $\lambda_{\mathrm{next}} > \Lambda$ for the next scalar eigenvalue, Parseval and (91) imply

$$\|\rho h_a\|_2^2 \le \frac{\|\nabla(\rho h_a)\|_2^2}{\lambda_{\mathrm{next}}} \le \frac{C_H B_W}{\lambda_{\mathrm{next}}}. \tag{100}$$

Equation (94) contradicts $q_\psi(a,a) \geq p$. The box eigenvalues are

$$\lambda_{\mathbf{n}} = \pi^2 \sum_{i=1}^{3} n_i^2/L_i^2, \qquad \mathbf{n} \in \{1,2,\dots\}^3. \tag{101}$$

For each point below the cutoff, the unit cell $\prod_i [n_i - 1, n_i]$ lies in the positive octant of $\sum_i x_i^2/L_i^2 \leq \Lambda/\pi^2$. These cells have disjoint interiors. Their total volume is at most the ellipsoid-octant volume, giving $N_{D,B}(\Lambda) \leq V_B \Lambda^{3/2}/(6\pi^2)$. Multiplication by three proves (99) without a Weyl asymptotic or a remainder depending on fine material interfaces. □

Theorem 6.9 (Cost averaged over an orthonormal input basis)**.** *Under the hypotheses of Theorem 6.8, let $a_1, \dots, a_N$ be any orthonormal basis of W, and set $\mathcal{E}_{\mathrm{sum}} = \sum_i \mathcal{E}_B(a_i)$, $B_{\mathrm{avg}} = \mathcal{E}_{\mathrm{sum}}/N$. If λ_j^{vec} lists the Dirichlet spectrum with three component multiplicity, then*

$$\mathcal{E}_{\mathrm{sum}} \geq \frac{p}{KC_H} \sum_{j=1}^{N} \lambda_j^{\mathrm{vec}} \geq \frac{3p}{5KC_H} \left(\frac{2\pi^2}{V_B}\right)^{2/3} N^{5/3}, \qquad N \leq \frac{V_B}{2\pi^2} \left(\frac{5KC_H B_{\mathrm{avg}}}{3p}\right)^{3/2}. \tag{102}$$

Proof. Let $A : \mathbb{C}^N \to H_0^1(B)^3$ take coefficients to $\rho h_{\sum_i c_i a_i}$. Its L^2 Gram matrix $S = A^*A$ obeys $S \geq (p/K)I$, by flux coercivity and (94). The columns u_i of $AS^{-1/2}$ are L^2-orthonormal. Let D_∇ be their positive semidefinite gradient Gram matrix. Cyclicity of finite matrix trace gives

$$\sum_i \|\nabla(\rho h_{a_i})\|_2^2 = \mathrm{Tr}(SD_\nabla) \geq \frac{p}{K} \,\mathrm{Tr}\, D_\nabla \geq \frac{p}{K} \sum_{j=1}^{N} \lambda_j^{\mathrm{vec}}. \tag{103}$$

For the last inequality, expand the u_i in a vector Dirichlet eigenbasis v_j. The weights $w_j = \sum_i |\langle u_i, v_j\rangle|^2$ are between zero and one by Bessel's inequality and sum to N. Among such weights, $\sum_j \lambda_j^{\mathrm{vec}} w_j$ is minimized by filling the first N positions; equivalently compare all weights with the cutoff λ_N^{vec}. All series are nonnegative. The left side of (103) is at most $C_H \mathcal{E}_{\mathrm{sum}}$. The box count gives $\lambda_j^{\mathrm{vec}} \geq (2\pi^2 j/V_B)^{2/3}$, and $\sum_{j=1}^{N} j^{2/3} \geq \int_0^N x^{2/3} dx = 3N^{5/3}/5$. This proves both inequalities. Basis independence of $\mathcal{E}_{\mathrm{sum}}$ follows because it is the trace of the positive resource quadratic form restricted to W. □

6.5 Absolute bypass supplies the sharp-section bridge

The preceding theorem concerns a smooth window, whereas the question is posed for the sharp square D. Choose a window equal to one on D and tapering to zero outside it. The correction introduced by the taper can have either sign, but its magnitude is at most the allowed absolute bypass. Passage and throughput supply the positive contribution $\eta\tau$ per unit incident power, leaving a positive margin precisely when the sufficient condition $\delta < \eta\tau$ holds. This is a condition for this bridge; it does not settle the other threshold regimes.

The following trace hypothesis states explicitly how the physical section measurement is related to Lemma 6.5. It is automatic for smooth fields on a neighborhood of the section, and also whenever the relevant plane Poynting integrals converge in L^1 to their plane-0 values. It is not inferred from $H(\mathrm{curl})$ alone.

Assumption 6.10 (Physical section compatibility)**.** *For each $a \in W$ there is a real flux density s_a on the entire section plane, integrable on D and absolutely integrable on its complement, such that*

$$P_D(a) = \int_D s_a, \qquad q_\psi(a,a) = \int_{\mathbb{R}^2} \psi s_a, \qquad \int_{\mathbb{R}^2 \setminus D} |s_a| \leq \delta \|a\|^2. \tag{104}$$

Here $s_a = \frac{1}{2}\operatorname{Re}(E_a \times \overline{H_a}) \cdot \hat{z}$ *when that classical trace exists. A separately specified regularized measurement may be used if it establishes these identities.*

Lemma 6.11 (An outer window preserves passage up to bypass)**.** *Take* $\psi = 1$ *on the same fixed section* D*, with* $0 \le \psi \le 1$ *and compact support in a slightly larger transverse region. Under Assumption 6.10 and the physical passage condition* $P_D(a) \ge \eta\|Ta\|^2$*, one has, for every* $a \in W$*,*

$$q_\psi(a,a) \ge \eta\|Ta\|^2 - \delta\|a\|^2. \tag{105}$$

If also (81) holds and $\delta < \eta\tau$*, then* $q_\psi(a,a) \ge p\|a\|^2$ *with* $p = \eta\tau - \delta > 0$*.*

Proof. Because $\psi = 1$ on D, $q_\psi(a,a) = P_D(a) + \int_{\mathbb{R}^2\setminus D} \psi s_a$. The second integral is at least $-\int_{\mathbb{R}^2\setminus D} |s_a|$. Apply the passage and bypass hypotheses, then the throughput bound. □

Remark 6.12 (Scope of the outer-window argument)**.** The physical section D has not been enlarged: its prescribed bypass condition controls the correction outside it. The window is only an analytical device. No limit of a discontinuous indicator, no unproved zero lateral flux, and no assumption about how much flux avoids an inner edge strip are used. The new restriction $\delta < \eta\tau$ is genuine for this coercivity argument. For larger tolerances this proof yields no positive lower bound, and makes no claim of impossibility or of a counterexample. A sharp flux defined on an exceptional plane without the compatibility in Assumption 6.10 is likewise outside the conclusion.

Theorem 6.13 (Approximation of the complete transmission map under stated resources)**.** *Let* W *be a closed input subspace satisfying passage and absolute bypass, Assumption 6.10, and the preceding local Maxwell hypotheses. Suppose for some finite* B_**,*

$$\mathcal{E}_B(a) \le B_*\|a\|^2 \qquad (a \in W). \tag{106}$$

For any $\Lambda \ge 0$*, let* $L_\Lambda a = \Pi_\Lambda(\rho h_a)$*, let* $\mathcal{K}_\Lambda = \ker L_\Lambda$*, and let* P_Λ *be the orthogonal projection of* W *onto* $\mathcal{K}_\Lambda^\perp$*. The operator* $R_\Lambda = T|_W P_\Lambda$ *satisfies*

$$\operatorname{rank} R_\Lambda \le 3N_{D,B}(\Lambda), \qquad \|T|_W - R_\Lambda\|^2 \le \frac{1}{\eta}\left(\delta + \frac{KC_H B_*}{\lambda_{\mathrm{next}}}\right), \tag{107}$$

where λ_{next} *is the first scalar box eigenvalue exceeding* Λ*. In particular, for* $p = \eta\tau - \delta > 0$ *and* $\Lambda = KC_H B_*/p$*, the norm error is strictly below* $\sqrt{\tau}$*. If every vector in* W *also satisfies (81), then*

$$\dim W \le \frac{V_B}{2\pi^2}\left(\frac{KC_H B_*}{\eta\tau - \delta}\right)^{3/2}. \tag{108}$$

Proof. The resource bound makes $a \mapsto \rho h_a$ bounded, so $\mathcal{K}_\Lambda$ is closed. Since L_Λ has rank at most $3N_{D,B}(\Lambda)$, its kernel has codimension at most that number; this proves the rank statement. For $b \in \mathcal{K}_\Lambda$, the spectral-tail estimate and Lemmas 6.7 and 6.11 give

$$\eta\|Tb\|^2 \le q_\psi(b,b) + \delta\|b\|^2 \le \left(\frac{KC_H B_*}{\lambda_{\mathrm{next}}} + \delta\right)\|b\|^2. \tag{109}$$

Apply this to $b = (I - P_\Lambda)a$, whose norm is at most $\|a\|$. Because $\lambda_{\mathrm{next}} > \Lambda = KC_H B_*/p$, the error is strictly below $\sqrt{\tau}$ (if $B_* = 0$, positivity of p already precludes a nonzero counted subspace). Lemma 6.1 and the explicit box count finish the proof. □

Corollary 6.14 (Conditional uniform family bound)**.** *Let $V_\tau = \operatorname{Ran} \mathbf{1}_{[\tau,\infty)}(T^*T)$. If passage, absolute bypass, trace compatibility, common local geometry, and a common finite resource B_* hold for every vector of V_τ, with $\delta < \eta\tau$, then (108) bounds $\dim V_\tau$, without an a priori compactness assumption on T. It is the usual count of squared singular values at least τ when T is compact. Alternatively a uniform bound on the basis-average resource over every finite-dimensional subspace gives the last bound in (102), with $p = \eta\tau - \delta$.*

Proof. The spectral theorem implies (81) on V_τ. Apply Theorem 6.13, or apply Theorem 6.9 to every finite-dimensional subspace. An infinite-dimensional Hilbert space contains finite orthonormal sets of arbitrarily large cardinality, so a common finite upper bound forces finite dimension. □

The map R_Λ is defined using the complete T, including all matching and resonant feedback. It is not obtained by deleting a component of an isolated link and then silently applying an uncontrolled inverse. Its cost is the explicitly retained norm B_* of the actual full field. Thus Theorem 6.13 discharges the output-approximation step under a resource hypothesis; it does not discharge that hypothesis.

Corollary 6.15 (Essential-norm consequence)**.** *Under Theorem 6.13's hypotheses, without assuming a throughput lower bound, the distance of $T|_W$ from the compact operators is at most $\sqrt{\delta/\eta}$. In particular, exact zero bypass makes $T|_W$ compact.*

Proof. The finite-rank R_Λ are compact and $\lambda_{\mathrm{next}} \to \infty$ as $\Lambda \to \infty$. Take the limit superior in (107). When $\delta = 0$, these finite-rank operators converge to $T|_W$ in operator norm. A norm limit of compact operators is compact: given any bounded input sequence, use a diagonal subsequence convergent under each approximant, then the uniform approximation makes its images under T Cauchy. □

6.6 An explicit area scaling with its extra resource exposed

Corollary 6.16 (Conditional square-enclosure area scaling)**.** *Suppose $D \subset [-L/2, L/2]^2$ and there is a source-free comparison box*

$$B = (-L/2 - 4r, L/2 + 4r)^2 \times (-3r, 4r), \qquad r > 0, \tag{110}$$

on which the material bounds and (106) hold. There are admissible cutoffs with

$$V_B = 7r(L+8r)^2, \quad G \le \sqrt{3}/r, \quad d_1, d_2 \le \sqrt{3}/r, \quad C_H \le k_0^2\varepsilon_+ + 3/r^2, \quad K \le \frac{c_0\sqrt{3}}{2r\sqrt{\varepsilon_-}}\sqrt{2 + \frac{12}{k_0^2\varepsilon_- r^2}}. \tag{111}$$

In particular, if $r = (k_0\sqrt{\varepsilon_+})^{-1}$ is admissible and $\kappa = \varepsilon_+/\varepsilon_-$, then, with $p = \eta\tau - \delta > 0$,

$$\dim W \le \frac{7}{2\pi^2}(k_0\sqrt{\varepsilon_+}L + 8)^2 \left(2\sqrt{3}\sqrt{\kappa}\sqrt{2 + 12\kappa}\,\frac{\omega B_*}{p}\right)^{3/2}. \tag{112}$$

For a scaled fixed shape with $L^2 \le c_D|D|$, this is $O(1 + k_0^2\varepsilon_+|D|)$ only if ωB_*, the material ratio, thresholds, shape constant, and the required collar remain controlled.

Proof. For a one-dimensional interval use the function equal to one on that interval, decreasing linearly to zero across an exterior strip of width r, and zero beyond the strip. Its Lipschitz constant is $1/r$. Let $Q_s = [-L/2 - s, L/2 + s]^2$. Take ψ as the product of the two one-dimensional cutoffs equal to one on Q_0 and zero outside Q_r, and take $\chi(z) = 1 - z/r$ on $(0, r)$. Then $|\nabla_\perp \psi| \le \sqrt{2}/r$ and $|g| \le \sqrt{3}/r$. Take ζ as the product cutoff equal to one on $Q_r \times [0, r]$, supported on $Q_{2r} \times [-r, 2r]$;

take ρ equal to one on the latter box and supported on $Q_{3r} \times [-2r, 3r]$. Each has gradient bounded by $\sqrt{3}/r$, and both supports are compact in (110). Equality on the indicated closed supports suffices in the preceding estimates. This proves (111). Substitute $r = (k_0\sqrt{\varepsilon_+})^{-1}$ in (108), using $\omega = c_0 k_0$; straightforward cancellation gives (112). Finally $(x+8)^2 \le 2x^2 + 128$ proves the asserted order with every additional dependency retained. □

Corollary 6.17 (Local extension to real symmetric anisotropy)**.** *All local estimates and their conditional channel consequences remain valid for measurable real symmetric tensors $\varepsilon_r(x)$ satisfying $\varepsilon_- I \le \varepsilon_r \le \varepsilon_+ I$, provided $\varepsilon_r|e|^2$ is replaced by $\overline{e} \cdot \varepsilon_r e$ in the resource.*

Proof. Symmetry and reality give the same cross-Poynting cancellation. The magnetic estimate uses $|\varepsilon_r e|^2 \le \varepsilon_+ \overline{e} \cdot \varepsilon_r e$. In the Caccioppoli step use the positive quadratic form of ε_r^{-1}, its Cauchy–Schwarz inequality, and $\varepsilon_r^{-1} \le \varepsilon_-^{-1} I$. The identity $k_0^{-2} \overline{\operatorname{curl} h} \cdot \varepsilon_r^{-1} \operatorname{curl} h = \overline{e} \cdot \varepsilon_r e$ replaces its scalar version. Every remaining step is unchanged. Constant scalar permeability is still essential to this proof of $\operatorname{div} h = 0$. □

6.7 The scope of the resource route

Remark 6.18 (Open question: removing the resource in the small-bypass regime)**.** There is no estimate here, from $1 \le \varepsilon_r \le \varepsilon_+$, the fixed section, passivity, passage, and absolute bypass alone, that uniformly bounds B_* or replaces its role by a uniform approximation estimate for the full T. A possible sufficient missing theorem is: every admitted counted subspace has a finite-rank approximation with error strictly below $\sqrt{\tau}$ and rank bounded solely by the frozen parameters. An area scaling additionally requires a rank of order $1 + k_0^2 \varepsilon_+ |D|$. Theorem 6.13 supplies such an approximation *with* B_*; it does not eliminate it. Even proving unbounded local amplification would only invalidate that proof route, not construct an arbitrarily large channel subspace. Conversely, pointwise compactness for each device would not make the bound uniform over a sequence of devices. Theorem 19.1 later disproves the unrestricted assertion in the allowed range $\delta > \eta$; it leaves the stricter regime $\delta < \eta\tau$ used here unresolved without resources.

7 Resonant amplification and candidate channel mechanisms

We examine several mechanisms relevant to the fixed-section channel question. A passive device can have large internal fields; locally evanescent fields can carry positive flux through interference; and a finite-dimensional resonator model does not by itself realize a Maxwell device. The examples distinguish exact Maxwell constructions from finite-dimensional models, and do not identify a model port with a physical channel through the prescribed section. The physical examples use the fixed real scalar material class $1 \le \varepsilon_r \le \varepsilon_+$ at one positive frequency, with vacuum exterior. The section and thresholds are fixed, whereas support size and resonance lifetime may grow. The radial, local-flux, and mirror-network examples originate in the prior report [20]; they are rederived here with their hypotheses explicit. The physical counterexample to the quantified fixed-section assertion is given separately in Theorem 19.1.

7.1 An exact bounded-index Maxwell amplification obstruction

First consider a single incoming spherical wave surrounded by concentric dielectric layers. Adding sufficiently many layer pairs makes the core field arbitrarily large while the outgoing wave still carries exactly the incident power. This provides a concrete reason that passivity alone cannot

supply the uniform local field bound needed by Section 6. It is a one-channel reflection example, so it does not itself establish many channels through the prescribed square.

Proposition 7.1 (Unbounded local amplification, one reflected channel)**.** *For every fixed $\varepsilon_+ > 1$ and $k_0 > 0$ there are a fixed ball B_{r_0} and finite radial dielectric structures ε_M, with $1 \le \varepsilon_M \le \varepsilon_+$, for which a unit-power incoming spherical radiation channel produces electric and magnetic squared field norms in B_{r_0} growing proportionally to q^{2M}, for some fixed $q > 1$. The exterior radius grows linearly with M. The selected scattering coefficient has modulus one and the net power through every concentric sphere is zero.*

Proof. Choose $1 < q < \sqrt{\varepsilon_+}$. Write $\widehat{j}_1(x) = xj_1(x) = \sin(x)/x - \cos(x)$. Its derivative has arbitrarily large positive roots: at $(m+1/2)\pi > 1$ its sign alternates, since its value is $(-1)^m(1-x^{-2})$. Choose such a root $x_0 > 1$ large enough that $q^2 + 2/x_0^2 \le \varepsilon_+$, and put $r_0 = x_0/k_0$. The root is not simultaneously a zero of $\widehat{j}_1$, by uniqueness for its second-order ordinary differential equation away from zero.

For a tangential, surface-divergence-free vector spherical harmonic X_{1m} with $\int_{S^2} |X_{1m}|^2 \, d\Omega = 1$, set

$$E = \frac{u(r)}{r} X_{1m}, \qquad H = \frac{1}{i\omega\mu_0} \nabla \times E, \qquad u'' + \left(k_0^2 \varepsilon_M(r) - \frac{2}{r^2} \right) u = 0. \tag{113}$$

This is the exact TE multipole reduction of both Maxwell curl equations. At radial interfaces continuity of tangential E and H is exactly continuity of u, u'; permeability is constant and the normal electric component vanishes. The integrated outgoing power is

$$P(r) = \frac{1}{2\omega\mu_0} \operatorname{Im}(\overline{u} u'). \tag{114}$$

In the core take $\varepsilon_M = 1$ and $u = C_M \widehat{j}_1(k_0 r)$, which is regular at zero and has $u'(r_0) = 0$.

Append M low/high shell pairs. A shell of type $n \in \{1, q\}$ has width $\pi/(2k_0 n)$ and coefficient $\varepsilon_M(r) = n^2 + 2/(k_0 r)^2$. Thus its radial equation is exactly $u'' + (k_0 n)^2 u = 0$. On the state $(u, u'/k_0)^T$, its transfer matrix is $\left(\begin{smallmatrix} 0 & 1/n \\ -n & 0 \end{smallmatrix} \right)$. A pair has transfer matrix $-\operatorname{diag}(q^{-1}, q)$, so

$$R_M = r_0 + \frac{M\pi}{2k_0}(1 + q^{-1}), \quad u(R_M) = (-q^{-1})^M C_M \widehat{j}_1(x_0), \quad u'(R_M) = 0. \tag{115}$$

All shells obey the claimed material bounds. In the vacuum exterior put $u = a\widehat{h}_1^{(2)}(k_0 r) + b_M \widehat{h}_1^{(1)}(k_0 r)$, where $\widehat{h}_1^{(1)}(x) = -e^{ix}(1 + i/x)$ and $\widehat{h}_1^{(2)} = \overline{\widehat{h}_1^{(1)}}$ on the positive real axis. Direct differentiation gives the Wronskian $2i$ and

$$|(\widehat{h}_1^{(1)})'(x)|^2 = 1 - x^{-2} + x^{-4}, \quad b_M = -a \frac{(\widehat{h}_1^{(2)})'(k_0 R_M)}{(\widehat{h}_1^{(1)})'(k_0 R_M)}, \quad u(R_M) = \frac{2ia}{(\widehat{h}_1^{(1)})'(k_0 R_M)}. \tag{116}$$

Incoming power is $k_0 |a|^2/(2\omega\mu_0)$; choose $|a|^2 = 2\omega\mu_0/k_0$. Consequently

$$|C_M|^2 = \frac{4q^{2M}|a|^2}{|\widehat{j}_1(x_0)|^2 |(\widehat{h}_1^{(1)})'(k_0 R_M)|^2}. \tag{117}$$

For $x \ge 1$ the derivative factor squared lies in $[3/4, 1]$. The core fields are fixed nonzero profiles times C_M, proving the norm statement. A fixed interior section on which their traces are nonzero has the corresponding trace growth. Equation (116) gives $|b_M| = |a|$, while the core radial function is a constant times a real function. Equation (114) and conservation then give zero total radial flux at every radius. No independently chosen trapped amplitude was inserted: C_M is fixed by the incoming amplitude and the interface matching. □

Remark 7.2 (Scope of the amplification example)**.** External passivity does not uniformly bound the incident-power-to-local-field map over the admitted class with unrestricted support. The prior report's $q = 2$ example required $\varepsilon_+ > 4$; choosing x_0 and q as above extends this obstruction to every $\varepsilon_+ > 1$. This does not disprove a uniform channel count, a fixed-support estimate, or a theorem restricted to counted fields with positive through-power. A complete spherical scattering phase is not an additional transmitted channel. This exact construction establishes neither an increasing number of transmitted directions nor the required absolute bypass bound.

7.2 Evanescent pairs can carry real power locally

An individual exponentially decaying or growing factor is often associated with reactive rather than transported power. A suitable phase relation between the two factors changes their interference: the combined field has positive real normal flux. The example below gives arbitrarily many such independent local solutions. Their existence in a collar does not show that they can all be generated by finite-power incident fields while meeting the global bypass requirement.

Proposition 7.3 (Infinite positive local flux index)**.** *On a fixed rectangular section $D = (0, L) \times (0, W)$ and homogeneous source-free collar $D\times(-h, h)$, the space of smooth local Maxwell solutions has positive flux subspaces of arbitrarily large finite dimension. This remains true if every superposition has zero real normal flux on the four collar sidewalls.*

Proof. Let $k^2 = \omega^2\mu_0\varepsilon_0\varepsilon_c$ and take every integer m with $q_m = m\pi/L > k$. Put $\kappa_m = \sqrt{q_m^2 - k^2}$ and

$$f_m(z) = a_m(e^{-\kappa_m z} + ie^{\kappa_m z}), \qquad |a_m|^2 = \frac{2\omega\mu_0}{\kappa_m LW}, \qquad E_m = (0, f_m \sin(q_m x), 0), \tag{118}$$

$$H_m = \frac{1}{\omega\mu_0}(if_m' \sin(q_m x), 0, -iq_m f_m \cos(q_m x)). \tag{119}$$

Both curl equations hold by $f_m'' = (q_m^2 - k^2)f_m$. The normal power density is

$$\frac{\operatorname{Im}(\overline{f}_m f_m') \sin^2(q_m x)}{2\omega\mu_0} = \frac{\kappa_m |a_m|^2 \sin^2(q_m x)}{\omega\mu_0}. \tag{120}$$

Sine orthogonality therefore gives, for every finite coefficient vector,

$$P_D\left(\sum_m c_m(E_m, H_m)\right) = \sum_m |c_m|^2. \tag{121}$$

On the x sidewalls E vanishes, and on the y sidewalls the normal Poynting component vanishes identically. Both statements hold for every finite superposition, not just for basis fields. □

Remark 7.4 (Scope of the local evanescent example)**.** A single decreasing exponential carries zero real normal power. Its coherent combination with an increasing exponential does not. Thus a propagating-wave count cannot be justified by discarding each evanescent term separately. These are exact *local* vector Maxwell fields in ordinary material, but their norms at the collar ends grow rapidly with transverse order. No finite passive dielectric device producing these data from power-normalized external channels has been constructed. Zero sidewall flux is a property of the fields, not permission to install conducting walls. Nor does it control the field on the rest of the infinite section plane. Hence this proposition does not establish global absolute bypass or a physical counterexample.

7.3 An exact feedback diagnostic independent of mode reduction

Proposition 7.5 (Lossless scattering algebra)**.** *For any N and any $0 < \xi_j \le 1$, reciprocal unitary two-port networks with isolated transmission powers ξ_j can be cascaded with lossless phases to produce N perfectly transmitted orthogonal network channels.*

Proof. For direction j, use two identical mirrors with $r_j = i\sqrt{1-\xi_j}$ and $t_j = \sqrt{\xi_j}$. The symmetric matrix $\left(\begin{smallmatrix} r_j & t_j \\ t_j & r_j \end{smallmatrix}\right)$ is unitary. With propagation phase $p_j = i$, the convergent reflection series gives

$$t_{\mathrm{all},j} = \frac{t_j^2 p_j}{1 - r_j^2 p_j^2} = i, \qquad r_{\mathrm{all},j} = r_j + \frac{t_j^2 r_j p_j^2}{1 - r_j^2 p_j^2} = 0. \tag{122}$$

The direct sum has transmission iI_N. The feedback inverse is exactly $\mathrm{diag}(\xi_j^{-1})$, compensating arbitrarily weak isolated links. □

What is disproved. An isolated-link singular-value tail together with external passivity does not control the completed scattering transmission. This proposition is stronger as an algebraic diagnostic than a coupled-mode approximation, but still supplies no bounded-index synthesis through the same physical D.

7.4 Matched resonator pairs: energy, bandwidth, and errors

The following model uses the energy/power normalization conventional in temporal coupled-mode theory [6, 18]. Its equations and all conclusions about them are proved directly; their agreement with a particular Maxwell device remains an additional question.

Definition 7.6 (MODEL: a reciprocal resonator pair)**.** Let x, y be energy-normalized resonator amplitudes, so stored model energy is $|x|^2 + |y|^2$. Let a, b be incoming amplitudes with incident power $|a|^2 + |b|^2$. For $J, \gamma > 0$, set

$$\begin{aligned} \dot{x} &= (-i\omega_0 - \gamma)x - iJy + \sqrt{2\gamma}\, a, & a_- &= -a + \sqrt{2\gamma}\, x, \\ \dot{y} &= (-i\omega_0 - \gamma)y - iJx + \sqrt{2\gamma}\, b, & b_- &= -b + \sqrt{2\gamma}\, y. \end{aligned} \tag{123}$$

The -1 direct reflection is part of the model's port convention.

Proposition 7.7 (Exact matching and cost in the model)**.** *For harmonic drive at $\omega = \omega_0 + \Delta$ with $a = 1, b = 0$, define $D_\Delta = (\gamma - i\Delta)^2 + J^2$. Then*

$$\begin{aligned} x &= \frac{\sqrt{2\gamma}(\gamma - i\Delta)}{D_\Delta}, & y &= \frac{-i\sqrt{2\gamma}J}{D_\Delta}, \\ t &= \frac{-2i\gamma J}{D_\Delta}, & r &= \frac{\gamma^2 + \Delta^2 - J^2}{D_\Delta}. \end{aligned} \tag{124}$$

The model is lossless and passive. At $\Delta = 0$, $\gamma = J$ it has $t = -i, r = 0$, internal energy J^{-1}, and left-to-right internal current 1*. At this matched setting,*

$$|t(\Delta)|^2 = \frac{1}{1 + \Delta^4/(4J^4)}, \qquad \mathrm{FWHM} = 2\sqrt{2}J. \tag{125}$$

Proof. Substitution of harmonic time dependence gives the linear system with matrix $\begin{pmatrix} \gamma - i\Delta & iJ \\ iJ & \gamma - i\Delta \end{pmatrix}$; inversion proves (124). Direct differentiation of the energy gives

$$\frac{d}{dt}(|x|^2 + |y|^2) = |a|^2 + |b|^2 - |a_-|^2 - |b_-|^2. \tag{126}$$

The internal left-to-right exchange is $I_{L\to R} = -2J\,\mathrm{Im}(\overline{x}y)$, from the individual energy derivatives. At matching $x = 1/\sqrt{2J}$ and $y = -ix$, giving the energy and current. Finally, $|D_\Delta|^2 = (2J^2 - \Delta^2)^2 + 4J^2\Delta^2 = 4J^4 + \Delta^4$ gives the line shape and its half-power frequencies. The poles are at $\Delta = \pm J - i\gamma$, and hence remain strictly below the real axis for every member of the family. □

Remark 7.8 (Model sensitivities)**.** At $\Delta = 0$, writing $s = \gamma/J$ gives $|t|^2 = 4s^2/(1+s^2)^2$. Thus $|t|^2 \geq \tau$ exactly when

$$\frac{1 - \sqrt{1-\tau}}{\sqrt{\tau}} \leq s \leq \frac{1 + \sqrt{1-\tau}}{\sqrt{\tau}}. \tag{127}$$

At matching, a common frequency detuning obeys the threshold exactly when $|\Delta| \leq \sqrt{2}J(\tau^{-1}-1)^{1/4}$. If both resonators instead have an additional unobserved amplitude decay $\kappa \geq 0$, replace the diagonal rate in the equations by $\gamma + \kappa$ while keeping the driven/output couplings $\sqrt{2\gamma}$. For $\gamma = J$ and $\Delta = 0$,

$$|t|^2 = \frac{4}{[(1+\kappa/J)^2 + 1]^2}. \tag{128}$$

Consequently fixed loss destroys the small-J limit. To approach unit transmission it is necessary here that $\kappa/J \to 0$. For a fixed threshold, the exact permitted ratio is $\kappa/J \leq \sqrt{2/\sqrt{\tau} - 1} - 1$. These costs cannot be suppressed by saying merely that each cavity has large Q: its leakage and errors must be compared to its weak link.

Theorem 7.9 (N weak directions and a stable certificate in the model)**.** *Let $J = \mathrm{diag}(J_1, \ldots, J_N)$ with all $J_j > 0$. At the common frequency ω_0, take N independent pairs with external rates J_j. Put*

$$G = \mathrm{diag}(J^{1/2}, J^{1/2}), \quad B_0 = \begin{pmatrix} I & iI \\ iI & I \end{pmatrix}, \quad A_0 = GB_0G, \quad E_La = (a,0)^T, \quad E_Ra = (0,a)^T. \tag{129}$$

Their transmission and reflection are $T_0 = -iI_N$, $R_0 = 0$; their internal energy matrix is J^{-1} and exchange-current matrix is I_N. If the system matrix changes to $A = A_0 + \mathcal{E}$, keeping the same port couplings, define $F = G^{-1}\mathcal{E}G^{-1}$ and $\rho = \|F\|$. Whenever $\rho < \sqrt{2}$, the system remains invertible and

$$\|T - T_0\| \leq \frac{\rho}{1 - \rho/\sqrt{2}}, \qquad T = 2E_R^*(B_0 + F)^{-1}E_L. \tag{130}$$

In particular every input is transmitted with power greater than τ if

$$\rho < \frac{1 - \sqrt{\tau}}{1 + (1-\sqrt{\tau})/\sqrt{2}}. \tag{131}$$

Proof. The unperturbed statement follows pairwise from Proposition 7.7. Also $B_0^*B_0 = 2I$, so $\|B_0^{-1}\| = 1/\sqrt{2}$ and $\|(B_0+F)^{-1}\| \leq 1/(\sqrt{2}-\rho)$ by the Neumann series. The resolvent identity gives

$$\|T - T_0\| \leq 2\|(B_0+F)^{-1}\|\|F\|\|B_0^{-1}\| \leq \frac{\sqrt{2}\rho}{\sqrt{2}-\rho}. \tag{132}$$

The triangle inequality gives $\|Ta\| \geq (1 - \|T - T_0\|)\|a\|$. Solving the sufficient strict inequality $\rho/(1-\rho/\sqrt{2}) < 1 - \sqrt{\tau}$ gives (131). □

Remark 7.10 (Model generality and port errors)**.** The perturbation may mix different pairs and need not be diagonal. A sufficient unweighted condition is $\|\mathcal{E}\|/\min_j J_j \to 0$, since $\rho \le \|\mathcal{E}\|/\min_j J_j$; weighted control can be much sharper. If normalized input/output couplings also change to $E_L + L$ and $E_R + R$, and there is a direct transmission correction D_0, the same proof yields

$$\|T - T_0\| \le \frac{\rho}{1 - \rho/\sqrt{2}} + \frac{2(\|L\| + \|R\| + \|L\|\|R\|)}{\sqrt{2} - \rho} + \|D_0\|. \tag{133}$$

The normalization here is relative to the original G; for example the physical input matrix in the model is $\sqrt{2}G(E_L + L)$. An arbitrary algebraic perturbation is not automatically passive or reciprocal. Any proposed physical realization must also establish those properties and the power normalization of its actual ports. The estimate is a sufficient matrix certificate once those facts hold.

7.5 Compression and coherent passage certification

For a proposed device, the relevant test is a bound on every vector in the input subspace. The compressed transmission matrix and the section-flux matrix below give convenient sufficient tests for that purpose. The absolute-bypass test is stronger than a bound on net signed flux: return flow outside the section must be counted even where opposite contributions cancel.

Proposition 7.11 (Physical channel certificate if its data exist)**.** *Let $T : \mathcal{H}_{\text{in}} \to \mathcal{H}_{\text{out}}$ be a bounded physical transmission operator between power Hilbert spaces. Let V and Z be isometries from $\mathbb{C}^N$ into its input and output spaces, and let $M = Z^*TV$. If U is unitary and $\|M - U\| \le e < 1 - \sqrt{\tau}$, then $\|TVa\|^2 > \tau\|a\|^2$ for every nonzero a. If T is a contraction, and its physical section-flux matrix on these inputs obeys $Q_D \succeq \eta I_N$, then the passage inequality $P_D(Va) \ge \eta\|TVa\|^2$ also holds for every a.*

Proof. The isometry Z gives $\|TVa\| \ge \|Z^*TVa\|$; the unitary comparison gives $\|Ma\| \ge (1 - e)\|a\|$. For the second statement, $P_D(Va) = a^*Q_Da \ge \eta\|a\|^2 \ge \eta\|TVa\|^2$. The exact, potentially weaker passage test is $Q_D - \eta V^*T^*TV \succeq 0$. None of these conclusions needs compactness or a discrete singular-value decomposition of the full operator. □

Lemma 7.12 (A sufficient absolute-bypass certificate)**.** *Suppose actual basis fields have well-defined pointwise traces on $\Pi \setminus D$, where Π is the section plane, and define the Hermitian matrix*

$$F_{ij}(s) = \frac{1}{4}\left(E_j(s) \times \overline{H_i(s)} + \overline{E_i(s)} \times H_j(s)\right) \cdot n. \tag{134}$$

If these traces are regular enough that $\int_{\Pi\setminus D} \|F(s)\|\, dA$ is defined and at most δ, then every coherent vector satisfies

$$\int_{\Pi\setminus D} |S_n(a; s)|\, dA \le \delta\|a\|^2. \tag{135}$$

Proof. Expansion gives $S_n(a; s) = a^*F(s)a$. Pointwise, $|a^*F(s)a| \le \|F(s)\|\|a\|^2$; integrate. □

Remark 7.13 (Limitations of basis-only and signed-flux tests)**.** Let $F(s) = h(s)\left(\begin{smallmatrix} 0 & L \\ L & 0 \end{smallmatrix}\right)$, with $\int |h| = 1$. Each coordinate basis vector has zero local flux, but $a = (1, 1)^T/\sqrt{2}$ has absolute integrated flux L. If additionally $\int h = 0$, the full *signed* integrated flux matrix vanishes while the same absolute bypass remains L. This elementary example disproves both inference rules for Hermitian flux data; it is not asserted to be a global Maxwell realization. The evanescent pair in Proposition 7.3 gives an actual local Maxwell instance of individually zero-flux exponential fields

acquiring power by interference. Likewise a basis test for signed passage can fail: $Q = \left(\begin{smallmatrix} 1 & 2 \\ 2 & 1 \end{smallmatrix}\right)$ has positive diagonal but a negative eigenvalue. Section-flux conditions require a full matrix inequality; absolute bypass requires additional control such as Lemma 7.12. Rough Maxwell traces are not silently assumed to have these pointwise products.

7.6 Physical realization attempts and their specific obstructions

Proposition 7.14 (A restricted radial angular-momentum obstruction)**.** *For a radial scalar dielectric with $\varepsilon(r) \le \varepsilon_+$ on $0 < r \le R$, a regular real TE radial solution of angular order $\ell \ge 1$ obeys*

$$u'' = \left(\frac{\ell(\ell+1)}{r^2} - k_0^2 \varepsilon(r) \right) u. \tag{136}$$

If $\ell(\ell+1) > k_0^2 \varepsilon_+ R^2$ and the nonzero leading coefficient in $u \sim c r^{\ell+1}$ is positive, then $u, u' > 0$ on $(0, R]$. In particular, neither $u(R) = 0$ nor $u'(R) = 0$ can hold.

Proof. The regular solution also satisfies $u'(r) \sim (\ell+1) c r^{\ell}$. To justify this from the equation rather than differentiate an asymptotic without control, put $v = r^{-\ell-1} u$. Then $(r^{2\ell+2} v')' = -k_0^2 \varepsilon(r) r^{2\ell+2} v$. The integration constant at zero must vanish for v to have its finite limit c, so boundedness of ε, v gives $v' = O(r)$. Thus both u and u' are positive for sufficiently small positive radius. As long as $u > 0$, the displayed strict inequality gives $u'' > 0$, so u' is increasing and remains positive. A first zero of either u or u' is consequently impossible. Across radial interfaces u, u' are continuous; the same argument applies piecewise and hence globally. □

Radial shells and partial waves. Proposition 7.1 proves that bounded-index reflectors can produce arbitrarily large internal amplitude. Repeating its exactly compensated shell profile for order ℓ would require $\varepsilon = n^2 + \ell(\ell+1)/(k_0 r)^2$. At a fixed inner radius this eventually violates the fixed material upper bound. Increasing the radius avoids that violation but does not place the high-order power through the original D. Proposition 7.14 also blocks the particular real-core Neumann or Dirichlet tuning in a fixed small ball at high ℓ. It is not a general exclusion of open resonances, nonspherical matching, or fields coupled from a larger exterior structure. The exact radial example is a one-port reflector; turning its stored energy into N independently driven opposite-side ports is an unproved step.

Planar dielectric Bragg cavities. At normal incidence, bounded-index quarter-wave layers do realize lossless one-dimensional mirrors; a symmetric resonant pair can realize the scalar feedback algebra. This statement follows by the same two-by-two transfer-matrix multiplication used above. Such an exact planar realization has infinite transverse extent and its plane waves are normalized per transverse area. It does not supply finite total incoming power with absolute flux confined to a prescribed finite D. Truncating the mirrors adds lateral leakage and diffraction. An N-cavity proposal must prove that these errors, along with off-diagonal mixing and detuning, satisfy the relative bounds of Theorem 7.9 for the weakest direction. Merely increasing the number of mirror layers supplies no such multidimensional estimate.

Many small tips coupled to large remote resonators. Arbitrarily fine dielectric tips or corners could create linearly independent local trace patterns. Linear independence does not bound the smallest singular value of the physical coupling matrix, and the field-to-output inverse is precisely where its weakness might be compensated. No bounded-index synthesis is established that makes all N resonances coincide at the prescribed frequency while controlling leakage, parasitic coupling, and model error relative to that smallest coupling. Remote support growth is allowed, so its expense

alone is not an obstruction. In contrast, assuming ideal independently tunable impedances or perfect conducting partitions would change the physical class. These routes remain candidates, not impossibility results.

Thin dielectric guides and broadened channels. A weakly confined guide mode, when it exists, does not automatically satisfy the fixed-aperture bypass requirement. The prior report's qualified planar-guide construction explicitly changes the lower permittivity bound toward zero, varies the section shape with unbounded diameter, and uses infinite leads. It therefore cannot be transferred to the present fixed ordinary-dielectric, fixed-background, same-section problem. Counting outputs at different frequencies, adding internal sources, or sending the threshold τ to zero would likewise answer different questions.

Remark 7.15 (Open physical realization of the network model)**.** For each N one would need an actual finite dielectric and power isometries V_N, Z_N at the same frequency whose completed compression obeys the bound in (133) with a fixed margin below $1-\sqrt{\tau}$, together with the physical section inequality in Proposition 7.11 and an absolute-bypass estimate such as (135). In a resonator implementation this requires a justified Maxwell reduction and a weighted error matrix; $o(\min_j J_j)$ unweighted error is sufficient but has not been proved. The matrices J^{-1} and I_N in Theorem 7.9 are model energy and internal-current matrices, not computed Maxwell energy or section-flux matrices. If this bridge were established for arbitrary N, the fixed-parameter finite channel bound would be false. Its absence means that neither a disproof nor a universal bound has been obtained by this network-model track. The different physical construction in Theorem 19.1 gives a counterexample in the regime $\delta > \eta$ without establishing this model reduction.

8 Coherent bypass and limits of local constructions

Theorem 19.1 gives a physical construction for $\delta > \eta$. Here we examine the implications of coherent passage and absolute bypass separately from that construction. These conditions imply a global feasibility restriction, but they do not bound the dimension of local Maxwell solutions normalized by total plane flux, even when bypass is controlled on the entire transverse plane. The local fields constructed below do not by themselves have the required far-field accessibility.

8.1 A global power-budget restriction

Proposition 8.1 (A necessary threshold condition)**.** *Consider the compact-scatterer vacuum-exterior class of Assumptions 1.1–1.2, with a legitimate integrable flux on the full plane $\Pi = \{z = 0\}$. Use the usual radiation normalization: the angular incoming and outgoing far-field amplitudes a_∞, b_∞ have squared norms equal to their powers, with $\|b_\infty\|^2 \le \|a_\infty\|^2 = \|a\|^2$. Then*

$$-\|a\|^2 \le P_\Pi(a) \le \|a\|^2, \qquad |P_D(a)| \le (1+\delta)\|a\|^2 \tag{137}$$

whenever the absolute bypass is at most $\delta\|a\|^2$. Consequently a nonzero counted subspace requires

$$\eta\tau \le 1+\delta. \tag{138}$$

In particular, its dimension is zero if $\eta\tau > 1+\delta$.

Proof. Apply the real Poynting conservation law in a large upper half-ball. Its flat face has outward normal $-\hat{z}$. On passing to infinity, the hemispherical outward flux is the outgoing upper-hemisphere power minus the incoming upper-hemisphere power. Thus

$$P_\Pi(a) = \|\mathbf{1}_{\Omega_+} b_\infty\|^2 - \|\mathbf{1}_{\Omega_+} a_\infty\|^2. \tag{139}$$

Here the far-field assertion can be checked directly: the magnetic amplitudes of outgoing and incoming waves are respectively $Z_0^{-1}\hat{r} \times E_{\text{out}}$ and $-Z_0^{-1}\hat{r} \times E_{\text{in}}$. The incoming–outgoing cross terms in the real radial Poynting flux cancel, leaving their squared-power difference. The definition of the radiation power amplitudes includes this integrated far-field limit. Integrability of the plane flux permits the disk integral to converge to P_Π. Each term on the right of (139) is nonnegative, and no larger than $\|a\|^2$, proving the first bound. Also $|P_D - P_\Pi| \le \int_{\Pi\setminus D} |S_z| \le \delta\|a\|^2$. Finally the counted inequalities give $\eta\tau\|a\|^2 \le P_D(a) \le (1+\delta)\|a\|^2$. □

Remark 8.2 (Loewner bounds do not count dimension)**.** On any finite counted input space let Q_D be its Hermitian section-flux matrix. Polarization and Proposition 8.1 give

$$\eta T^*T \preceq Q_D \preceq (1+\delta)I, \qquad \tau I \preceq T^*T \preceq I. \tag{140}$$

For $0 < \eta \le 1$, the choice $T = I_N$, $Q_D = I_N$, with zero signed and absolute bypass, satisfies these algebraic inequalities for every N. This is not a physical construction. It establishes precisely that the coherent Loewner inequalities and global power budget alone supply no rank bound. A spatial Maxwell-to-input accessibility restriction is necessary.

8.2 Arbitrarily many local fields with whole-plane coherent bypass control

The next theorem strengthens the local evanescent example of Proposition 7.3: it certifies absolute bypass on all of $\Pi \setminus D$, rather than only vanishing flux on the sides of a finite collar. Its normalization is total *local plane flux*, not power supplied by asymptotic incoming channels.

Theorem 8.3 (Coherent local passage with arbitrarily small bypass)**.** *Fix $k_0 > 0$, $L > 0$, $h > 0$, an integer $N \ge 1$, and $0 < \delta < 1$. Let $D = (-L/2, L/2)^2$ and $\Omega_h = \mathbb{R}^2 \times (-h, h)$. There are N linearly independent, smooth, source-free vacuum Maxwell fields on Ω_h, with finite weighted field norm there, such that every coefficient vector $a \in \mathbb{C}^N$ has*

$$S_z(a; x, y, 0) \ge 0, \quad P_\Pi(a) = \|a\|^2, \quad P_D(a) \ge (1-\delta)\|a\|^2, \quad \int_{\Pi\setminus D} |S_z(a)| \le \delta\|a\|^2. \tag{141}$$

All tangential Fourier supports can be chosen above any prescribed transverse wavenumber. Thus local source-free Maxwell equations and all-superposition passage and whole-plane bypass alone do not bound the dimension, even at fixed section, frequency, and homogeneous permittivity.

Proof. Use the unitary Fourier transform on each transverse coordinate. For $b > 0$, define

$$\widehat{\phi_b}(\xi) = (2b)^{-1/2}\mathbf{1}_{[-b,b]}(\xi), \qquad \phi_b(x) = \frac{\sin(bx)}{\sqrt{\pi b}\, x}, \qquad g_b(x,y) = \phi_b(x)\phi_b(y), \tag{142}$$

with the continuous value at zero. Plancherel gives $\|\phi_b\|_2 = \|g_b\|_2 = 1$. Since $|\sin(bx)| \le 1$,

$$\int_{|x|\ge L/2} |\phi_b(x)|^2\, dx \le \frac{4}{\pi b L}, \qquad \int_{\mathbb{R}^2\setminus D} |g_b|^2 \le \frac{8}{\pi b L}. \tag{143}$$

Choose $b \ge 8N/(\pi L\delta)$, and choose $Q > k_0$ as large as desired. For $j = 1, \dots, N$, put

$$K_j = Q + 3bj, \qquad f_j(x,y) = e^{iK_j x} g_b(x,y), \qquad f_a = \sum_{j=1}^{N} a_j f_j. \tag{144}$$

Their Fourier supports are disjoint rectangles $[K_j - b, K_j + b] \times [-b, b]$. Thus the f_j are orthonormal and $\|f_a\|_2^2 = \|a\|^2$. Pointwise Cauchy–Schwarz gives $|f_a|^2 \le N|g_b|^2\|a\|^2$, hence

$$\int_{\mathbb{R}^2 \setminus D} |f_a|^2 \le \delta \|a\|^2. \tag{145}$$

Every support lies in $\xi_x \ge Q + 2b > k_0$, entirely in the evanescent sector, but its union is bounded for each finite N, Q, b.

Use the normalized fields $e = \sqrt{\varepsilon_0}E$, $h = \sqrt{\mu_0}H$ of (84), and set $C = \sqrt{2/c_0}$. Prescribe the tangential data at $z = 0$ by

$$e_t = (0, Cf_a), \qquad h_t = (-Cf_a, 0), \qquad e_z = \frac{iC}{k_0}\partial_y f_a, \qquad h_z = -\frac{iC}{k_0}\partial_x f_a. \tag{146}$$

The normal components are determined by the two normal curl equations. For completeness, the full extension is constructed, not assumed. Put $J(v_x, v_y) = (-v_y, v_x)$ and evolve the tangential components by

$$\begin{aligned} e_z &= \frac{i}{k_0}(\partial_x h_y - \partial_y h_x), \qquad \partial_z e_t = \nabla_t e_z - ik_0 J h_t, \\ h_z &= -\frac{i}{k_0}(\partial_x e_y - \partial_y e_x), \quad \partial_z h_t = \nabla_t h_z + ik_0 J e_t. \end{aligned} \tag{147}$$

After transverse Fourier transformation this is a four-component constant coefficient ordinary differential equation for each ξ. Its matrix entries are polynomials of degree at most two in ξ, with fixed coefficients depending on k_0. On the bounded Fourier support the matrix exponential and every fixed number of its derivatives are bounded for $|z| \le h$. Inverse Fourier transformation therefore supplies smooth fields, with every transverse derivative and every z derivative in $L^2(\Omega_h)$. In particular their weighted field norm is finite. The normal definitions and the tangential evolution are exactly all six curl equations, so $\operatorname{curl} e = ik_0 h$ and $\operatorname{curl} h = -ik_0 e$. This also proves the divergence conditions.

At the measurement plane, $S_z = (c_0/2)\operatorname{Re}(e \times \overline{h}) \cdot \hat{z} = (c_0 C^2/2)|f_a|^2 = |f_a|^2$. Orthogonality and (145) give all four assertions in (141). They hold for every vector, not merely for the basis fields or a sample of random inputs. Nonzero f_a also proves linear independence of the fields. □

Proposition 8.4 (The flux normalization permits unbounded field resource)**.** *For the fields in Theorem 8.3, set $q_{\min} = Q + 2b$. Their local slab resource satisfies*

$$\int_{\Omega_h} (|e_a|^2 + |h_a|^2)\, dx\, dy\, dz \ge \frac{4h}{c_0 k_0^2} q_{\min}^2 \|a\|^2. \tag{148}$$

Thus the same coherent flux and bypass bounds coexist with arbitrarily large resource at fixed N, D, h, k_0, δ in this local class.

Proof. The vacuum Maxwell equations imply $(\Delta + k_0^2)h_z = 0$. For each Fourier frequency in the support, put $\kappa(\xi) = \sqrt{|\xi|^2 - k_0^2} > 0$. The component has the form $u(z) = u(0)\cosh(\kappa z) + u'(0)\sinh(\kappa z)/\kappa$. When $|u|^2$ is integrated on $(-h, h)$ its cross term is odd, and both remaining terms are nonnegative. Hence $\int_{-h}^{h} |u(z)|^2 dz \ge 2h|u(0)|^2$. Plancherel and (146) yield

$$\int_{\Omega_h} |h_z|^2 \ge \frac{2hC^2}{k_0^2}\|\partial_x f_a\|_2^2 \ge \frac{4h}{c_0 k_0^2} q_{\min}^2 \|a\|^2, \tag{149}$$

which is bounded above by the total resource. □

8.3 Why the local theorem is not the requested counterexample

Proposition 8.5 (Failure of a vacuum outgoing completion)**.** *No nonzero field of Theorem 8.3 can be continued into an entire homogeneous vacuum upper half-space with the outgoing condition that every evanescent Fourier component decays as $z \to +\infty$.*

Proof. The transverse Fourier support is preserved by vacuum evolution and contains only $|\xi| > k_0$, with a positive distance from the light circle. An outgoing continuation therefore has exponentially decaying L^2 electric and magnetic slices as $z \to +\infty$, implying $P_\Pi(z) \to 0$ by Cauchy–Schwarz. On the other hand, the full-plane integrated flux of a source-free vacuum solution with these L^2 slices is independent of z. One way to justify this is to integrate the divergence-free real Poynting vector over a transverse cutoff of radius R. Its lateral error is bounded by C/R times the L^1 norm of the transverse Poynting field integrated over the finite z interval. That norm is finite by Cauchy–Schwarz, so the error tends to zero. Conservation would give $P_\Pi(z) = P_\Pi(0) = \|a\|^2 > 0$, a contradiction. □

The example therefore cannot acquire a physical incoming-power normalization by simply declaring its coefficient space to be an incident channel space. Formally appending $T = I_N$ would satisfy throughput and, for $\eta \le 1 - \delta$, passage, but it would not construct the global field-to-port map required in Assumption 1.2.

Proposition 8.6 (No exact realization of these entire slab data by a compact exterior device)**.** *Suppose a proposed dielectric perturbation is compactly supported outside Ω_h and the exterior convention consists of propagating incoming radiation and outgoing scattered radiation. It cannot have a nonzero field of Theorem 8.3 as its exact total field on all of Ω_h.*

Proof. The Fourier Cauchy construction defines a homogeneous Maxwell solution $F^0 = (e^0, h^0)$ on all of $\mathbb{R}^3$: for every finite z its bounded Fourier support makes the matrix exponential well defined. Let F be the proposed scattering field. The difference $F - F^0$ is a homogeneous vacuum Maxwell field in the unbounded connected component of the complement of the material support, and is zero on the entire open slab. Each component satisfies the constant-coefficient Helmholtz equation, so analytic continuation implies equality throughout that connected component, in particular everywhere outside a sufficiently large ball.

Choose z_0 above that ball. The entire half-space $z > z_0$ is vacuum, and $F = F^0$ there. Its transverse spectrum is the same bounded set $|\xi| > k_0$ as before. In a homogeneous exterior half-space the stated radiation convention permits incoming propagating components, outgoing propagating components, and evanescent components decaying toward infinity; it excludes growing evanescent components. This follows as well by transverse Fourier transformation of the outgoing vacuum Green function and of the incident propagating angular spectrum: the longitudinal root for $|\xi| > k_0$ has positive imaginary part. There are no propagating components in the present support. The field therefore decays toward $+\infty$ in L^2 slices, contradicting its conserved flux $\|a\|^2 > 0$, exactly as in Proposition 8.5. □

Thus even the exact local packet data are not a ready-made physical counterexample. A resonant construction would need a quantitatively controlled *approximation* to suitable concentrated data, or different accessible fields, with input power and every coherent error tracked. Proposition 8.6 does not exclude that possibility, nor does it exclude arbitrary external resonant matching.

8.4 Matching theory and the global realization problem

The reflectionless-scattering analysis of Stone and coauthors [17] gives a Maxwell formulation of reflection zeros and structural tuning to a real-frequency reflectionless state. Its multichannel state is a selected coherent input vector. Such a state does not assert an N-dimensional subspace with uniformly high transmission at the same frequency, nor does it certify passage and absolute bypass through a fixed small section. Applying that framework therefore still requires the simultaneous synthesis and error control identified in Remark 7.15.

Remark 8.7 (Global bridge required beyond these local packets)**.** The local analysis identifies two substantive global tasks. A proof must restrict the radiatively accessible trace subspaces of all admitted bounded-index devices strongly enough to give the uniform finite-rank estimate of Lemma 6.1, despite arbitrary external support and feedback. A disproof must realize an unbounded sequence of positive-flux trace subspaces with power-normalized incident and delivered channels and controlled absolute bypass. Theorem 8.3 shows that local Maxwell equations and even a whole-plane coherent bypass certificate cannot replace that global step. Proposition 8.1 only closes the empty parameter regime $\eta\tau > 1 + \delta$; it does not resolve the meaningful positive-throughput regime. These packet arguments do not give a physical counterexample. The subsequent edge-sphere construction in Theorem 19.1 does supply one for $\delta > \eta$, without completing these exact packets.

Remark 8.8 (Formalization boundary)**.** Finite-dimensional Loewner consequences, norm perturbation certificates, and dimension lemmas can be formalized independently. Such Lean statements do not formalize the existence of a Maxwell scattering realization. The local packet argument requires Fourier analysis, the stated Maxwell evolution, and flux integration; finite-dimensional certificates alone cannot supply a global realization. The later edge-sphere construction in Theorem 19.1 supplies that realization through its actual material volume equation and whole-plane error estimates. Section A.2 identifies its complete Lean existence endpoint, including the physical incoming Hilbert space and the same-device passivity identity. The global bridge is proved within this chain, rather than introduced as a mathematical axiom.

9 Radial channels: bypass, local synthesis, and gain limits

The large multiplicity $2\ell+1$ of a spherical partial wave and the unbounded radial Bragg amplification in Proposition 7.1 suggest a concrete possible counterexample. This section tests that proposal directly at the physical section. The resulting obstruction does not assume a field-energy bound or a bound on the exterior support. It applies to a single angular order in a homogeneous core, including arbitrary coherent combinations of all azimuthal indices and both electric and magnetic multipoles. Mixed angular orders and a structured core remain outside its scope.

The distinction between field amplitude and transported power is central to this test. A high-order spherical mode can have many angular patterns and a large field in the core, but neither fact says that all of those patterns carry power through D without a comparable return outside it. We first isolate that return using symmetry, then examine a single spherical order. The later synthesis and gain estimates show how far one can go by adjusting the radial medium; they do not by themselves supply a counted channel space.

9.1 Inversion parity and the threshold regime

Proposition 9.1 (An odd plane flux must return outside the section)**.** *Let $s \in L^1(\mathbb{R}^2)$ be a real normal power density, and suppose $s(2c - x) = -s(x)$ almost everywhere for some point c in the*

section plane. For any measurable section D,

$$\int_{\mathbb{R}^2\setminus D} |s|\,dA \;\geq\; \left|\int_D s\,dA\right|. \tag{150}$$

Consequently a nonzero counted input with this symmetry requires $\delta \geq \eta\tau$. This conclusion does not require that D be centered at c.

Proof. The intersection $D \cap (2c - D)$ is invariant under $x \mapsto 2c - x$, so its signed integral is zero. The reflection of $D \setminus (2c - D)$ is contained in the complement of D, and has the opposite signed integral. Taking its absolute integral proves (150). The counted-input inequalities then give $\delta\|a\|^2 \geq P_D(a) \geq \eta\tau\|a\|^2$. □

Remark 9.2 (Application to a Maxwell parity sector)**.** In a medium invariant under inversion about c, a field satisfying $E(2c - x) = \sigma E(x)$, $\sigma \in \{1, -1\}$, satisfies $H(2c - x) = -\sigma H(x)$ by the first curl equation. Its real Poynting vector is therefore odd. If c lies in the section plane and the required traces are integrable, Proposition 9.1 applies. In particular, a coherent sum of electric-type multipoles of one angular order has one parity, as does a coherent sum of magnetic-type multipoles of that order. Merely using their azimuthal degeneracy does not give passage in the regime $\delta < \eta\tau$. If the square is centered at c, its signed passage is exactly zero. Mixing the two parities is necessary for this centered construction; it is not sufficient, as the next theorem shows.

9.2 Both polarizations of a regular spherical partial wave

Fix a homogeneous ball centered at the center of D, with real permittivity $n^2\varepsilon_0$ and permeability μ_0. Write $k = nk_0$ and $Z = \sqrt{\mu_0/(n^2\varepsilon_0)}$. Let $\nu = \ell(\ell + 1)$, $\ell \geq 1$, and let $Y_{\ell m}$ be any orthonormal complex spherical-harmonic basis. For coefficient vectors $A, B \in \mathbb{C}^{2\ell+1}$ define

$$Y_A = \sum_m A_m Y_{\ell m}, \quad \Psi_A = \nu^{-1/2}\nabla_{\mathbb{S}^2} Y_A, \quad X_A = \widehat{r} \times \Psi_A, \tag{151}$$

and similarly for B. With $j = j_\ell(kr)$, put

$$u = rj, \qquad a_\ell(r) = \frac{\sqrt{\nu}\, j}{kr}, \qquad b_\ell(r) = \frac{u'}{kr}. \tag{152}$$

The notation a_ℓ, b_ℓ in this section denotes radial functions, not external incoming amplitudes. The general regular field at this one angular order can be written

$$\begin{aligned} E &= jX_A - a_\ell Y_B \widehat{r} - b_\ell \Psi_B, \\ H &= -\frac{i}{Z}(-a_\ell Y_A \widehat{r} - b_\ell \Psi_A + jX_B). \end{aligned} \tag{153}$$

The usual two regular spherical Maxwell waves give this representation: if $M_A = jX_A$ and $N_A = k^{-1}\nabla \times M_A$, direct spherical differentiation gives $N_A = -a_\ell Y_A \widehat{r} - b_\ell \Psi_A$, $\nabla \times N_A = kM_A$, and hence both Maxwell curl equations hold in (153). Regularity excludes the singular spherical Bessel solution. All possible complex coefficients, including those generated by a distant resonant dielectric, are allowed.

Lemma 9.3 (The plane flux separates into opposite parities)**.** *On the equatorial plane $z = 0$, a field (153) has*

$$S_z(r, \varphi) = F_\ell(r)O(\varphi) + G_\ell(r)C(\varphi), \tag{154}$$

where the real angular functions satisfy $O(\varphi+\pi)=-O(\varphi)$ and $C(\varphi+\pi)=C(\varphi)$, and

$$F_\ell=\frac{a_\ell j}{2Z}=\frac{\sqrt{\nu}\,u^2}{2Zkr^3},\qquad G_\ell=\frac{a_\ell b_\ell}{2Z}=\frac{\sqrt{\nu}\,uu'}{2Zk^2r^3}. \tag{155}$$

Explicitly, with all angular expressions evaluated at $\theta=\pi/2$,

$$\begin{aligned} O&=-\operatorname{Im}(\overline{Y_A}\Psi_{A,\theta}+\overline{Y_B}\Psi_{B,\theta}),\\ C&=\operatorname{Im}(Y_B\overline{X_{A,\theta}}-\overline{Y_A}X_{B,\theta}). \end{aligned} \tag{156}$$

Proof. At the equator $\widehat{z}=-\widehat{\theta}$. In $E\times\overline{H}$, the tangential terms arise only by crossing one radial and one tangential component. Substituting (153), and using $X\times\widehat{r}=\Psi$, $\Psi\times\widehat{r}=-X$, $\widehat{r}\times X=-\Psi$, gives (154)–(156). For completeness, the tangential vector inside the factor i/Z is

$$a_\ell j(Y_B\overline{\Psi_B}-\overline{Y_A}\Psi_A)+a_\ell b_\ell(Y_B\overline{X_A}-\overline{Y_A}X_B). \tag{157}$$

Taking one half its real part after multiplication by i/Z, then changing from the θ component to z, gives the stated signs.

The spherical-harmonic inversion identity gives $Y_A(\pi/2,\varphi+\pi)=(-1)^\ell Y_A(\pi/2,\varphi)$, whereas its θ derivative gains the opposite sign. Since $X_\theta=-\nu^{-1/2}\partial_\varphi Y$ at the equator, X_θ gains the same sign as Y. These facts prove the two angular parity assertions for arbitrary coherent coefficients. □

Lemma 9.4 (Radial growth below the angular turning scale)**.** *Let $R_2>0$ and assume $\nu>k^2R_2^2$. Define*

$$\gamma=\frac{1+\sqrt{1+4(\nu-k^2R_2^2)}}{2}>1. \tag{158}$$

Then the regular real solution $u=rj_\ell(kr)$ is positive with $u'>0$ for $0<r\le R_2$, and

$$\gamma\le\frac{ru'(r)}{u(r)}\le\ell+1,\qquad \frac{u(t)}{u(s)}\ge(t/s)^\gamma\quad(0<s\le t\le R_2). \tag{159}$$

Proof. The radial equation is $u''=(\nu/r^2-k^2)u$ and $u(r)=cr^{\ell+1}(1+O(r^2))$ with $c>0$. The coefficient of u is positive throughout this interval, so a first zero of u or u' is impossible. For $w=ru'/u$ the equation is

$$rw'=\nu-k^2r^2+w-w^2. \tag{160}$$

At $w=\gamma$ its right side is $k^2(R_2^2-r^2)\ge0$, and at $w=\ell+1$ it is $-k^2r^2<0$. The initial expansion has $w=\ell+1-k^2r^2/(2\ell+3)+O(r^4)$, so w begins in the interval $[\gamma,\ell+1]$ and cannot exit it. A first crossing at the lower endpoint can equivalently be excluded by the scalar comparison equation, including the equality case at R_2. Integrating $u'/u\ge\gamma/r$ proves the ratio bound. □

Theorem 9.5 (High angular degeneracy cannot evade absolute bypass in a homogeneous core)**.** *Let $R=L/\sqrt{2}$ be the circumradius of the fixed square D, fix $1<s<t$, and assume a homogeneous source-free ball of radius tR about its center. Consider any regular Maxwell field in this ball supported in one angular order ℓ, with arbitrary coefficients A,B in (153). If $\ell(\ell+1)>k^2t^2R^2$, let γ be (158) with $R_2=tR$, and set*

$$B_\ell(s,t)=\frac{\gamma}{\ell+1}\big(t^{2\gamma-2}-s^{2\gamma-2}\big). \tag{161}$$

Then its physical flux obeys the local, amplitude-independent estimate

$$\int_{sR<r<tR,\ z=0}|S_z|\,dA\ \ge\ B_\ell(s,t)\,|P_D|. \tag{162}$$

In particular any nonzero counted input whose core field is of this angular order must satisfy

$$\delta \geq B_\ell(s,t)\eta\tau. \tag{163}$$

At fixed k, R, s, t, $B_\ell(s,t) \to \infty$ exponentially as $\ell \to \infty$. Neither exterior field energy nor a radial mirror's quality factor appears in this inequality.

Proof. By Lemma 9.4, $G_\ell > 0$ on $(0, tR]$. The square is centrally symmetric, so the integral of the odd term $F_\ell O$ in (154) over D is zero. Writing the square in polar coordinates and using its circumradius,

$$|P_D| \leq \left(\int_0^R G_\ell(r) r\, dr\right)\left(\int_0^{2\pi} |C(\varphi)|\, d\varphi\right). \tag{164}$$

On the full annulus, opposite angles have fluxes $FO + GC$ and $-FO + GC$. The triangle inequality $|x+y| + |-x+y| \geq 2|y|$ gives

$$\int_{sR<r<tR} |S_z|\, dA \geq \left(\int_{sR}^{tR} G_\ell(r) r\, dr\right)\left(\int_0^{2\pi} |C(\varphi)|\, d\varphi\right). \tag{165}$$

There is no basis-only estimate here: both bounds apply to the full coherent field with its actual A, B.

The common positive factor $\sqrt{\nu}/(2Zk^2)$ cancels in the ratio of the radial integrals, leaving integrals of uu'/r^2. By (159),

$$\begin{aligned} \int_0^R \frac{uu'}{r^2}\, dr &\leq \frac{\ell+1}{2\gamma-2}\frac{u(R)^2}{R^2}, \\ \int_{sR}^{tR} \frac{uu'}{r^2}\, dr &\geq \frac{\gamma}{2\gamma-2}\frac{u(R)^2}{R^2}\left(t^{2\gamma-2} - s^{2\gamma-2}\right). \end{aligned} \tag{166}$$

For the first inequality use $u(r) \leq u(R)(r/R)^\gamma$ and $u' \leq (\ell+1)u/r$; for the second use the reverse growth bound for $r \geq R$ and $u' \geq \gamma u/r$. Combining (164)–(166) proves (162); if C vanishes identically, then $P_D = 0$ and the assertion is immediate. The annulus lies outside D, so the counted-input conditions imply (163). Finally $\gamma = \ell + 1 + O(\ell^{-1})$ at fixed ktR, which proves the claimed divergence. □

Corollary 9.6 (A limitation of the degenerate Bragg proposal)**.** *Fix the homogeneous core, the section, and the annulus in Theorem 9.5, together with finite $\delta \geq 0$ and $\eta, \tau > 0$. There is a finite angular-order cutoff beyond which no nonzero counted input can have a pure ℓ core field. This remains true if arbitrary passive dielectric layers outside the core make either or both polarization amplitudes arbitrarily large. In particular increasing $2\ell + 1$ at a single resonance does not by itself yield an unbounded counted subspace through this fixed section.*

Proof. The constant $B_\ell(s,t)$ tends to infinity, whereas $\delta/(\eta\tau)$ is fixed. All exterior amplification is already included in the arbitrary coefficients A, B and cancels in the ratio. □

Remark 9.7 (Scope and the remaining constructive alternatives)**.** This is a genuine Maxwell exclusion for the stated spherical route, not a uniform theorem for Conjecture 1.4. A coherent mixture of different angular orders has additional interference terms with different radial factors; the proof does not bound them. Nor does it cover a dielectric structured throughout the core, a spherical center moving away with angular order, or a plane that does not pass through that center. Such changes are allowed by the unrestricted target and require a new argument.

The parameter regime $\delta \geq \eta\tau$ permits the return-flow mechanism in Proposition 9.1; it does not prove that an arbitrarily large physical counted subspace exists. A large bypass tolerance, a choice of the full lossless scattering map as T, or a single circulating high-Q field is not by itself a quantifier counterexample. The throughput threshold still requires independent physical inputs, and passage must hold for every coherent vector. No admissible all-device counterexample for either threshold regime is inferred here.

9.3 An actual local inverse-synthesis step for mixed angular orders

The preceding obstruction does not make a mixed-order proposal impossible. Conversely, saying that radial layers can independently tune every partial wave is an extra claim. The following local version of that claim can be proved for finite ordinary dielectrics, including control of the interior amplitude rather than only the scattering phase.

Theorem 9.8 (Local independent control of finitely many complex core amplitudes)**.** *Fix $k_0 > 0$, $\varepsilon_+ > 1$, a radius $R_0 > 0$, an annulus $0 < r_- < r_+ < R_0$, and distinct positive angular orders $l_1, \dots, l_m$. Choose $1 < n_b^2 < \varepsilon_+$. There exist $2m$ real smooth radial functions h_j supported in (r_-, r_+) such that the finite scalar dielectric*

$$\varepsilon_\theta(r) = \begin{cases} n_b^2 + \sum_{j=1}^{2m} \theta_j h_j(r), & r < R_0, \\ 1, & r > R_0 \end{cases} \tag{167}$$

has the following property for all sufficiently small real $\theta \in \mathbb{R}^{2m}$.

For each $l = l_i$, fix the leading coefficient at the origin of the regular real TE radial solution u_l independently of θ. In the vacuum exterior write

$$u_l(r;\theta) = A_l(\theta)\, \xi_l^-(k_0 r) + \overline{A_l(\theta)}\, \xi_l^+(k_0 r), \qquad \xi_l^\pm(x) = x h_l^{(2/1)}(x). \tag{168}$$

Here ξ_l^- uses $h_l^{(2)}$ and ξ_l^+ uses $h_l^{(1)}$. Each A_l is nonzero. The map

$$\theta \longmapsto \left(\operatorname{Re} \log \frac{A_{l_i}(\theta)}{A_{l_i}(0)}, \operatorname{Im} \log \frac{A_{l_i}(\theta)}{A_{l_i}(0)} \right)_{i=1}^{m} \tag{169}$$

is a real-analytic local diffeomorphism at zero. Thus every sufficiently small prescribed change of all m core gains and all m scattering phases is realized by a physical radial permittivity in the same fixed interval $[1, \varepsilon_+]$.

Here is one explicit, retained neighborhood certificate. Denote the map in (169) by $\mathcal{F}$, let σ be the smallest singular value of $J = D\mathcal{F}(0)$, and choose a parameter ball of radius ρ on which

$$\rho \left(\sum_j \|h_j\|_\infty^2 \right)^{1/2} < \min(n_b^2 - 1, \varepsilon_+ - n_b^2), \qquad \sup_{|\theta| \leq \rho} \|D\mathcal{F}(\theta) - J\| \leq \sigma/2. \tag{170}$$

The logarithms are taken on their continuous branches near zero. Then every target vector of Euclidean norm less than $\sigma\rho/2$ is attained in this parameter ball. No lower bound on $\sigma\rho$ uniform in m is asserted.

Proof. The TE equation, its interface conditions, and its regular normalization are

$$u_l'' + \left(k_0^2 \varepsilon_\theta(r) - \frac{l(l+1)}{r^2} \right) u_l = 0, \qquad u_l, u_l' \text{ continuous.} \tag{171}$$

Since every control vanishes near zero, the regular initial data can be set at any fixed radius below r_-. Standard successive integration of this first-order system on a finite interval gives real-analytic dependence on the finite parameters. The two vacuum Hankel solutions have Wronskian $2ik_0$, with the convention $W(f,g) = fg' - f'g$. The real nonzero regular solution has conjugate exterior coefficients, so $A_l = 0$ would force the solution to vanish outside and then everywhere. This proves its nonvanishing and the local analytic logarithms.

Let $z_l(r)$ be the outgoing radial solution, equal to $\xi_l^+(k_0 r)$ outside R_0, continued inward through the base material at $\theta = 0$. A real variation $h(r)$ changes the regular solution by $\dot{u}_l$ satisfying

$$\dot{u}_l'' + \left(k_0^2 \varepsilon_0 - l(l+1)/r^2\right) \dot{u}_l = -k_0^2 h u_l, \qquad \dot{u}_l = \dot{u}_l' = 0 \quad (r < r_-). \tag{172}$$

Differentiate $W(\dot{u}_l, z_l)$, using the unperturbed equation for z_l, and integrate. Evaluation in the exterior gives the exact first-variation formula

$$D \log A_l(0)[h] = \frac{k_0}{2i A_l(0)} \int_{r_-}^{r_+} h(r) u_l(r) z_l(r)\, dr. \tag{173}$$

This formula controls the complex incoming coefficient, not just the phase of a unit-modulus scattering coefficient.

Put $\kappa = n_b k_0$, $\psi_l(x) = x j_l(x)$, and $\zeta_l(x) = x y_l(x)$. Inside the base sphere, $u_l = c_l \psi_l(\kappa r)$ with real $c_l \neq 0$, while

$$z_l = \alpha_l \psi_l(\kappa r) + \beta_l \zeta_l(\kappa r). \tag{174}$$

The real Wronskian of $\psi_l(\kappa r)$ and $\zeta_l(\kappa r)$ is κ. In the vacuum exterior, $W(z_l, \overline{z_l}) = -2ik_0$; consequently

$$\operatorname{Im}(\alpha_l \overline{\beta_l}) = -k_0/\kappa \neq 0. \tag{175}$$

Thus the real and imaginary parts of the kernel in (173) are obtained by an invertible real two-by-two change of basis from

$$\psi_l(\kappa r)^2, \qquad \psi_l(\kappa r)\zeta_l(\kappa r). \tag{176}$$

We now prove independence of all $2m$ real functions in (176). Their expressions extend analytically through zero: the first functions are even and the second odd, since the zero of ψ_l cancels the pole of ζ_l. An identity on the prescribed annulus therefore extends to all real arguments and separates into its even and odd parts. The squares are independent because their first nonzero Taylor orders $2l_i + 2$ are distinct.

For the odd products use the exact finite Hankel expressions

$$\xi_l^+(x) = (-i)^{l+1} e^{ix} p_l(x), \qquad \xi_l^-(x) = i^{l+1} e^{-ix} \widetilde{p}_l(x), \tag{177}$$

where $p_l, \widetilde{p}_l$ are polynomials of degree l in $1/x$ with nonzero leading coefficients. These follow directly by the spherical-Bessel recurrence starting from the sine and cosine solutions at $l = 0$; they are also displayed in (70). Since

$$\psi_l \zeta_l = \frac{(\xi_l^+)^2 - (\xi_l^-)^2}{4i}, \tag{178}$$

a nontrivial linear relation among the odd products would imply $e^{4ix} P(1/x) = Q(1/x)$ for two polynomials P, Q. If P is nonzero, the quotient $Q(1/x)/P(1/x)$ has either a finite limit, zero limit, or diverging modulus as $x \to +\infty$; none equals e^{4ix}. Thus $P = Q = 0$. The coefficient of the highest remaining power x^{-2l_i} in P then forces the coefficient of the largest l_i to vanish. Descending induction forces all coefficients to vanish. This proves the claimed independence.

For any $2m$ independent continuous real functions on an interval, there exist $2m$ evaluation points whose value matrix is invertible. Indeed, if the span of all evaluation vectors were proper, a nonzero linear combination of the functions would vanish everywhere. Choose such points for the real derivative kernels in (173). Real smooth unit-integral bumps h_j in sufficiently small, disjoint neighborhoods of those points make the derivative matrix as close as desired to that invertible evaluation matrix. Hence J is invertible and $\sigma > 0$. The inverse-function theorem proves the qualitative local assertion.

For the retained certificate, write $\mathcal{F}(\theta) = J\theta + \mathcal{R}(\theta)$. The second condition in (170) makes $\mathcal{R}$ Lipschitz with constant $\sigma/2$ on the parameter ball and $\mathcal{R}(0) = 0$. For a target y with $|y| < \sigma\rho/2$, the map $\theta \mapsto J^{-1}(y - \mathcal{R}(\theta))$ is a contraction of that ball into itself. Its fixed point realizes y. The first condition in (170) keeps the permittivity strictly within its prescribed bounds.

Finally, for the angular normalization $\int_{S^2} |X_{lm}|^2 \, dS = 1$, an incoming TE radial amplitude A carries physical power $|A|^2/(2Z_0)$ in the vacuum exterior. Thus the field produced by unit incoming power has regular-core amplitude $\sqrt{2Z_0}/A_l$ in the normalization above, while its outgoing-to-incoming coefficient is $\overline{A_l}/A_l$. The real and imaginary logarithms controlled in (169) are precisely the logarithmic core gain with a minus sign, and minus one half the scattering phase. The vacuum power convention does not change with the controls. □

Remark 9.9 (The local synthesis range is not an arbitrary matching network)**.** Theorem 9.8 supplies actual radial Maxwell material controls for a finite set of angular orders. It neither makes A_l arbitrarily small simultaneously nor estimates the absolute flux on the whole section plane. The certified target neighborhood may shrink with the number and size of the angular orders. Iterating local invertibility without a continuation estimate would not prove global reachability within the fixed permittivity bounds. Independent tuning of finitely many scattering phases alone would be still weaker, because it would not control the gain represented by $|A_l|^{-1}$.

Corollary 9.10 (Local control of both polarizations at separated orders)**.** *If the selected positive angular orders additionally satisfy $|l_i - l_j| \geq 3$ for $i \neq j$, there exist $4m$ smooth real radial controls in the same prescribed annulus that independently vary, locally, the complex regular-core incoming coefficients of both TE and TM polarizations at all selected orders. All material and physical normalization conclusions of Theorem 9.8 remain valid, with a $4m$-dimensional Jacobian and its own retained neighborhood constants.*

Proof. For the TM polarization choose the magnetic radial amplitude u. Its real equation and transmission conditions are

$$(\varepsilon^{-1}u')' + \left(k_0^2 - \frac{l(l+1)}{\varepsilon r^2}\right) u = 0, \qquad u,\ \varepsilon^{-1}u' \text{ continuous.} \tag{179}$$

It has the same regular/irregular basis inside a constant-index core and the same vacuum radial Hankel basis outside. If z_l is its continued outgoing solution, differentiating the weighted Wronskian $\varepsilon^{-1}W(\dot{u}_l, z_l)$ and integrating by parts gives

$$D \log A_l^{\mathrm{TM}}(0)[h] = \frac{1}{2ik_0 A_l^{\mathrm{TM}}(0) n_b^4} \int h(r) \left(u_l' z_l' + \frac{l(l+1)}{r^2} u_l z_l\right) dr. \tag{180}$$

Indeed $\dot{p} = -h/n_b^4$ for $p = \varepsilon^{-1}$, and the integrated weighted-Wronskian derivative is $-\int \dot{p}(u_l' z_l' + l(l+1)u_l z_l/r^2)$. The endpoint terms vanish since the control has compact support inside the annulus. The exterior weighted Wronskian is again $2ik_0 \dot{A}_l^{\mathrm{TM}}$.

Inside the sphere write $u_l = c_l\psi_l(\kappa r)$ and $z_l = \alpha_l\psi_l(\kappa r) + \beta_l\zeta_l(\kappa r)$. The weighted outgoing Wronskian gives $\operatorname{Im}(\alpha_l\overline{\beta_l}) = -n_b \neq 0$. Consequently the real and imaginary derivative kernels are an invertible real change of basis from

$$(\psi_l')^2 + \frac{l(l+1)}{x^2}\psi_l^2, \qquad \psi_l'\zeta_l' + \frac{l(l+1)}{x^2}\psi_l\zeta_l, \quad x = \kappa r. \tag{181}$$

The common factor κ^2 is immaterial for independence.

The elementary recurrences $\psi_{l-1} = \psi_l' + l\psi_l/x$ and $\psi_{l+1} = (l+1)\psi_l/x - \psi_l'$, and the identical recurrences for ζ_l, imply

$$\begin{aligned}(\psi_l')^2 + \frac{l(l+1)}{x^2}\psi_l^2 &= \frac{l+1}{2l+1}\psi_{l-1}^2 + \frac{l}{2l+1}\psi_{l+1}^2,\\ \psi_l'\zeta_l' + \frac{l(l+1)}{x^2}\psi_l\zeta_l &= \frac{l+1}{2l+1}\psi_{l-1}\zeta_{l-1} + \frac{l}{2l+1}\psi_{l+1}\zeta_{l+1}.\end{aligned} \tag{182}$$

The independence proof for the product kernels in the preceding theorem also includes order zero. The triples $\{l_i - 1, l_i, l_i + 1\}$ are disjoint by hypothesis. The TE pair uses the middle index of each triple; the TM pair is a nonzero combination of its two unused neighboring indices, separately in the even and odd kernel families. All $4m$ derivative functions are therefore independent. The same evaluation-point, smooth-bump, and inverse-function argument now proves the corollary. For the magnetic normalization of TM waves, incoming power is $Z_0|A|^2/2$, another fixed vacuum factor independent of the controls. □

Proposition 9.11 (Fixed-annulus controls have a finite gain ceiling)**.** *Keep $r_- > 0$, R_0, the interior material on $r < r_-$, and an angular order l fixed. Let the material vary arbitrarily on $r_- < r < R_0$ within $1 \le \varepsilon \le \varepsilon_+$, with finitely many smooth pieces, and let it be vacuum beyond R_0. For either polarization, the incoming coefficient A_l of the same origin-normalized regular solution obeys a strictly positive lower bound independent of the number and thickness of radial layers.*

Here is an explicit bound. For TE let $v = (u, u'/k_0)^T$; for TM let $v = (u, \varepsilon^{-1}u'/k_0)^T$. Set

$$\begin{aligned}C_l &= k_0(R_0 - r_-)\max\left(\varepsilon_+, 1 + \frac{l(l+1)}{k_0^2 r_-^2}\right),\\ V_l &= \begin{pmatrix}\operatorname{Re}\xi_l^-(k_0R_0) & -\operatorname{Im}\xi_l^-(k_0R_0)\\ \operatorname{Re}(\xi_l^-)'(k_0R_0) & -\operatorname{Im}(\xi_l^-)'(k_0R_0)\end{pmatrix}.\end{aligned} \tag{183}$$

The primes in V_l are argument derivatives. Then

$$|A_l| \ge \frac{e^{-C_l}|v(r_-)|}{2\|V_l\|} > 0. \tag{184}$$

Proof. The states are continuous across every radial interface. Away from interfaces their first-order systems are respectively

$$v' = k_0\begin{pmatrix}0 & 1\\ l(l+1)/(k_0^2r^2) - \varepsilon & 0\end{pmatrix}v, \qquad v' = k_0\begin{pmatrix}0 & \varepsilon\\ l(l+1)/(k_0^2\varepsilon r^2) - 1 & 0\end{pmatrix}v. \tag{185}$$

For a real matrix with off-diagonal entries a, b and zero diagonal, the Euclidean operator norm is $\max(|a|, |b|)$. Both generators are therefore bounded by $C_l/(R_0 - r_-)$ on the interval. Gronwall applied also to reverse propagation gives $|v(R_0)| \ge e^{-C_l}|v(r_-)|$. The initial state is fixed and nonzero by uniqueness of the regular radial solution. On the vacuum side of the final interface, (168) gives $v(R_0) = 2V_l(\operatorname{Re}A_l, \operatorname{Im}A_l)^T$. The Hankel Wronskian makes V_l invertible, and its norm is finite. This proves (184). □

Remark 9.12 (Focused global continuation attempt and its exact limits)**.** The local controls can leave every selected scattering phase fixed while changing the selected core gains: prescribe zero imaginary coordinates in (169). Thus phase matching by itself does not determine the internal response. But the controls cannot be iterated inside their fixed bounded annulus to obtain arbitrarily large gains; Proposition 9.11 gives an explicit obstruction to that proposed iteration, even with arbitrarily many increasingly thin layers.

Allowing the controlled radius to increase removes this particular ceiling, as the frozen unrestricted target permits. It also adds an uncontrolled portion of the physical section plane. Endpoint radial transfer data A_l do not estimate its absolute normal flux. The single-order estimate in Theorem 9.5 gives a concrete case in which the exterior plane cost grows rather than disappears under amplification. Theorem 11.6 below supplies approximate global reachability for any finite set of TE orders with increasing support, including independent core gains up to a common phase. It does not supply simultaneous whole-plane bypass control. Corollary 14.6 further bounds the counted dimension in a sufficiently large vacuum core for every fixed finite angular band, regardless of gain. The unrestricted finite-channel statement is still unresolved by this route.

10 Growing radial support: simultaneous gain and its flux cancellation

This section carries a growing-support construction through the actual radial Maxwell equations. It proves simultaneous large gains for any prescribed finite band of partial waves. It also proves why this particular construction does not give many power channels: the gains of opposite electric inversion parities are reciprocal, whereas signed flux through a centered section couples those opposite parities. The resulting channel bound is independent of the mirror length and radius within the prescribed band. It is not a bound for arbitrary dielectric geometry or for partial waves outside that band.

The useful comparison is between two effects of the same layers: they can amplify certain field components, but they amplify their partners by the reciprocal factor. The flux couples those partners, so large internal fields need not yield a correspondingly large passage operator. We first bound the vacuum reference flux, construct the layers, and then evaluate their effect on the flux form in the chosen finite band.

10.1 A vacuum flux trace estimate with physical normalization

Lemma 10.1 (Trace-class vacuum section flux)**.** *Let $\mathcal{H} = L^2_t(S^2)$ be the power-normalized incoming vacuum space. For the regular vacuum Maxwell fields generated by (56), let Q^0_D be the Hermitian signed flux operator through a bounded planar section of area A. Then*

$$\|Q^0_D\|_1 \le \frac{2k_0^2 A}{\pi}. \tag{186}$$

If D is centrally symmetric about the origin, the positive part has

$$\mathrm{Tr}(Q^0_D)_+ \le \frac{k_0^2 A}{\pi}. \tag{187}$$

Consequently a subspace V with $\langle b, Q^0_D b\rangle \ge t\|b\|^2$ for all $b \in V$, $t > 0$, has dimension at most $k_0^2 A/(\pi t)$ in the symmetric case.

Proof. Denote the two restriction maps to $L^2(D;\mathbb{C}^3)$ by E and H. The physical normalization is

$$\mathsf{E}g(x) = \frac{k_0\sqrt{Z_0}}{\sqrt{2}\,\pi}\int_{S^2} g(d)e^{ik_0 d\cdot x}\,dS(d),$$
$$\mathsf{H}g(x) = \frac{k_0}{\sqrt{2Z_0}\,\pi}\int_{S^2} d\times g(d)e^{ik_0 d\cdot x}\,dS(d). \tag{188}$$

The incoming far-field amplitude is $\sqrt{2Z_0}\,g(-\widehat{x})/r$ up to a unit-modulus phase, so $\|g\|^2$ is incoming power. At each direction the tangential projection has trace two, and cross product by d is an isometry on its tangential range. Direct integration of the squared kernels therefore gives

$$\|\mathsf{E}\|_{\mathrm{HS}}^2 = \frac{4k_0^2 Z_0 A}{\pi}, \qquad \|\mathsf{H}\|_{\mathrm{HS}}^2 = \frac{4k_0^2 A}{\pi Z_0}. \tag{189}$$

For $Jv = v\times\widehat{z}$, $\|J\|\le 1$, and the flux operator is

$$Q_D^0 = \tfrac{1}{4}(\mathsf{E}^* J\mathsf{H} + \mathsf{H}^* J^*\mathsf{E}). \tag{190}$$

The product of two Hilbert–Schmidt operators is trace class, with trace norm bounded by the product of their Hilbert–Schmidt norms. The triangle inequality proves (186).

The electric inversion map $E(x)\mapsto E(-x)$ acts unitarily on the incoming space. Its two eigenspaces are the electric parity sectors. For a same-parity field the magnetic field has the opposite parity by the curl equation, so its Poynting density is odd and its flux through centered D vanishes. Polarization of this identity makes both diagonal blocks of Q_D^0 zero. The parity involution therefore conjugates Q_D^0 to $-Q_D^0$. Its positive and negative spectra have equal multiplicities, and their trace norms are equal. This proves (187). The compact selfadjoint min–max principle, followed by summing positive eigenvalues at least t, proves the dimension assertion. □

10.2 An explicit finite ordinary-dielectric stack

Fix $1 < q < \sqrt{\varepsilon_+}$, a positive integer L, and a number $M \ge 1$ of mirror periods. The dimensionless radius is $x = k_0 r$. Each period consists of a low-index interval of length $\pi/2$ followed by a high-index interval of length $\pi/(2q)$. The total dimensionless mirror length is

$$d_M = \frac{M\pi}{2}(1+q^{-1}). \tag{191}$$

Choose x_0 to be an integer multiple of π, and put $x_1 = x_0 + d_M$. The relative permittivity is vacuum for $x < x_0$ and $x > x_1$, and in a mirror interval with reference index $n\in\{1,q\}$ it is

$$\varepsilon(x) = n^2 + 2/x^2. \tag{192}$$

This is a compact, real, scalar, nonmagnetic dielectric with finitely many smooth radial pieces. If $x_0 \ge \sqrt{2/(\varepsilon_+ - q^2)}$, it obeys $1\le\varepsilon\le\varepsilon_+$ everywhere.

Here are explicit finite-band radius requirements. Write

$$p_l(x) = 1 + \sum_{s=1}^{l} a_{ls}x^{-s}, \qquad S_l = \sum_{s=1}^{l}|a_{ls}|, \quad T_l = \sum_{s=1}^{l} s|a_{ls}|, \quad K_L = 1 + \max_{1\le l\le L}(2S_l + T_l), \tag{193}$$

where a_{ls} are the finite Hankel coefficients in (70), and set $D_L = L(L+1)+2$. In addition to the material bound, require

$$x_0 \ge 1, \qquad x_0 \ge 8K_L q^{2M}, \qquad x_0^2 \ge 32 D_L d_M q^{4M+4}. \tag{194}$$

An integer multiple of π satisfying these finitely many lower bounds always exists. The growing radius is an allowed resource of this construction and is not hidden in a fixed-support claim.

Theorem 10.2 (Simultaneous reciprocal gain of all prescribed partial waves)**.** *For the dielectric (192) with (194), let $1 \le l \le L$ and consider either polarization. Normalize its real regular radial solution in the vacuum core to $u_l(x) = \psi_l(x) = x j_l(x)$, and write outside the device*

$$u_l(x) = A_l \xi_l^-(x) + \overline{A_l} \xi_l^+(x). \tag{195}$$

The coefficient is nonzero. For TE use the electric radial amplitude, and for TM the magnetic radial amplitude. Uniformly over the prescribed band and all azimuthal indices,

$$\frac{3}{16\sqrt{2}}\, q^{\sigma M} \le |A_l| \le \frac{5\sqrt{2}}{4}\, q^{\sigma M}, \tag{196}$$

where $\sigma = -1$ for TE odd l and TM even l, and $\sigma = +1$ for TE even l and TM odd l. Relative to the free-space regular solution with the same physical incoming amplitude, the core multiplier is $g_l = (2A_l)^{-1}$. Thus the electric-odd parity sector has gain q^M times a complex factor whose modulus lies between $2/(5\sqrt{2})$ and $8\sqrt{2}/3$; the electric-even sector has gain q^{-M} times such a factor.

Proof. For TE take the dimensionless state $v = (u, u_x')^T$, and for TM take $v = (u, \varepsilon^{-1} u_x')^T$. These states are continuous at every layer interface, and satisfy, respectively,

$$v' = \begin{pmatrix} 0 & 1 \\ l(l+1)/x^2 - \varepsilon & 0 \end{pmatrix} v, \qquad v' = \begin{pmatrix} 0 & \varepsilon \\ l(l+1)/(\varepsilon x^2) - 1 & 0 \end{pmatrix} v. \tag{197}$$

Their reference generators on an index-n interval are obtained by discarding the x^{-2} terms and setting $\varepsilon = n^2$. The exact quarter-period reference matrices are

$$T_n^{\mathrm{TE}} = \begin{pmatrix} 0 & 1/n \\ -n & 0 \end{pmatrix}, \qquad T_n^{\mathrm{TM}} = \begin{pmatrix} 0 & n \\ -1/n & 0 \end{pmatrix}. \tag{198}$$

The full reference products, in physical layer order, are

$$U_0^{\mathrm{TE}}(x_1, x_0) = (-1)^M \operatorname{diag}(q^{-M}, q^M), \qquad U_0^{\mathrm{TM}}(x_1, x_0) = (-1)^M \operatorname{diag}(q^M, q^{-M}). \tag{199}$$

Within an individual reference interval, each propagator and its inverse has norm at most q. Combining complete period products with the at most two partial intervals gives the safe bounds

$$\|U_0(x, x_0)\|,\ \|U_0(x, x_0)^{-1}\| \le q^{M+2} \quad (x_0 \le x \le x_1). \tag{200}$$

For either polarization the difference of the actual and reference generators has norm at most D_L/x_0^2. For TE it is the single entry $(l(l+1) - 2)/x^2$. For TM its entries are $2/x^2$ and $l(l+1)/(\varepsilon x^2)$, with $\varepsilon \ge 1$.

Writing the actual propagator as $U = U_0 W$ gives a Volterra equation whose coefficient norm integrates to at most

$$\beta = \frac{D_L d_M q^{2M+4}}{x_0^2} \le \frac{q^{-2M}}{32}. \tag{201}$$

Gronwall, followed by the exact endpoint norm in (199), gives

$$\|U(x_1, x_0) - U_0(x_1, x_0)\| \le q^M (e^\beta - 1) \le 2 q^M \beta. \tag{202}$$

This estimate retains the possible growth of the reference transfer matrix; no small generator error is identified with a small endpoint error without this amplification factor.

The finite Hankel formulas give, for $x \geq 1$,

$$|\psi_l(x) - \sin(x - l\pi/2)| + |\psi_l'(x) - \cos(x - l\pi/2)| \leq K_L/x. \tag{203}$$

They also give $|\xi_l^+(x)|, |\xi_l^{+\prime}(x)| \leq 2$ for $x \geq K_L$. At the multiple x_0 of π, the ideal initial state is a signed first coordinate vector for odd l and a signed second coordinate vector for even l. Its error has norm at most $K_L/x_0 \leq q^{-2M}/8$, and the actual initial state has norm at most two. Combining this with (202) shows that the actual final state differs from its ideal value in (199) by at most

$$q^M \frac{K_L}{x_0} + 4q^M\beta \leq \frac{1}{4}q^{-M}. \tag{204}$$

Therefore, with σ as in the theorem,

$$\tfrac{3}{4}q^{\sigma M} \leq |v(x_1)| \leq \tfrac{5}{4}q^{\sigma M}. \tag{205}$$

In the exterior both state conventions equal (u, u'). Since $W(\xi_l^-, \xi_l^+) = 2i$, the exterior coefficient satisfies $A_l = (u\xi_l^{+\prime} - u'\xi_l^+)/(2i)$. The Hankel bounds and the conjugate coefficient representation give both inequalities

$$|v(x_1)|/(4\sqrt{2}) \leq |A_l| \leq \sqrt{2}|v(x_1)|. \tag{206}$$

This proves (196). Nonvanishing also follows directly from uniqueness: a zero incoming coefficient of a real regular solution would make both exterior coefficients zero.

For a vacuum regular wave $\psi_l = (\xi_l^- + \xi_l^+)/2$, so its incoming coefficient is $1/2$. Fixed vacuum power normalization therefore gives the exact relative core multiplier $1/(2A_l)$ for either polarization. Finally the electric parity is $(-1)^l$ for TE and $(-1)^{l+1}$ for TM. This identifies the amplified and suppressed sectors as stated. □

10.3 What happens to physical passage in this entire finite band

Theorem 10.3 (An area bound survives the common-stack gains)**.** *Let $D = (-L_D/2, L_D/2)^2 \times \{0\}$, with area $A = L_D^2$, be inside the vacuum core of the preceding construction. Let $\mathcal{H}_L$ contain all power-normalized incoming TE and TM partial waves with $1 \leq l \leq L$ and all their azimuthal indices. For any physical selected-output contraction T of this device, every counted subspace $W \subset \mathcal{H}_L$ satisfies*

$$\dim W \leq \frac{128}{9\pi}\frac{k_0^2 A}{\eta\tau}. \tag{207}$$

The bound is independent of L, M, x_0, the local resonant field norm, and the exterior support size, provided the explicit radius conditions are met. Its proof uses no bypass hypothesis, so it applies in particular whenever the frozen absolute-bypass condition also holds. It does not assert a bound for inputs in angular orders above L.

Proof. Identify the finite physical incoming basis with the corresponding orthonormal vacuum basis. On the core, every actual field equals the regular vacuum field with its coefficient in each mode multiplied by g_l. Let P_- and P_+ be the electric-odd and electric-even parity projections. Theorem 10.2 writes this diagonal multiplier exactly as

$$G = (q^M P_- + q^{-M} P_+)B, \qquad \|B\| \leq C := 8\sqrt{2}/3, \tag{208}$$

where every diagonal entry of B is nonzero. Its complex phases are included in B; no common phase is assumed.

Both diagonal parity blocks of the vacuum section-flux operator vanish, by the inversion argument in Lemma 10.1. The two real gain factors in (208) therefore cancel in each cross block, giving the exact identity

$$Q_D^{\mathrm{device}}\big|_{\mathcal{H}_L} = G^* Q_D^0 G = B^* Q_D^0 B. \tag{209}$$

For counted inputs, $\langle a, Q_D^{\mathrm{device}} a\rangle \geq \eta\tau\|a\|^2$. Hence $V = BW$ has the same dimension as W and obeys

$$\langle b, Q_D^0 b\rangle \geq \frac{\eta\tau}{C^2}\|b\|^2 \quad (b \in V). \tag{210}$$

Apply (187) and $C^2 = 128/9$. This proves (207) for all coherent inputs, without replacing the device transmission by an isolated link. □

Theorem 10.4 (Arbitrary-rank physical field amplification with zero plane flux)**.** *Fix $N \geq 1$, a ball B_R centered on the section plane, the same frequency and material upper bound. There is a sequence of the finite ordinary dielectrics above and an N-dimensional physically power-normalized input subspace U_N such that the full scattering map is unitary on U_N, every coherent field has $S_z = 0$ almost everywhere on the entire plane, and*

$$\int_{B_R} |E_a|^2\, dx \;\geq\; \frac{16Z_0}{25} q^{2M} \min_{1\leq j\leq N} \int_0^R |\psi_{2j-1}(k_0 r)|^2\, dr\; \|a\|^2 \qquad (a \in U_N). \tag{211}$$

The positive constant after q^{2M} is independent of M. Thus every unit vector in this physical subspace has diverging local field energy while full-map throughput is one and absolute bypass is zero. Its passage through D is also zero, so it is not a counted subspace for any $\eta > 0$.

Proof. Take $L = 2N-1$ and the TE modes $(l, m_{\mathrm{az}}) = (2j-1, 0)$, $1 \leq j \leq N$. Choose x_0 also greater than $k_0 R$ for each M. Radial real dielectrics preserve these orthogonal channels. In each channel the outgoing-to-incoming coefficient is $\overline{A_l}/A_l$, of modulus one, so their full physical scattering map is unitary.

On the equatorial plane, $Y_{l0} = 0$ for odd l and $\partial_\varphi Y_{l0} = 0$. A TE electric field there is purely azimuthal, whereas its magnetic field is normal to the plane. These component properties persist for every radius, in every layer, and for every coherent sum of the selected channels. Their normal Poynting component is consequently zero everywhere except possible interface circles, a set of plane measure zero.

A free unit-power TE partial wave has electric radial coefficient $2\sqrt{2Z_0}\,\psi_l(k_0 r)/r$ with unit-normalized X_{l0}. The actual coefficient is multiplied by g_l. The lower bound in Theorem 10.2 gives $|g_l| \geq 2q^M/(5\sqrt{2})$ for these odd orders. Angular orthogonality on B_R removes all cross terms and proves (211). Each radial integral is strictly positive because the regular Bessel solution is not identically zero. The frozen passage inequality would require $0 = P_D(a) \geq \eta\|Ta\|^2 > 0$ for a nonzero efficient input; thus no such input is counted. □

Remark 10.5 (What the growing-support test establishes)**.** The simultaneous gain theorem closes a specific global synthesis step for actual finite dielectrics: there is no assumed coupled-mode model, no independent lumped loads, and no unproved extension of local Cauchy data. It also shows that an estimate of local field norm from passivity, throughput, and bypass alone cannot be uniform, even on an arbitrarily large fixed-dimensional physical subspace.

The positive-passage condition remains essential. For this common radial stack its required opposite-parity product cancels the large gain, leading to the rigorous bandwise area bound (207). To escape that result by angular-selective inner layers one would have to change the parity-dependent radial gain pattern while retaining full-plane bypass control. The local inverse-synthesis theorem

does not prove this nonlocal statement. Neither the construction nor its bandwise exclusion settles the unrestricted channel conjecture.

11 Global finite-order radial TE control with bounded positive index

The following construction turns the angular-momentum term in the actual radial Maxwell equation into a controllable finite ensemble. It uses only finite concentric layers with $1 \le \varepsilon \le q^2 < \varepsilon_+$. Its support may grow. The result is approximate global transfer control for every prescribed finite set of TE orders. It is not a bypass theorem.

Think of a radial layer as a two-by-two transfer map for each angular order. The same physical layer acts on every order, so the challenge is to control several maps at once rather than tune a separate device for each one. The identity loop below nearly restores the reference transfer while retaining a small dependence on angular order. Repeating such loops at large radius turns that dependence into a useful shear; combinations of shears then give the finite-order approximation theorem.

11.1 An identity loop with an amplified angular derivative

Use $x = k_0 r$, the electric TE state $v = (u, u')^T$, and

$$X = \begin{pmatrix} 0 & 1 \\ 0 & 0 \end{pmatrix}, \qquad Y = \begin{pmatrix} 0 & 0 \\ 1 & 0 \end{pmatrix}, \qquad J = X - Y. \tag{212}$$

For $\nu = l(l+1)$ the exact equation in an index-n layer is

$$v' = (X - n^2 Y + \nu x^{-2} Y)v. \tag{213}$$

The state is continuous at dielectric interfaces. No magnetic or surface parameter is being varied.

Fix $1 < q < \sqrt{\varepsilon_+}$. A high quarter layer has index q and length $\pi/(2q)$; a low quarter layer has index one and length $\pi/2$. The reference equation omits $\nu x^{-2} Y$. Its quarter matrix is $T_n = \left(\begin{smallmatrix} 0 & 1/n \\ -n & 0 \end{smallmatrix}\right)$. A loop consists of M high–low pairs followed by M low–high pairs. Its length and reference endpoint are

$$\ell_M = M\pi(1 + q^{-1}), \qquad U_0(\ell_M) = I. \tag{214}$$

Indeed, the first half gives $(-1)^M \operatorname{diag}(q^M, q^{-M})$ and the second its inverse.

Lemma 11.1 (Angular derivative of a dielectric loop)**.** *Let $B_M = \int_0^{\ell_M} U_0(s)^{-1} Y U_0(s)\, ds$. Then*

$$\begin{aligned} B_M &= \begin{pmatrix} 0 & -d_M \\ b_M & 0 \end{pmatrix}, \\ b_M &= \frac{\pi(q^2 + q^{-1})}{2(q^2 - 1)}(q^{2M} - 1), \\ d_M &= \frac{\pi(1 + q^{-1})}{2(q^2 - 1)}(1 - q^{-2M}), \\ \frac{d_M}{b_M} &= \kappa_q q^{-2M}, \qquad \kappa_q = \frac{1}{q^2 - q + 1} < 1. \end{aligned} \tag{215}$$

Moreover

$$\int_0^{\ell_M} \|U_0(s)^{-1} Y U_0(s)\|\, ds = b_M + d_M \le 2b_M. \tag{216}$$

Proof. If the first row of U_0 is (a, b), determinant one gives

$$U_0^{-1} Y U_0 = \begin{pmatrix} -ab & -b^2 \\ a^2 & ab \end{pmatrix}. \tag{217}$$

This rank-one matrix has norm $a^2 + b^2$. In high and low layers use $0 \le \theta \le \pi/2$, with $ds = d\theta/q$ and $ds = d\theta$, respectively. Up to an irrelevant common sign, the first-row pairs in the forward half, for $0 \le j < M$, are

$$(q^j \cos\theta, q^{-j-1} \sin\theta), \qquad (-q^{j+1} \sin\theta, q^{-j-1} \cos\theta). \tag{218}$$

Those in the reverse half, for $M \ge h \ge 1$, are

$$(q^h \cos\theta, q^{-h} \sin\theta), \qquad (-q^{h-1} \sin\theta, q^{-h} \cos\theta). \tag{219}$$

Integrating a^2 over these layers gives $b_M = \frac{\pi}{2}(q^{-1} + q^2) \sum_{j=0}^{M-1} q^{2j}$. Integrating b^2 gives $d_M = \frac{\pi}{2}(q^{-3} + q^{-2}) \sum_{j=0}^{M-1} q^{-2j}$. The integral of ab in each forward pair is $(q^{-2} - 1)/2$, and in each reverse pair its negative. The diagonal entries therefore vanish exactly. Summing the geometric series gives (215). The rank-one norm identity gives (216). □

Lemma 11.2 (Finite-radius error for one actual Maxwell loop)**.** *Let $U_\nu(r)$ be the actual transfer through this loop starting at dimensionless radius $r > 0$, and let $0 \le \nu \le V$. Then*

$$\left\| U_\nu(r) - I - \frac{\nu}{r^2} B_M \right\| \le \frac{4\nu \ell_M b_M}{r^3} + \frac{2\nu^2 b_M^2}{r^4} \exp(2\nu b_M / r^2). \tag{220}$$

Also $\|U_\nu(r)\| \le \exp(2\nu b_M / r^2)$.

Proof. Writing the actual fundamental matrix as $U_0 W$ gives

$$W'(s) = \frac{\nu}{(r+s)^2} U_0(s)^{-1} Y U_0(s) W(s), \qquad W(0) = I.$$

The integrated coefficient norm is at most $\beta = 2\nu b_M / r^2$. The Volterra series beyond its linear term is bounded by $e^\beta - 1 - \beta \le \beta^2 e^\beta / 2$. Replacing $(r+s)^{-2}$ in that linear term by r^{-2} costs at most $2\nu \ell_M (b_M + d_M)/r^3 \le 4\nu \ell_M b_M / r^3$. Since $U_0(\ell_M) = I$, these are the endpoint errors. The same series bounds $\|W(\ell_M)\|$ by e^β. □

11.2 A macroscopic angular shear in a thin distant annulus

Theorem 11.3 (Simultaneous angular shear from positive-index layers)**.** *Fix finitely many orders $l_1, \dots, l_m \ge 1$, put $\nu_j = l_j(l_j + 1)$ and $V = \max_j \nu_j$, and fix $t \ge 0$. For every sufficiently large starting radius R there are finite layers of index one or q in an annulus of dimensionless thickness $o(R)$ whose actual TE transfers converge simultaneously to*

$$\exp(t\nu_j Y) = I + t\nu_j Y, \qquad 1 \le j \le m. \tag{221}$$

The material bound is independent of R, t, and the orders.

Proof. For $t = 0$ use no layers. Otherwise fix $a \in (1/2, 1)$ and set

$$M = \lfloor a \log_q R \rfloor, \quad h = b_M / R^2, \quad K = \lfloor t/h \rfloor \tag{222}$$

for sufficiently large R. Use K consecutive loops, starting at $r_i = R + i\ell_M$, $0 \le i < K$. The explicit formula for b_M gives

$$h \to 0, \qquad K\ell_M/R = O(R^{1-2a}\log R) \to 0, \qquad q^{-2M} \to 0.$$

Set $\epsilon_M = \kappa_q q^{-2M}$. One actual loop differs from $I + h\nu Y$ by at most

$$\nu h\epsilon_M + \frac{2\nu hK\ell_M}{R} + \frac{4\nu h\ell_M}{R} + 2\nu^2 h^2 e^{2\nu h}. \tag{223}$$

The first two terms compare $(\nu/r_i^2)B_M$ with $h\nu Y$, using $B_M/b_M = Y - \epsilon_M X$ and $|R^2/r_i^2 - 1| \le 2i\ell_M/R$. The last two terms are (220).

Each actual step has norm at most e^{2Vh} and each ideal step at most e^{Vh}. Telescoping the K-fold products bounds their difference by Ke^{2Vt} times (223) with $\nu = V$. Since $Y^2 = 0$, the ideal product is $I + Kh\nu Y$, whose difference from the target is at most Vh. Thus the simultaneous endpoint error is at most

$$e^{2Vt}t\left[V\epsilon_M + \frac{2VK\ell_M}{R} + \frac{4V\ell_M}{R} + 2V^2 he^{2Vh}\right] + Vh. \tag{224}$$

Every term tends to zero. The total thickness is $K\ell_M = o(R)$. Every layer has real permittivity one or q^2, and every structure at finite R has finitely many interfaces. □

11.3 Finite-ensemble global transfer control

Definition 11.4. For the fixed finite orders, a tuple $(G_1, \dots, G_m) \in \mathrm{SL}(2,\mathbb{R})^m$ is *asymptotically realizable* if, for every sufficiently large R, a finite radial dielectric in $[R, R + d_R]$, with $d_R/R \to 0$ and $1 \le \varepsilon \le q^2$, has simultaneous TE transfers converging to that tuple as $R \to \infty$.

Lemma 11.5 (Common real symplectic control and closure)**.** *Every common tuple $(G, \dots, G)$, $G \in \mathrm{SL}(2,\mathbb{R})$, is asymptotically realizable. The realizable tuples form a closed multiplicative semigroup.*

Proof. In the reference equation a vacuum layer realizes $e^{\theta J}$ for any real θ, by adding a multiple of 2π to make the length nonnegative. A high–low quarter pair with adjustable high index $1 \le s \le q$ realizes $-\mathrm{diag}(s, s^{-1})$; a vacuum half-period removes the sign. Products give any positive diagonal $\mathrm{diag}(s, s^{-1})$, $s > 0$, with inverses obtained by interchanging layer order. The singular-value decomposition expresses every real determinant-one matrix as two proper rotations and such a diagonal. Thus finite bounded-index layers realize any common G exactly in the reference equation. For this fixed sequence, the interaction estimate above bounds the angular correction by $O(R^{-2})$, uniformly over the finite orders. Its length is fixed, proving common realizability.

Two realizing families concatenate: the first endpoint divided by R tends to one, so use the second family at that endpoint. Total thickness remains $o(R)$ and transfers converge to the product. For closedness let realizable tuples $G^{(n)} \to G$. Choose increasing thresholds $R_n \to \infty$ so that the family for $G^{(n)}$, for every $R \ge R_n$, has transfer error at most $1/n$ and thickness at most R/n. On $R_n \le R < R_{n+1}$ use that family. Transfers converge to G and relative thickness to zero. All tuple norms are maxima of the finitely many matrix norms. The same reasoning permits limits of finite products. □

Theorem 11.6 (Global approximate finite-order TE transfer control)**.** *For distinct positive integers $l_1, \dots, l_m$ and arbitrary $G_1, \dots, G_m \in \mathrm{SL}(2,\mathbb{R})$, their tuple is asymptotically realizable by actual finite ordinary dielectrics, for any fixed $1 < q < \sqrt{\varepsilon_+}$. Consequently each prescribed accuracy is attained by a finite bounded positive scalar radial structure. No uniform radius, layer-count, or thickness bound is asserted as target or accuracy varies.*

Proof. In tuple notation put $A = (\nu_j Y)_j$, $B = (-\nu_j X)_j$, and $C = A + B = (-\nu_j J)_j$. Theorem 11.3 supplies e^{tA} for $t \geq 0$. Common conjugation by J supplies e^{tB} for $t \geq 0$, because $JYJ^{-1} = -X$. The finite-dimensional product formula

$$e^{tC} = \lim_{n\to\infty} (e^{tA/n} e^{tB/n})^n$$

and semigroup closure supply e^{tC} for $t \geq 0$. Every ν_j is an integer, hence $e^{2\pi C} = I$. Reduction modulo 2π supplies e^{tC} for every real t. Another product formula gives

$$e^{-tB} = e^{t(A-C)} = \lim_{n\to\infty} (e^{tA/n} e^{-tC/n})^n, \qquad t \geq 0.$$

Common conjugation then supplies e^{-tA}. This explicitly generates inverses without negative physical layer thicknesses.

Put $H = [X, Y] = \mathrm{diag}(1, -1)$. The Lie algebra generated by common X, Y, H and $(\nu_j Y)_j$ contains

$$(\nu_j^p X)_j, \quad (\nu_j^p Y)_j, \quad (\nu_j^p H)_j \qquad (p = 0, 1, 2, \ldots).$$

Indeed $[H, X] = 2X$, $[H, Y] = -2Y$, and bracketing $(\nu_j^p X)_j$ with $(\nu_j Y)_j$ raises the power to $p + 1$. The distinct numbers $\nu_j = l_j(l_j + 1)$ give an invertible Vandermonde matrix for powers $0, \ldots, m - 1$. Linear combinations therefore isolate X, Y, H in each coordinate. The generated Lie algebra is all of $\mathfrak{sl}(2, \mathbb{R})^m$.

For completeness this yields global group control as follows. Let Γ be the subgroup generated by the common one-parameter groups and e^{tA} for all real t. The span of their generators conjugated by Γ is invariant under their adjoint flows. Differentiating these flows shows it contains the generated Lie algebra, hence the full algebra just computed. Select $3m$ conjugated generators forming a basis. The product of their one-parameter groups has invertible derivative at the identity, so the inverse function theorem puts an open identity neighborhood in Γ. It is an open subgroup. The singular-value decomposition also shows $\mathrm{SL}(2, \mathbb{R})^m$ is connected, so Γ is the whole group. Every generator and inverse belongs to the closed realizable semigroup, so all of Γ does. This proves the claim using actual radial Maxwell transfer matrices. □

Corollary 11.7 (Prescribed finite TE core gains and relative phases)**.** *Fix finitely many distinct TE orders and arbitrary nonzero complex numbers g_j. There is a sequence of the finite ordinary radial dielectrics above, with vacuum-core radius tending to infinity, whose physical core multipliers converge to g_j up to one common unit-modulus factor. This includes simultaneous large gains for both electric inversion parities. After removing that common phase, convergence of the fields and their derivatives is uniform on every fixed compact subset of the vacuum core, for every coherent input in the chosen finite angular band.*

Proof. Restrict the starting radius to $R = 2\pi n \to \infty$. The origin-normalized regular solution is $\psi_l(x) = x j_l(x)$; its state at R tends to the unit vector

$$v_l^0 = (\sin(-l\pi/2), \cos(-l\pi/2))^T.$$

For each order choose a nonzero real vector w_j satisfying $w_{j,1} + i w_{j,2} = i^{l_j+1}/g_j$. There is a real determinant-one matrix taking $v_{l_j}^0$ to w_j, for example

$$G_j = \left[w_j, \frac{-Jw_j}{|w_j|^2} \right] \left[v_{l_j}^0, -Jv_{l_j}^0 \right]^{-1}.$$

Apply Theorem 11.6 to these fixed targets. The actual regular state at the outer endpoint $X_R = R + d_R$ then converges to w_j.

The exterior incoming coefficient is $A_j = (u\xi_{l_j}^{+\prime} - u'\xi_{l_j}^{+})/(2i)$. The finite Hankel formula at $X_R \to \infty$ gives

$$\xi_l^+(X_R) = (-i)^{l+1}e^{iX_R}(1+o(1)), \qquad \xi_l^{+\prime}(X_R) = i(-i)^{l+1}e^{iX_R}(1+o(1)).$$

Consequently $e^{-iX_R}A_j \to 1/(2g_j)$. A free regular wave has incoming coefficient $1/2$, so the physical relative core multiplier is $(2A_j)^{-1}$. Multiplying that multiplier by the common phase e^{iX_R} gives the asserted limit g_j. The selected band is finite and its regular vacuum basis is smooth on each compact set, which proves uniform coherent field and derivative convergence there. All azimuthal indices within an order have the same multiplier. □

Remark 11.8 (Scope and the remaining channel requirement)**.** Theorem 11.6 overcomes the fixed-annulus ceiling by proving global approximate reachability when support may grow. It neither assumes a circuit model nor infers global reachability from the earlier local inverse theorem. Only TE and finitely many prescribed orders are controlled; all azimuthal indices of an order share its transfer. Corollary 11.7 shows that the reciprocal-parity gain pattern of the common stack is not a restriction on all bounded positive radial structures.

Transfer targets alone do not supply counted channels. A proposed subspace must additionally satisfy positive passage and absolute whole-plane bypass for every coherent input, in the physical input power norm. Fields in the many concentric layers can be large. No estimate of their normal plane flux follows from endpoint control. Neither a bypass estimate nor a qualifying many-channel subspace is asserted here.

12 Paired electric and magnetic radial control

The distant finite-order control construction can be tracked in both polarizations simultaneously. Its limiting TE and TM transfers obey a specific inverse-transpose relation. This supplies controlled amplification of an electric-wall reflection sector and suppression of its opposite sector, within any prescribed finite band. It does not bound unselected partial waves or the Green operator of a perturbed device.

This distinction matters because a physical dielectric cannot choose its electric and magnetic layer responses independently. The paired equations below follow both responses through the same stack. The resulting relation is later used to identify the amplified and suppressed parity sectors; it is not yet a statement about the response to a source inserted in the core.

12.1 The same physical layers control a paired transfer graph

Retain $X, Y, J, q, \ell_M, b_M, d_M$ from Section 11. For TE use $v_{\mathrm{E}} = (u, u')^T$ and for TM use $v_{\mathrm{M}} = (u, n^{-2}u')^T$ in an index-n layer. With $\nu = l(l+1)$ their exact dimensionless equations are

$$v_{\mathrm{E}}' = (X - n^2Y + \nu x^{-2}Y)v_{\mathrm{E}}, \qquad v_{\mathrm{M}}' = (n^2X - Y + \nu n^{-2}x^{-2}Y)v_{\mathrm{M}}. \tag{225}$$

Both states are continuous across each material interface.

Lemma 12.1 (Paired angular derivatives of the identity loop)**.** *For the high–low, then low–high loop of Lemma 11.1, its two reference propagators satisfy $U_{0,\mathrm{M}} = U_{0,\mathrm{E}}^{-T}$ at every prefix. Their integrated angular derivatives are*

$$B_{\mathrm{E},M} = \begin{pmatrix} 0 & -d_M \\ b_M & 0 \end{pmatrix}, \qquad B_{\mathrm{M},M} = \begin{pmatrix} 0 & -b_M \\ d_M & 0 \end{pmatrix} = -B_{\mathrm{E},M}^T. \tag{226}$$

For both polarizations the integrated interaction-generator norm is $b_M + d_M \le 2b_M$. Consequently the one-loop error (220) and the repeated-loop error (224) apply simultaneously, with the same constants. The limiting repeated-loop transfers are

$$\left(e^{t\nu Y}, e^{-t\nu X}\right), \qquad t \ge 0. \tag{227}$$

Proof. The two reference generators are negative transposes: $n^2X - Y = -(X - n^2Y)^T$. Differentiating an inverse transpose proves the prefix identity, including across continuous state interfaces. Write the TE prefix as $U = \left(\begin{smallmatrix} a & b \\ c & d \end{smallmatrix}\right)$. The TM prefix is $U^{-T} = \left(\begin{smallmatrix} d & -c \\ -b & a \end{smallmatrix}\right)$. Its angular interaction matrix, including the actual factor n^{-2}, is therefore

$$n^{-2}U_{0,\mathrm{M}}^{-1} Y U_{0,\mathrm{M}} = n^{-2} \begin{pmatrix} cd & -c^2 \\ d^2 & -cd \end{pmatrix}. \tag{228}$$

Its norm is $(c^2 + d^2)/n^2$.

For completeness, in the forward half with $0 \le j < M$, the TE second rows during the high and low quarters, up to a common sign, are

$$(-q^{j+1}\sin\theta, q^{-j}\cos\theta), \qquad (-q^{j+1}\cos\theta, -q^{-j-1}\sin\theta).$$

In the reverse half with $M \ge h \ge 1$, the corresponding low and high rows are

$$(-q^{h}\sin\theta, q^{-h}\cos\theta), \qquad (-q^{h}\cos\theta, -q^{1-h}\sin\theta).$$

Use $ds = d\theta/q$ in a high quarter and $ds = d\theta$ in a low quarter. Integrating c^2/n^2 gives exactly the same b_M as the integral of a^2 in the TE calculation; integrating d^2/n^2 gives d_M. These identities follow on each quarter by interchanging $\sin^2\theta$ and $\cos^2\theta$. The integral of cd/n^2 in a forward pair is $(1 - q^{-2})/2$, and in a reverse pair its negative. Thus its integral over the loop is zero, proving (226) and the norm assertion.

The TM interaction equation differs from its reference equation by $\nu(r+s)^{-2}$ times (228). Its integrated norm and the error from freezing $(r+s)^{-2}$ are consequently exactly bounded as in Lemma 11.2. Since $B_{\mathrm{M},M}/b_M = -X + \kappa_q q^{-2M} Y$, the repeated-loop proof applies with Y replaced by $-X$. Both square to zero and have norm one, so every constant in (224) is unchanged. □

Theorem 12.2 (Global finite-order paired TE/TM transfer control)**.** *For distinct positive integers $l_1, \dots, l_m$ and arbitrary $G_j \in \mathrm{SL}(2,\mathbb{R})$, there are actual finite radial dielectrics with $1 \le \varepsilon \le q^2 < \varepsilon_+$ in $[R, R + d_R]$, $d_R = o(R)$, whose simultaneous transfers converge to*

$$(G_j, G_j^{-T}) \qquad (1 \le j \le m) \tag{229}$$

as $R \to \infty$. The first component is TE and the second TM. This is a constructed family of paired targets, not a universal identity for arbitrary physical radial structures.

Proof. Define asymptotic realizability for the $2m$ transfers together, using the maximum of their matrix norms. Concatenation and closedness follow by exactly the threshold-selection proof of Lemma 11.5. Every common reference transfer G in that lemma is now paired with G^{-T}, since the reference generators are negative transposes. For a fixed layer word both angular errors are $O(R^{-2})$, so the common paired tuple is realizable. Lemma 12.1 supplies the weighted shear pair (227).

The map $\iota : G \mapsto (G, G^{-T})$ is an injective continuous group homomorphism: $(GH)^{-T} = G^{-T}H^{-T}$. Its infinitesimal map is $A \mapsto (A, -A^T)$. Thus common conjugation, the product formulas, and the integer-frequency signed-time construction in Theorem 11.6 all remain within this graph. In particular the paired shear inverses are supplied by positive layers through the same periodic rotation argument. The Vandermonde and open-subgroup proof applies to the first components and hence, by ι, to their whole graph. It supplies every tuple (229) in the closed paired realizable semigroup. No step replaces TM behavior by an independently assumed transfer. □

12.2 Reflection parity and finite-band isolation

Let $R_z(x, y, z) = (x, y, -z)$. An electric-wall field means

$$E(R_z x) = -R_z E(x), \qquad H(R_z x) = R_z H(x). \tag{230}$$

It has $E_t = 0$ and $H_z = 0$ on the plane. The opposite, magnetic-wall field has the reversed two signs and satisfies $E_z = 0$ and $H_t = 0$. Each sector has identically zero normal Poynting density on the plane, for every coherent combination.

Lemma 12.3 (Spherical-wave reflection sectors)**.** *For azimuthal index m, a TE spherical wave is electric-wall exactly when $l + m$ is even; a TM wave is electric-wall exactly when $l + m$ is odd. On the subspace invariant under a rotation by π around the z axis, with the vector rotated as well, only even m occur. Within this C_2-even subspace the electric-wall sector is precisely TE even l together with TM odd l.*

Proof. The scalar identity is $Y_{lm}(\pi - \theta, \varphi) = (-1)^{l+m} Y_{lm}(\theta, \varphi)$. For $X_{lm} = \widehat{r} \times \nabla_{S^2} Y_{lm}/\sqrt{l(l+1)}$, reflection reverses the cross product, giving $X_{lm}(R_z x) = (-1)^{l+m+1} R_z X_{lm}(x)$. This is the TE electric-field parity. Taking a curl reverses that reflection sign, so the TM electric-field parity is $(-1)^{l+m}$. The Maxwell curl equation gives the opposite magnetic-field sign in each case. This proves the wall classification. Rotation by π contributes $e^{im\pi}$ after the vector rotation, so its invariant sector has even m. □

Theorem 12.4 (Controlled finite-band wall amplification and suppression)**.** *Fix any finite set of angular orders and positive numbers A_l. In the C_2-even input band of those orders, there is a sequence of finite ordinary radial dielectrics with vacuum-core radius tending to infinity such that, after one common rephasing, the physical core multipliers converge to*

	TE	TM
l even	A_l	A_l^{-1}
l odd	A_l^{-1}	A_l

. (231)

Thus the electric-wall sector has gain A_l and its opposite sector gain A_l^{-1}, for each controlled order. For a uniform $A_l = A > 0$, the finite-band core operator converges to $AP_{\mathrm{e}} + A^{-1}P_{\mathrm{m}}$ after that rephasing. Convergence of all coherent fields and their derivatives is uniform on each fixed compact core subset. The wall boundary identities themselves hold exactly at every stage, by symmetry.

Proof. Take the paired targets $G_l = \mathrm{diag}(A_l, A_l^{-1})$ and restrict starting radii to $R = 2\pi n$. The regular radial state tends to $v_l^0 = (\sin(-l\pi/2), \cos(-l\pi/2))^T$ in either polarization, because the inner core is vacuum. For even l this is a signed second coordinate vector; for odd l it is a signed first one. Thus the limiting endpoint multiplier on this real state is A_l^{-1} for TE even and TM odd, and A_l for the opposite two cases.

At the outer endpoint X_R, the incoming radial coefficient obeys the same Wronskian formula in either polarization. The exterior and core are both vacuum, so their state conventions agree there. The Hankel calculation in Corollary 11.7 gives $e^{-iX_R} A_l^{\mathrm{in}} \to c_l/2$ when the endpoint state is $c_l v_l^0$. Its physical core multiplier, relative to the free wave with the same physical incoming amplitude, is $(2A_l^{\mathrm{in}})^{-1}$. After multiplication by e^{iX_R} it therefore tends to c_l^{-1}, proving (231). This relative multiplier is valid for TM as well as TE; their different fixed impedance factors cancel in the free/actual comparison.

Lemma 12.3 identifies these gains with the two wall sectors for even m. All azimuthal indices within an order have the same radial transfer. Finite-band convergence gives uniform compact field

and derivative convergence. Radial symmetry preserves reflection and C_2 sectors exactly for every finite device, establishing the final assertion. □

Remark 12.5 (What the suppression does and does not provide)**.** For uniform A the limiting multiplier $D_A = AP_{\mathrm{e}} + A^{-1}P_{\mathrm{m}}$ preserves the vacuum plane flux form pointwise:

$$D_A^* Q_z^0(x) D_A = Q_z^0(x) \qquad (z = 0). \tag{232}$$

Indeed both diagonal wall blocks vanish pointwise, and the two real factors cancel in the remaining blocks. Amplifying the electric-wall background alone creates no plane passage.

The theorem supplies a controlled finite set of opposite-parity TM and TE input responses. It supplies no uniform estimate for unselected angular orders, a total Green operator, a source inside a new inclusion, or a geometry after a nearby inclusion breaks the reflection symmetry. Such estimates are required before a proposed small-transducer construction can be claimed to satisfy physical positive passage and absolute bypass.

13 Arbitrary physical passage dimension when bypass is omitted

The global control theorem supplies a sharper obstruction to a power-only channel proof. The following fields are responses of actual finite positive dielectrics with physically normalized incoming waves. They satisfy positive passage on arbitrarily large coherent subspaces. Their absolute bypass is not uniformly controlled.

Here the experiment is deliberately narrower than the original channel test: measure forward power on the square, but do not demand a bound on the absolute flux elsewhere. The theorem is useful because it shows exactly why the bypass condition cannot be dropped from a power-counting argument. It does not establish the full counterexample on its own.

Proposition 13.1 (Unbounded positive local-flux trace)**.** *Fix $k > 0$, $\varepsilon_+ > 1$, and the centered square D. In the finite scalar dielectric class $1 \le \varepsilon \le \varepsilon_+$, the positive part of the section-flux operator has no uniform trace or operator-norm bound in the physical incoming-power norm. This remains true for radial dielectrics with a vacuum core containing D.*

Proof. Let R_D be the circumradius of D, choose odd l with $l(l+1) > k^2 R_D^2$, and put $m = l + 1$. Use real normalized axisymmetric spherical harmonics and set

$$c_l = \frac{\partial_\theta Y_{l0}(\pi/2)}{\sqrt{l(l+1)}}, \qquad d_m = Y_{m0}(\pi/2).$$

These constants are nonzero. The radial positivity argument of Theorem 9.5 gives $j_l(kr), j_m(kr) > 0$ for $0 < r \le R_D$. Hence

$$I_{lm} = \int_D \frac{j_l(kr) j_m(kr)}{r}\, dA > 0, \qquad K_{lm} = 4k\sqrt{m(m+1)}\,|c_l d_m| I_{lm} > 0. \tag{233}$$

The apparent singularity at the origin is integrable.

In the physical convention of Lemma 10.1, a free unit-incoming-power TE wave, with its fixed phase absorbed into the input basis, has electric field $2k\sqrt{2Z}\, j_l(kr) X_{l0}$. Denote the actual core multipliers by g_l, g_m and the two physical incoming coefficients by a, b. On the plane, the odd TE wave has azimuthal electric field and normal magnetic field. The even TE wave has zero electric field and radial tangential magnetic field there, with

$$H_r = i\frac{2k\sqrt{2Z}}{Z}\, b g_m \sqrt{m(m+1)}\frac{j_m(kr)}{kr} d_m.$$

Since $\widehat{\varphi} \times \widehat{r} = -\widehat{z}$ on that plane, the exact section form is

$$P_D(a,b) = -4k\sqrt{m(m+1)}c_l d_m I_{lm}\,\mathrm{Im}(a\bar{b}\,g_l\overline{g_m}). \tag{234}$$

Its two eigenvalues are $\pm K_{lm}|g_l g_m|/2$. Corollary 11.7 supplies actual finite radial devices with g_l, g_m approaching any common $G > 0$, up to common phase. The positive eigenvalue can therefore be arbitrarily large. It bounds below the operator norm, the positive trace, and the nuclear norm whenever those traces are defined; equivalently the same divergence already holds on this two-dimensional compression. □

Theorem 13.2 (Arbitrary coherent physical passage rank)**.** *For every integer $N \geq 1$ and $p_* > 0$, there is a finite radial dielectric with the same fixed k, D, and material bounds, and an N-dimensional physical incoming space W_N, such that*

$$\|Sa\|^2 = \|a\|^2, \qquad P_D(a) \geq p_*\|a\|^2 \quad (a \in W_N). \tag{235}$$

Here S is the complete scattering map. No common absolute-bypass bound is asserted.

Proof. First construct local target fields. Choose distinct $q_j > k$ and put $\alpha_j = \sqrt{q_j^2 - k^2}$. In cylindrical coordinates define

$$E_j = J_1(q_j\rho)\left[\cosh(\alpha_j z) + i\frac{k}{\alpha_j}\sinh(\alpha_j z)\right]\widehat{\varphi}, \qquad H_j = \frac{1}{i\omega\mu_0}\,\mathrm{curl}\,E_j. \tag{236}$$

The quotient $J_1(q_j\rho)/\rho$ is an entire function of ρ^2, so the Cartesian vector field is smooth at the axis. Its divergence vanishes, and the order-one Bessel equation gives $(\Delta + k^2)E_j = 0$. Both vacuum Maxwell curl equations follow. At $z = 0$, $\partial_z E_j = ikE_j$, whence every coherent combination satisfies

$$S_z(a;\rho,0) = \frac{1}{2Z}\left|\sum_{j=1}^{N} a_j J_1(q_j\rho)\right|^2. \tag{237}$$

Its section Gram matrix is positive definite. A combination vanishing on D vanishes on a radial interval; its Taylor series then gives a Vandermonde system in the distinct q_j^2, after extracting the nonzero factors q_j. All coefficients must vanish.

Next approximate these targets by a finite regular TE band. Each axisymmetric azimuthal electric field in (236) has a regular TE spherical expansion with azimuthal order zero. For the needed convergence, choose $R' > R_D$ avoiding zeros of the finitely many possibly oscillatory $j_l(kR')$. All sufficiently large orders are positive at R'. Expand the smooth tangential trace on that sphere in X_{l0}. Angular projection of the vector Helmholtz equation yields the regular radial factor $j_l(kr)$. The smooth trace coefficients decay faster than any fixed power of l; the large-order Bessel series gives a bound of the form $C(r/R')^l$ on $j_l(kr)/j_l(kR')$, with polynomial factors for first derivatives on any smaller ball. The expansion therefore converges with its first derivatives on a ball containing D. Projection of the radial equations and angular completeness identify its sum with the original field.

Truncate all N expansions at a common finite order L. Uniform convergence of E, H on D preserves strict positivity of their finite Hermitian Gram matrix once L is sufficiently large. In the physical incoming norm, the resulting coefficient span V_N consequently satisfies

$$\dim V_N = N, \qquad P_D^0(a) \geq p_N\|a\|^2, \qquad p_N > 0.$$

The constant p_N may depend on N and may be very small. Apply Corollary 11.7 with a common real gain G for every TE order through L. After common rephasing, the actual finite-device section matrix converges to G^2 times the free section matrix on V_N. Choose G with $G^2 p_N > p_*$ and then a sufficiently accurate finite device. This gives the second inequality of (235) on the physical coefficient space $W_N = V_N$. The device is finite, real, positive, and radial, so its complete power-normalized scattering map is unitary. This gives the first equality. The exponentially growing local targets themselves were used only for compact approximation, never as physical inputs. □

Remark 13.3 (Why this does not close the unrestricted channel target)**.** For these finite angular-band devices, normal plane flux is absolutely integrable. It is regular on bounded regions up to the finitely many interfaces, and its exterior leading spherical Poynting vector is radial and tangent to the plane, leaving an $O(r^{-3})$ normal tail. Upper-half-space conservation with the physical radiation convention gives

$$P_\Sigma = P_{\mathrm{out,upper}} - P_{\mathrm{in,upper}}, \qquad |P_\Sigma(a)| \le \|a\|^2.$$

Consequently

$$\int_{\Sigma\setminus D} |S_z(a)| \ge |P_D(a) - P_\Sigma(a)| \ge P_D(a) - \|a\|^2. \tag{238}$$

The unbounded positive eigenvalue in Proposition 13.1 therefore entails unbounded bypass. On a subspace satisfying a fixed absolute-bypass bound, conservation only implies $\|Q_D\| \le 1 + \delta$. That operator-norm estimate alone cannot bound the number of positive eigenvalues. The spatial information in the absolute-bypass condition remains essential, and Theorem 14.6 obstructs using the construction of Theorem 13.2 at fixed bypass for arbitrarily large N.

14 A flux-only count for globally propagating vacuum fields

This section gives a second kind of restricted channel theorem: the entire planar fields must arise from propagating vacuum Herglotz waves. Their amplitudes may be arbitrarily large relative to the chosen input norm. Absolute bypass then supplies a finite dimension bound without an electric or magnetic field-resource bound. The conclusion is not an area law and does not apply to general dielectric fields or local evanescent solutions. It also identifies an obstruction to completing a remote radial-control construction by sending controls to infinity around a fixed regular-wave target.

The extra hypothesis is global: every field in this section is made from propagating vacuum waves across the whole plane. It is stronger than knowing the field only near D. The proof uses that bandwidth to control how much positive flux can be concentrated in the square while the absolute flux outside remains limited. This provides a useful comparison with the later construction, whose structured device is not covered by this hypothesis.

14.1 An explicit scalar observation estimate

Use the Fourier convention $\widehat{f}(\xi) = \int f(x) e^{-i\xi\cdot x}\, dx$. For $\kappa, L > 0$, define the explicit numbers

$$n = 2 + \lceil 4e\kappa L \rceil, \qquad C_{\kappa,L} = 2\left[1 + 2n(16e)^{n-1}\right]. \tag{239}$$

Here e in the numerical constants is the base of the natural logarithm.

Lemma 14.1 (Observation outside an interval)**.** *If $f \in L^1(\mathbb{R})$ and $\operatorname{supp} \widehat{f} \subset [-\kappa, \kappa]$, then, for $I = (-L/2, L/2)$,*

$$\|f\|_{L^1(\mathbb{R})} \le C_{\kappa,L} \|f\|_{L^1(\mathbb{R}\setminus I)}. \tag{240}$$

Proof. Fourier inversion applies because $\widehat{f}$ is bounded and compactly supported. In particular f has a smooth representative, and

$$\|f^{(j)}\|_\infty \le \frac{\kappa^{j+1}}{\pi(j+1)}\|f\|_1 \quad (j \ge 0). \tag{241}$$

Write $F = \|f\|_1$ and $G = \|f\|_{L^1(\mathbb{R}\setminus I)}$. In the adjacent interval $[L/2, 3L/2]$, take the n subintervals

$$J_j = [L/2 + jL/n,\ L/2 + (j+1/2)L/n]\,, \qquad 0 \le j < n. \tag{242}$$

Each has length $h = L/(2n)$. Averaging gives a point $x_j \in J_j$ with $|f(x_j)| \le G/h = 2nG/L$. For $j > i$, $x_j - x_i \ge (j-i)h$. Let P be the polynomial of degree at most $n-1$ interpolating these values. For $x \in I$, all distances $|x - x_j|$ are at most $2L$, so its Lagrange formula gives

$$\sum_{j=0}^{n-1}\left|\prod_{i\ne j}\frac{x-x_i}{x_j-x_i}\right| \le \frac{(4n)^{n-1}2^{n-1}}{(n-1)!} \le (16e)^{n-1},$$

$$|P(x)| \le \frac{2n}{L}(16e)^{n-1}G. \tag{243}$$

The last inequality uses $m! \ge (m/e)^m$ with $m = n-1 \ge 1$. The divided-difference integral remainder, obtained by repeated integration of the fundamental theorem of calculus, applies also to complex-valued f:

$$|f(x) - P(x)| \le \frac{(2L)^n}{n!}\|f^{(n)}\|_\infty. \tag{244}$$

It uses derivative values only on the real convex hull of the nodes and x; no complex mean-value theorem is being assumed. Integrating over I and using (241),

$$\|f\|_{L^1(I)} \le 2n(16e)^{n-1}G + \frac{\kappa L}{\pi(n+1)}\frac{(2\kappa L)^n}{n!}F. \tag{245}$$

Our choice $n \ge 4e\kappa L$ implies $(2\kappa L)^n/n! \le 2^{-n}$. Hence the coefficient of F is at most $2^{-n}/(4e\pi) < 1/2$. Add G to both sides of (245) and absorb this term to obtain (240). □

Corollary 14.2 (Planar observation outside the fixed square)**.** *Let $D = (-L/2, L/2)^2$. If $f \in L^1(\mathbb{R}^2)$ and* $\operatorname{supp}\widehat{f} \subset \{\xi : |\xi| \le \kappa\}$*, then*

$$\|f\|_{L^1(\mathbb{R}^2)} \le C_{\kappa,L}\|f\|_{L^1(\mathbb{R}^2\setminus D)}, \qquad \|\nabla f\|_\infty \le \frac{\kappa^3}{6\pi}\|f\|_1. \tag{246}$$

Proof. Almost every horizontal slice is in $L^1(\mathbb{R})$ and has one-dimensional Fourier support in $[-\kappa, \kappa]$. To justify the support statement, test its partial Fourier transform against a smooth function supported outside that interval. Fourier transformation in the second variable gives zero by the global support assumption; injectivity and Fubini give zero for almost every slice. A countable dense collection of tests suffices. Apply Lemma 14.1 on these slices and integrate in the second variable. The observed strip $\{|x| \ge L/2\}$ is contained in $\mathbb{R}^2 \setminus D$, proving the first assertion. For the second, Fourier inversion and $|\widehat{f}| \le \|f\|_1$ give

$$|\nabla f(x)| \le \frac{\|f\|_1}{(2\pi)^2}\int_{|\xi|\le\kappa}|\xi|\,d\xi = \frac{\kappa^3}{6\pi}\|f\|_1. \tag{247}$$

□

14.2 Finite positive trace from actual pointwise flux

Theorem 14.3 (Channel finiteness from propagating bandwidth and bypass)**.** *Let W be a complex linear input space equipped with a Hilbert norm. Suppose its electric and magnetic fields depend linearly on the input, and are entire regular vacuum Maxwell Herglotz fields at real wavenumber $k > 0$. There is no assumed bound on their Herglotz density norms in terms of $\|a\|$. Suppose every coherent $a \in W$ satisfies*

$$P_D(a) = \int_D s_a \geq p\|a\|^2, \qquad \int_{\mathbb{R}^2 \setminus D} |s_a| \leq \delta\|a\|^2, \quad s_a = \tfrac{1}{2}\operatorname{Re}(E_a \times \overline{H_a}) \cdot \widehat{z}, \tag{248}$$

where $D = (-L/2, L/2)^2$, $p > 0$, and $\delta \geq 0$. Set $\kappa = 2k$ and $A = L^2$. Then

$$\dim W \leq \frac{A\kappa^2 C_{\kappa,L}\delta}{\pi p} = \frac{4Ak^2 C_{2k,L}\delta}{\pi p}. \tag{249}$$

If $\delta = 0$, in fact $W = \{0\}$. For a counted physical subspace one may take $p = \eta\tau$; no condition $\delta < \eta\tau$ is needed here.

Proof. On the plane each electric and magnetic component is the Fourier transform of a finite complex measure supported in the transverse disk of radius k. Indeed, push its spherical Herglotz density forward under $d \mapsto kd_\perp$; the measure is finite because $L^2(S^2) \subset L^1(S^2)$. Products of a component and a conjugate component correspond to convolution with a reflected conjugate measure. Thus

$$\operatorname{supp} \widehat{s_a} \subset \{|\xi| \leq 2k\}. \tag{250}$$

The fields are continuous, hence s_a is integrable on the bounded square. Its assumed absolute bypass implies global L^1 integrability. In particular, global flux integrability is not being inferred from an arbitrary L^2 Herglotz density alone.

Corollary 14.2 now gives

$$\|s_a\|_1 \leq C_{\kappa,L}\delta\|a\|^2, \qquad |s_a(x)| \leq \frac{\kappa^2 C_{\kappa,L}\delta}{4\pi}\|a\|^2. \tag{251}$$

The pointwise bound follows from Fourier inversion, since the frequency disk has area $\pi\kappa^2$ and $|\widehat{s_a}| \leq \|s_a\|_1$. This controls the absolute flux *inside* D as well as outside it; the signed passage alone would not do so.

Restrict to an arbitrary finite-dimensional input subspace $V \subset W$ of dimension N. At each point x, write its Hermitian normal-flux form as $s_a(x) = \langle a, Q(x)a\rangle$. This form factors through the linear map

$$a \longmapsto \big(E_{a,x}(x), E_{a,y}(x), H_{a,x}(x), H_{a,y}(x)\big) \in \mathbb{C}^4. \tag{252}$$

Consequently $\operatorname{rank} Q(x) \leq 4$, and (251) bounds its operator norm by $\kappa^2 C_{\kappa,L}\delta/(4\pi)$. Thus

$$\operatorname{Tr} Q(x) \leq \operatorname{Tr}(Q(x))_+ \leq 4\|Q(x)\| \leq \frac{\kappa^2 C_{\kappa,L}\delta}{\pi}. \tag{253}$$

For an orthonormal basis $a_1, \ldots, a_N$ of V, the passage hypothesis gives

$$pN \leq \sum_{j=1}^{N} P_D(a_j) = \int_D \operatorname{Tr} Q(x)\, dx \leq \frac{A\kappa^2 C_{\kappa,L}\delta}{\pi}. \tag{254}$$

Only a finite sum is interchanged with integration. This proves (249), including infinite-dimensional W by restriction to finite-dimensional subspaces. If $\delta = 0$, (251) gives $s_a = 0$, and positive passage excludes every nonzero input. □

Remark 14.4 (Scope of the explicit estimate)**.** This is a flux-resource estimate, not a field-energy estimate. It permits unbounded electric and magnetic field norms and arbitrary coherent interference. The explicit observation constant grows exponentially in kL, and the resulting bound is not the proposed area scaling. Neither local vacuum Maxwell equations nor the existence of an entire extension alone implies (250): entire solutions with evanescent transverse content can grow in the normal direction and fall outside the propagating Herglotz class. The earlier local packet examples therefore do not contradict this theorem. General fields on a plane intersecting a dielectric also fall outside its hypotheses.

14.3 The limitation of moving controls to infinity

Lemma 14.5 (Uniform tails in a fixed regular-wave band)**.** *Fix a positive integer J, and let $\mathcal{F}_J$ be the real linear space of planar Hermitian cross-flux densities of regular vacuum vector spherical waves with angular orders $1 \le l \le J$, both polarizations and all azimuthal indices. Then $\mathcal{F}_J$ is finite dimensional and contained in $L^1(\mathbb{R}^2)$. For every $\epsilon > 0$ there is a finite radius $R_{J,\epsilon}$ such that*

$$\int_{|x|>R_{J,\epsilon}} |f(x)|\, dx \le \epsilon \|f\|_1 \qquad (f \in \mathcal{F}_J). \tag{255}$$

Proof. There are finitely many vector waves, so their Hermitian cross-fluxes span a finite-dimensional function space. They are smooth near the origin. Their finite spherical Hankel formulas give, uniformly in direction,

$$\begin{aligned} E(r\widehat{x}) &= r^{-1}\big(e^{ikr}A_+(\widehat{x}) + e^{-ikr}A_-(\widehat{x})\big) + O(r^{-2}), \\ H(r\widehat{x}) &= (Z_0 r)^{-1}\widehat{x} \times \big(e^{ikr}A_+(\widehat{x}) - e^{-ikr}A_-(\widehat{x})\big) + O(r^{-2}), \end{aligned} \tag{256}$$

with $A_\pm \cdot \widehat{x} = 0$. For any pair of such waves the leading cross-Poynting vector is radial, by $A \times (\widehat{x} \times \overline{B}) = \widehat{x}(A \cdot \overline{B})$ for transverse A, B. On the measurement plane its normal component therefore vanishes. Each cross-flux is $O(r^{-3})$, which is integrable in the two-dimensional plane. For every fixed $f \in \mathcal{F}_J$ its L^1 tail tends to zero. The unit sphere of the actual function space $\mathcal{F}_J$, with its L^1 norm, is compact. The tail functionals are all Lipschitz with constant one in that norm. A finite net of the unit sphere consequently makes this convergence uniform, proving (255). □

Corollary 14.6 (Finite-band control beyond a sufficiently large vacuum core)**.** *Fix J and choose $R_J \ge L/\sqrt{2}$ so that (255) holds with $\epsilon = 1/(2C_{2k,L})$. Consider any device whose material is outside the ball B_{R_J} and whose fields on its counted input space, within that ball, are linear combinations of regular vacuum vector waves of orders $l \le J$. If the actual fields satisfy (248), then*

$$\dim W \le \frac{2A(2k)^2 C_{2k,L}\delta}{\pi p}. \tag{257}$$

There is no bound on the coefficients or gains in this finite band. The radius threshold R_J may depend on the band, while the displayed count does not.

Proof. Extend each regular-wave combination to an entire vacuum field, and let $f_a \in \mathcal{F}_J$ be its plane flux. It agrees with the actual flux in the radius-R_J disk. Corollary 14.2 and the uniform tail estimate imply

$$\begin{aligned} \|f_a\|_1 &\le C_{2k,L} \int_{\mathbb{R}^2\setminus D} |f_a| \\ &\le C_{2k,L} \int_{\{|x|\le R_J\}\setminus D} |s_a| + \tfrac{1}{2}\|f_a\|_1 \le C_{2k,L}\delta\|a\|^2 + \tfrac{1}{2}\|f_a\|_1. \end{aligned} \tag{258}$$

Hence $\|f_a\|_1 \le 2C_{2k,L}\delta\|a\|^2$. The pointwise Fourier and rank-four trace argument in (253)–(254) applies with this doubled constant, while passage is unchanged on D. This proves (257). □

Corollary 14.7 (Fixed-target remote-control obstruction under explicit convergence)**.** *Let a sequence of physical devices be vacuum on balls with radii tending to infinity. Identify a fixed finite-dimensional normed input space W for the sequence. Assume that, for every $a \in W$, its electric and magnetic fields converge uniformly on compact subsets of the measurement plane to an entire propagating vacuum Herglotz family (E_a^0, H_a^0). If all devices satisfy (248) with the same p, δ, then their fixed input dimension obeys (249).*

Proof. Compact uniform convergence gives convergence of the flux on D, so $\int_D s_a^0 \ge p\|a\|^2$. Pointwise convergence on the complement and Fatou's lemma give $\int_{\mathbb{R}^2\setminus D} |s_a^0| \le \delta\|a\|^2$. The limit satisfies all hypotheses of Theorem 14.3. □

Remark 14.8 (Scope: varying targets and nearby material)**.** The convergence and propagating-limit hypotheses in Corollary 14.7 are essential parts of its statement. Finite-band transfer control, by itself, supplies no global bypass estimate. Allowing the angular band to grow with the remote-control radius, together with changing coefficients, can produce local superoscillatory limits with large vacuum tails beyond that radius. No uniform compactness or global Fourier-support claim for such sequences is made here. Changing coefficients alone in a fixed band does not evade Corollary 14.6 once its radius threshold is reached. Likewise this argument does not constrain devices whose material remains near the section. It proves an obstruction to a fixed-target remote-control completion. The nearby spheres used in Theorem 19.1 lie outside its hypotheses and permit the subsequent counterexample for $\delta > \eta$.

15 A nonradial channel bound with small total material volume

The following result controls physical excitation without a bound on the diameter, location, number of pieces, or minimum feature size of the material support. It imposes a small *total material volume*, which is an additional resource absent from Conjecture 1.4. Thus it proves a new restricted channel theorem, not the unrestricted conjecture. All frequency estimates in this section are at a positive *real* wavenumber k.

Small volume limits the strength of the material's total response, even when that material is distributed across a large region. The argument first bounds the free-space response kernel, then uses that bound to control the actual field in the physical incoming-power norm. Combining this field control with the earlier flux estimate yields a count. The conclusion is conditional on the quantitative volume restriction stated below, not on section area alone.

15.1 An exact real-frequency kernel estimate

Let $\chi = \varepsilon_r - 1$ be supported in a bounded measurable set $\Omega \subset \mathbb{R}^3$ of volume $V > 0$, with $0 \le \chi \le C := \varepsilon_+ - 1$. Write

$$a = \left(\frac{3V}{4\pi}\right)^{1/3}, \qquad \Phi_k(x) = \frac{e^{ik|x|}}{4\pi|x|}, \qquad \mathsf{K}_k = (k^2 I + \nabla\nabla)\Phi_k. \tag{259}$$

Distributionally on the whole space,

$$\mathsf{K}_k = -\mathsf{P} + \mathsf{R}_k, \qquad \mathsf{R}_k = k^2\Phi_k I + \nabla\nabla(\Phi_k - \Phi_0), \tag{260}$$

where P is the longitudinal orthogonal projection on $L^2(\mathbb{R}^3)^3$, with Fourier symbol $\xi\xi^{\mathsf{T}}/|\xi|^2$. In particular $\|\mathsf{P}\| = 1$. The static distributional term, including its diagonal contribution, is entirely contained in $-\mathsf{P}$.

Lemma 15.1 (Diameter-independent dynamic kernel estimate)**.** *For real $k > 0$ and $x \neq 0$,*

$$\|\mathsf{R}_k(x)\|_{\mathbb{C}^3\to\mathbb{C}^3} \le \frac{3k^2}{8\pi|x|}. \tag{261}$$

If U is another bounded measurable set of positive volume and $b = (3|U|/(4\pi))^{1/3}$, then

$$\|\mathbf{1}_U \mathsf{R}_k \mathbf{1}_\Omega\|_{2\to2} \le \frac{3}{4}k^2 ab. \tag{262}$$

Proof. Put $r = |x|$, $z = kr$, $n = x/r$, and $C_z = e^{iz}(1 - iz) - 1$. Direct radial differentiation gives

$$\mathsf{R}_k(x) = \frac{z^2e^{iz} - C_z}{4\pi r^3}(I - nn^{\mathsf{T}}) + \frac{2C_z}{4\pi r^3}nn^{\mathsf{T}}. \tag{263}$$

Since $C_0 = 0$ and $C_z' = ze^{iz}$, real $z \ge 0$ satisfies $|C_z| \le z^2/2$. The two real orthogonal projections in (263) give a normal matrix, whose operator norm is the larger modulus of its two eigenvalues. The tangential modulus is at most $3z^2/(8\pi r^3)$ and the radial modulus at most $z^2/(4\pi r^3)$. This proves (261). Near zero the difference $\Phi_k - \Phi_0 = ik/(4\pi) + O(r)$ has a locally integrable Hessian with no point mass: its first derivative is bounded and its surface integral on a radius-r sphere is $O(r^2)$. Thus this computation introduces no unaccounted distributional term.

For any measurable set A of volume $4\pi d^3/3$, and any center x,

$$\int_A |x - y|^{-p}\,dy \le \frac{4\pi d^{3-p}}{3-p} \quad (0 < p < 3). \tag{264}$$

Indeed, remove the portion of A outside the radius-d ball about x and fill its equally sized missing portion inside the ball. The decreasing radial kernel cannot reduce the integral. Integration over the ball gives the stated expression; truncation justifies the argument at its singularity. For the kernel majorant in (261), the row integral over Ω is at most $3k^2a^2/4$ and the column integral over U at most $3k^2b^2/4$. The vector-valued Schur estimate, obtained by applying the scalar Schur argument to the pointwise Euclidean norms, gives (262). □

Theorem 15.2 (Real-frequency response controlled by total volume)**.** *Suppose*

$$t := \frac{3}{4}C(ka)^2 < 1. \tag{265}$$

For a physical incident Maxwell field e^{inc}, let e be its outgoing total electric field in the normalization $e = \sqrt{\varepsilon_0}E$. Then

$$\|\sqrt{\chi}\,e\|_{L^2(\Omega)} \le \frac{\|\sqrt{\chi}\,e^{\mathrm{inc}}\|_{L^2(\Omega)}}{1-t}, \qquad \|\chi e\|_{L^2(\Omega)} \le \frac{\sqrt{C}\,\|\sqrt{\chi}\,e^{\mathrm{inc}}\|_{L^2(\Omega)}}{1-t}. \tag{266}$$

The inverse estimate is uniform over all supports of this volume and all measurable contrasts in the stated interval. No lower positive bound on χ is required.

Proof. The outgoing volume equation is $e = e^{\mathrm{inc}} + \mathsf{K}_k(\chi e)$. Set $s = \sqrt{\chi}$ and $j = se$, with functions on Ω extended by zero before applying whole-space operators. Its weighted form is

$$(I + s\mathsf{P}s - s\mathsf{R}_k s)j = se^{\mathrm{inc}}. \tag{267}$$

The operator $B = I + s\mathsf{P}s$ is self-adjoint and $B \geq I$, so $\|B^{-1}\| \leq 1$. Lemma 15.1, with $U = \Omega$, gives $\|s\mathsf{R}_k s\| \leq t$. Factor the left side as $B(I - B^{-1}s\mathsf{R}_k s)$ and invert the second factor by its norm convergent geometric series. This gives an inverse norm at most $(1-t)^{-1}$, which proves the first inequality; the second follows from $\|sj\| \leq \sqrt{C}\|j\|$.

Conversely the solution j reconstructs the outgoing field $e = e^{\mathrm{inc}} + \mathsf{K}_k(sj)$, and (267) gives $se = j$. Thus it solves the distributional Maxwell volume equation. A homogeneous outgoing solution has $j = 0$ by the same inverse, and its volume representation then gives $e = 0$. In the piecewise smooth physical class this is the ordinary unique outgoing scattering solution. The estimate therefore controls the actual physical field, rather than a formal Born approximation. □

15.2 Physical incoming power and the full local field resource

Take the physical incoming space to be transverse $L^2(S^2)^3$ with $g(d) \cdot d = 0$ and incoming power $\|g\|_2^2$. In the normalized variables $e = \sqrt{\varepsilon_0}E$, $h = \sqrt{\mu_0}H$, $c_0 = (\varepsilon_0\mu_0)^{-1/2}$, use

$$\begin{aligned} e_g^{\mathrm{inc}}(x) &= \frac{k}{\pi\sqrt{2c_0}} \int_{S^2} g(d) e^{ikd\cdot x}\, dS(d), \\ h_g^{\mathrm{inc}}(x) &= \frac{k}{\pi\sqrt{2c_0}} \int_{S^2} d \times g(d) e^{ikd\cdot x}\, dS(d). \end{aligned} \tag{268}$$

Stationary phase for smooth g gives incoming electric amplitude of modulus $\sqrt{2/c_0}|g(-\widehat{x})|/r$. Multiplication by the flux factor $c_0/2$ and integration over the incoming sphere gives $\|g\|_2^2$. Density extends this power normalization to L^2 data. In particular no plane wave of infinite incoming power is substituted for a unit input. Cauchy–Schwarz gives, pointwise,

$$|e_g^{\mathrm{inc}}(x)|,\ |h_g^{\mathrm{inc}}(x)| \leq k\sqrt{\frac{2}{\pi c_0}}\, \|g\|_2. \tag{269}$$

Theorem 15.3 (Explicit physical-power bound on local electric and magnetic fields)**.** *Under* (265)*, fix a bounded measurable observation set U of positive volume, and put*

$$\begin{aligned} b &= \left(\frac{3|U|}{4\pi}\right)^{1/3}, \quad I_U = k\sqrt{\frac{2|U|}{\pi c_0}}, \qquad P_V = \frac{Ck}{1-t}\sqrt{\frac{2V}{\pi c_0}}, \\ A_k(r) &= r + \frac{k}{2}r^2, \qquad D_E = 1 + \frac{3}{4}k^2 ab, \quad D_H = k\sqrt{A_k(a)A_k(b)}. \end{aligned} \tag{270}$$

For every physical incoming g,

$$\begin{aligned} \|\chi e_g\|_{L^2(\Omega)} &\leq P_V \|g\|_2, \\ \|e_g\|_{L^2(U)} &\leq (I_U + D_E P_V)\|g\|_2, \\ \|h_g\|_{L^2(U)} &\leq (I_U + D_H P_V)\|g\|_2. \end{aligned} \tag{271}$$

Consequently the complete local resource satisfies

$$\int_U (\varepsilon_r |e_g|^2 + |h_g|^2)\, dx \leq B_U \|g\|_2^2, \qquad B_U = \varepsilon_+ (I_U + D_E P_V)^2 + (I_U + D_H P_V)^2. \tag{272}$$

These bounds are independent of the distance between U and the material, and of the diameter and fine structure of the material support.

Proof. Apply (266) and (269) to obtain the first inequality. Put $p = \chi e_g$, extended by zero. The exact electric scattered field is $e^{\mathrm{sc}} = -\mathsf{P}p + \mathsf{R}_k p$. The whole-space projection has norm one, and (262) bounds the restriction of the dynamic term to U. Adding the incident-field bound gives the second inequality.

Taking the curl of the volume representation and using $\nabla \times e = ikh$ removes the Hessian part and gives

$$h^{\mathrm{sc}} = \frac{k}{i}\nabla \times (\Phi_k * p), \qquad |\nabla \Phi_k(x)| \le \frac{1}{4\pi}\left(\frac{k}{|x|} + \frac{1}{|x|^2}\right). \tag{273}$$

The cross-product kernel has operator norm at most $|\nabla \Phi_k|$. Equation (264), for $p = 1, 2$, bounds its row integral over Ω by $A_k(a)$ and its column integral over U by $A_k(b)$. The Schur estimate therefore gives $\|h^{\mathrm{sc}}\|_{L^2(U)} \le D_H \|p\|_2$. This proves the magnetic inequality. The coefficient bound $\varepsilon_r \le \varepsilon_+$ proves (272). □

Proposition 15.4 (Outgoing scattering is uniformly close to vacuum)**.** *With the same normalization and hypotheses, the radiated scattered power satisfies*

$$P_{\mathrm{sc}}(g) \le \left[\frac{Ck^3V}{2\pi(1-t)}\right]^2 \|g\|_2^2. \tag{274}$$

Equivalently, the full scattering operator differs from the vacuum scattering operator in power norm by at most $Ck^3V/[2\pi(1-t)]$.

Proof. For $p = \chi e_g$, the normalized electric far field is

$$e_\infty^{\mathrm{sc}}(d) = \frac{k^2}{4\pi}(I - dd^{\mathsf{T}}) \int_\Omega p(y) e^{-ikd\cdot y}\, dy. \tag{275}$$

Cauchy–Schwarz in Ω and then integration over S^2 give $P_{\mathrm{sc}} = (c_0/2)\|e_\infty^{\mathrm{sc}}\|_2^2 \le c_0 k^4 V \|p\|_2^2/(8\pi)$. Insert the first bound in (271) to obtain (274). The difference of the outgoing amplitudes is exactly the scattered outgoing amplitude; the incoming amplitudes agree. □

15.3 A genuine restricted channel theorem and its remaining limit

Corollary 15.5 (Uniform channel count under a small-volume cap)**.** *Fix the section, real frequency, material interval, and thresholds of Definition 1.3, with $\delta < \eta\tau$. Restrict the material support by $|\Omega| \le V_{\max}$, where*

$$\frac{3}{4}(\varepsilon_+ - 1)k^2 \left(\frac{3V_{\max}}{4\pi}\right)^{2/3} < 1. \tag{276}$$

Use physical incoming amplitudes (268) and retain the physical section compatibility of Assumption 6.10. Let B be the fixed comparison box and K, C_H its constants in (88). Define B_B by (270)–(272), taking $U = B$ and $V = V_{\max}$. Then every counted subspace satisfies

$$\dim W \le \frac{|B|}{2\pi^2}\left(\frac{KC_H B_B}{\eta\tau - \delta}\right)^{3/2}. \tag{277}$$

No enclosing radius, interface count, separation, or minimum feature size enters this bound.

Proof. All quantities on the right side of (272) are nondecreasing in V while (265) holds. Thus the common volume cap gives the input-to-resource estimate with constant B_B. Apply Theorem 6.13 to any finite-dimensional subspace of W. If W had larger or infinite dimension, it would contain a finite-dimensional subspace violating the same bound. □

Remark 15.6 (Open question: removal of the volume cap)**.** This argument excludes arbitrarily many counted channels formed solely by redistributing a sufficiently small amount of bounded-contrast dielectric, even among distant nonradial pieces. It does not exclude large remote resonators or matching structures: their total material volume is unrestricted in the primary target. If $t \geq 1$, the geometric-series proof supplies no inverse bound; it does not assert that the scattering problem is singular. Likewise an L^2 bound does not bound pointwise electric peaks and is fully compatible with the conical hotspot constructions. Finally, (261) uses $|e^{iz}| = 1$ for real z. At complex resonance frequencies it gives no diameter-independent estimate, and no resonance-free complex neighborhood is claimed.

16 Edge circulation and its physical completion

The absolute-bypass condition permits a qualitatively different mechanism when $\delta > \eta$: positive circulation inside a sharp section edge may be accompanied by an equal negative return immediately outside it. This section proves an exact electrostatic cross-flux calculation and a finite-dimensional Maxwell jet-interpolation result for that mechanism. It then states the additional global estimate needed to make the mechanism an admissible counterexample. Theorems 17.3 and 18.7 discharge that estimate in the following sections, leading to Theorem 19.1. In particular, no impressed dipole is included in the admissible material class and no electrostatic field is presented as an exact solution at the fixed nonzero frequency.

The proposed mechanism exploits the difference between signed passage and absolute bypass. A small inclusion close to the edge creates a local pattern with forward flux on one side and return flux on the other. By assigning independent local field data to different edge points, one can make this pattern for every coherent input in a finite-dimensional space. That is a local calculation: the device must still generate those data and keep the error small on the entire plane. The next two sections supply those global ingredients for the particular family used in the final theorem.

16.1 Exact local profile and physical coherent jets

Use the physical fields, the convention $e^{-i\omega t}$, and $Z_0 = \sqrt{\mu_0/\varepsilon_0}$. At one straight edge introduce orthonormal coordinates (x, y, z) with the section locally $x < 0$, outward normal $\widehat{x}$, tangent $\widehat{y}$, and $\widehat{x} \times \widehat{y} = \widehat{z}$. Fix dimensionless numbers $0 < \rho < h$ and $1 < \varepsilon_p \leq \varepsilon_+$. Set

$$\alpha = 4\pi\rho^3 \frac{\varepsilon_p - 1}{\varepsilon_p + 2} > 0. \tag{278}$$

Lemma 16.1 (Electrostatic edge cross-flux)**.** *For $s > 0$, put a dielectric sphere of radius ρs at $(0, 0, hs)$. Its exact electrostatic exterior response to a uniform normal electric field $Ae\widehat{z}$, where $A > 0$ and $e \in \mathbb{C}$, has dipole moment $\varepsilon_0 \alpha s^3 Ae\widehat{z}$. On the plane $z = 0$ its scattered tangential electric field is*

$$E_t^{\mathrm{stat}}(s\xi, s\upsilon, 0) = -\frac{3\alpha h A e}{4\pi} \frac{(\xi, \upsilon)}{(\xi^2 + \upsilon^2 + h^2)^{5/2}}. \tag{279}$$

Cross this field with a constant tangential magnetic jet $Ab\widehat{y}$, $b \in \mathbb{C}$. The resulting real cross-flux profile is exactly

$$f_s(s\xi, s\upsilon) := \tfrac{1}{2} \operatorname{Re}(E_t^{\mathrm{stat}} \times A\bar{b}\widehat{y}) \cdot \widehat{z} = -\frac{3\alpha h A^2}{8\pi} \operatorname{Re}(e\bar{b}) \frac{\xi}{(\xi^2 + \upsilon^2 + h^2)^{5/2}}. \tag{280}$$

If $q = \mathrm{Re}(e\bar{b}) \geq 0$, *then*

$$\int_{x<0} f_s \, dx \, dy = \int_{x>0} |f_s| \, dx \, dy = \frac{s^2 A^2 \alpha q}{4\pi h}, \qquad \int_{\mathbb{R}^2} f_s \, dx \, dy = 0. \tag{281}$$

The profile is nonnegative inside the edge and nonpositive outside. These are exact statements about the stated electrostatic cross-term.

Proof. Center coordinates at the sphere. Write the exterior potential as $-Aez + cAe(\rho s)^3 z/r^3$ and the interior potential as $-dAez$. Continuity of potential and normal electric displacement gives $d = 1 - c$ and $\varepsilon_p(1 - c) = 1 + 2c$. Therefore $c = (\varepsilon_p - 1)/(\varepsilon_p + 2)$, proving the polarizability. The dipole field is $[3(p \cdot \widehat{r})\widehat{r} - p]/(4\pi\varepsilon_0 r^3)$. At the observation plane the center-relative vector is $s(\xi, \upsilon, -h)$, which gives (279). Taking its cross product gives (280). Finally,

$$\int_{\mathbb{R}} \frac{d\upsilon}{(\xi^2 + \upsilon^2 + h^2)^{5/2}} = \frac{4}{3(\xi^2 + h^2)^2}, \qquad \int_{-\infty}^{0} \frac{-\xi \, d\xi}{(\xi^2 + h^2)^2} = \frac{1}{2h^2}.$$

Together with $dx\,dy = s^2 d\xi\, d\upsilon$ these prove the half-plane integrals. Oddness in ξ proves the last identity. □

An electric-wall vacuum Maxwell field satisfies (230); in particular $E_t = H_z = 0$ on the plane. Its normal Poynting density is identically zero there, including for every coherent combination of fields in that sector. We next prescribe the nonzero jets E_z, H_x, H_y while retaining this exact cancellation.

Lemma 16.2 (Finite even-TE jet interpolation)**.** *Let* $p_1, \ldots, p_N$ *be nonzero points of* $z = 0$, *with* $p_i \neq p_j$ *and* $p_i \neq -p_j$ *for* $i \neq j$. *Arbitrary complex values of* (E_z, H_x, H_y) *at these* N *points can be realized by a finite linear combination of regular vacuum TE spherical waves with even angular order* $l \geq 2$ *and even azimuthal index* m. *The field is electric-wall and invariant, with the vectors rotated, under a rotation by* π *about the* z *axis. In particular*

$$E_z(-p_j) = E_z(p_j), \qquad H_t(-p_j) = -H_t(p_j). \tag{282}$$

The interpolating regular waves have finite physical incoming power. No bound uniform in the interpolation points or target jets is asserted.

Proof. Consider a scalar regular Helmholtz solution u that is even in z and invariant under $(x, y) \mapsto (-x, -y)$, and set

$$E = \nabla \times (xu) = \nabla u \times x, \qquad H = \frac{\nabla \times E}{i\omega\mu_0}. \tag{283}$$

Since $\nabla \cdot E = 0$ and $(\Delta + k_0^2)E = 0$, these fields satisfy both vacuum Maxwell equations. They have precisely the electric-wall and rotation symmetries just stated. Their scalar spherical-harmonic expansion contains only even m and even l; the $l = 0$ term gives zero in (283). Thus finite truncations are regular TE fields of the required kind.

The full tangential scalar two-jets can first be prescribed at $p_1, \ldots, p_N$. To see this without assuming a Runge theorem, write $r_t = (x, y)$ and use the entire scalar solutions

$$u_\xi(r_t, z) = \cos(\xi \cdot r_t) \cos\!\big(\sqrt{k_0^2 - |\xi|^2}\, z\big), \qquad |\xi| < k_0.$$

If a linear functional on those finitely many two-jets annihilates every u_ξ, its value is an exponential polynomial in ξ, vanishing on the real open disk. Its entire continuation therefore vanishes identically.

It is the Fourier transform of the symmetrized finite distribution of derivatives of point masses supported at p_j and $-p_j$. These support points are all distinct, so uniqueness of the Fourier transform forces every coefficient of the original jet functional to be zero. Finite-dimensional duality proves the surjectivity of the scalar jet map.

For clarity, the resulting scalar jets really do prescribe the three Maxwell jets independently. Rotate coordinates in the plane so that one point is $(r, 0, 0)$ with $r > 0$. Formula (283) gives

$$E_z = -ru_y, \qquad H_x = \frac{2u_x + ru_{xx} + k_0^2 ru}{i\omega\mu_0}, \qquad H_y = \frac{2u_y + ru_{xy}}{i\omega\mu_0}. \tag{284}$$

Choose u_y for E_z, then u_{xy} for H_y, and u_{xx} for H_x. This gives a surjective map at each point, hence at all points simultaneously.

Each u_ξ is a finite sum of plane waves with real wavevectors of length k_0. Replace its point-supported angular measures by smooth, symmetrized densities on the sphere; their fields and any fixed finite set of derivatives converge on compact sets. Thus the jet map of smooth symmetric scalar Herglotz fields is onto: choose finitely many approximately interpolating columns close enough to an invertible interpolation matrix. For each of these smooth fields, truncate the spherical-harmonic expansion, preserving both symmetries. Compact derivative convergence again preserves the invertibility of that finite matrix. Invert it to obtain exact jets using one finite angular band. Its Maxwell fields are finite regular TE sums; their incoming spherical amplitudes have finite power. The parity identities give (282). □

Lemma 16.3 (Balancing the physical input Gram matrix)**.** *For any finite collection of target jets covered by Lemma 16.2, there are interpolants $v_1, \dots, v_N$ in a common finite even-TE band whose physical incoming Gram matrix is λI_N for some $0 < \lambda < \infty$. Consequently $g_j = v_j/\sqrt{\lambda}$ are orthonormal physical incoming data. All v_j retain their prescribed jets.*

Proof. Start with arbitrary interpolants u_j and their positive semidefinite incoming Gram matrix G. The space of finite even-TE regular waves has unbounded dimension, whereas the jet map has finite rank. Enlarge its finite band until its jet kernel contains an N-dimensional subspace orthogonal, in physical incoming power, to the span of the u_j. Choose $\lambda > \|G\|$. In an orthonormal basis of that kernel subspace, a matrix square root of $\lambda I - G$ supplies vectors w_j with Gram matrix $\lambda I - G$. They have zero prescribed jets and are orthogonal to all u_j. Hence $v_j = u_j + w_j$ has the same jets as u_j and Gram matrix $G + (\lambda I - G) = \lambda I$. □

16.2 Finite-rank diagonal edge circulation

Choose distinct points $p_j = (L/2, y_j, 0)$ on the interior of the right edge of the square, with $-L/2 < y_j < L/2$. Their partners $-p_j$ lie on the left edge. Let $\ell_0 = k_0^{-1}$. By Lemmas 16.2–16.3, take interpolants with jets

$$E_z^{v_j}(p_i) = \frac{\sqrt{Z_0}}{\ell_0}\delta_{ij}, \qquad H_t^{v_j}(p_i) = \frac{\widehat{y}}{\sqrt{Z_0}\ell_0}\delta_{ij}, \qquad \langle v_i, v_j\rangle_{\mathrm{in}} = \lambda\delta_{ij}. \tag{285}$$

Physical field units are implicit in the unit-power normalization of this display. Its relevant product is exactly $1/\ell_0^2$.

For each fixed amplification $A > 0$, Theorem 12.4 can amplify every even TE order in this finite band by the same factor $A\sqrt{\lambda}$, up to a common phase and arbitrarily small compact derivative errors. Applied to the orthonormal inputs $g_j = v_j/\sqrt{\lambda}$, its ideal core jets at p_j are

$$E_z(c; p_j) = \frac{A\sqrt{Z_0}}{\ell_0}c_j, \qquad H_t(c; p_j) = \frac{A}{\sqrt{Z_0}\ell_0}c_j\widehat{y}, \qquad c \in \mathbb{C}^N. \tag{286}$$

The original radial-device background has zero plane flux exactly, at every finite stage, by reflection symmetry. Compact derivative approximation concerns its illumination only, before adding spheres.

For $a > 0$ set $s = a\ell_0$ and $A = t/a$, with fixed $t > 0$. At each of p_j and $-p_j$, put the electrostatic cross-profile of Lemma 16.1, with the local outward/tangent directions $(\widehat{x}, \widehat{y})$ on the right and $(-\widehat{x}, -\widehat{y})$ on the left. Use the jets (286), and denote the sum of these $2N$ profiles by $F_a(c; x, y)$. Thus F_a is defined on the whole plane by explicit functions; it is quadratic in c and diagonal in the coefficients $|c_j|^2$.

Proposition 16.4 (Coherent local-model passage and absolute bypass)**.** *For each fixed finite N, the profiles just defined obey*

$$\sup_{\|c\|=1} \left| \int_D F_a(c)\, dA - p_0 \right| \longrightarrow 0, \qquad \sup_{\|c\|=1} \left| \int_{\mathbb{R}^2 \setminus D} |F_a(c)|\, dA - p_0 \right| \longrightarrow 0, \qquad p_0 = \frac{\alpha t^2}{2\pi h}. \tag{287}$$

Also $\int_{\mathbb{R}^2} F_a(c)\, dA = 0$ exactly. The geometric spheres associated with these profiles have radius $\rho a \ell_0$, lie strictly above the plane, are disjoint for sufficiently small a, and preserve the rotation by π symmetry. Their contrasts remain in the fixed ordinary dielectric interval.

Proof. For one point, the product in Lemma 16.1 is $q = |c_j|^2/\ell_0^2$, so its positive half-plane mass equals $\alpha t^2 |c_j|^2/(4\pi h)$. Its partner has the same mass: both the local tangent and H_t reverse at $-p_j$, leaving the scalar product and the orientation of positive interior flux unchanged. Summing gives $p_0 \sum_j |c_j|^2$.

Choose disjoint fixed disks about the $2N$ edge points, avoiding corners. Within each disk the square is exactly its interior half-plane. The rescaled profile has an integrable envelope bounded by a constant times $(1 + \xi^2 + \upsilon^2)^{-2}$, so its L^1 mass outside its disk tends to zero. More precisely its tail outside scaled radius R is $O(R^{-2})$. On each disk retain only its own profile. The L^1 difference between this truncated sum and F_a tends to zero, uniformly for $\sum_j |c_j|^2 = 1$, since there are finitely many centers. The retained profiles have the required signs on the two sides. The inequality $\big||u| - |v|\big| \le |u - v|$ proves both limits, including the absolute-value limit for arbitrary coherent c. Oddness gives zero total signed integral for every individual profile. Finally $h > \rho$ leaves a vacuum gap above the plane, and the fixed distinct centers ensure disjointness when a is small. □

Remark 16.5 (Why conditioning of the interpolation is not a bypass loss)**.** The number λ in Lemma 16.3 can be large and depends on N and the points. It is fixed before $a \downarrow 0$ and is absorbed into the common core gain $A\sqrt{\lambda}$. The incoming data remain orthonormal. Thus the model's passage and bypass matrices are both $p_0 I_N$ in physical input coordinates, rather than matrices whose ratio deteriorates with an interpolation condition number. This is a finite-dimensional statement and does not supply a bound on the perturbed Maxwell Green operator.

16.3 The precise physical estimate still required

For each a, the finite-band control theorem permits choosing a finite radial background with vacuum core large enough that its unperturbed fields approximate (286) and any prescribed finite number of derivatives as accurately as desired on a fixed neighborhood of all the edge points. The target gain $t\sqrt{\lambda}/a$ is finite for each a. This diagonal choice is legitimate for illumination. Add the $2N$ actual dielectric spheres to that background, and let $S_{z,a}(c)$ denote the plane flux of the resulting exact total scattering field for the same orthonormal incoming inputs. A background approximation theorem alone does not estimate this new field.

Proposition 16.6 (Conditional global completion estimate)**.** *Fix $0 < \tau < 1$ and $0 < \eta < \delta$. Choose t so that the constant p_0 of (287) lies strictly between η and δ. Suppose that for each fixed N one can choose the finite radial backgrounds and sphere sizes above so that the actual physical scattering fields have legitimate integrable plane fluxes and satisfy*

$$\sup_{\|c\|=1} \|S_{z,a}(c) - F_a(c)\|_{L^1(\mathbb{R}^2)} \longrightarrow 0. \tag{288}$$

Take the selected output map to be the full unitary scattering map of each finite lossless dielectric. Then for sufficiently small a the span of those N physical incoming data is counted under Definition 1.3, with the same fixed τ, η, δ. Consequently if *(288) can be established for every finite N, the unrestricted finiteness target is false for this one admissible fixed threshold tuple.*

Proof. Orthonormality gives input power $\|c\|^2$; unitarity gives $\|Tc\|^2 = \|c\|^2 \geq \tau\|c\|^2$. Equations (287)–(288) imply, uniformly for unit c, that actual passage tends to p_0 and actual absolute bypass tends to p_0. Their strict margins from η and δ prove the other two counting inequalities. Homogeneity covers all c. For each member the sphere-to-plane gap is positive, so it supplies a source-free vacuum neighborhood of the section; its shrinking size is not a forbidden resource. □

Remark 16.7 (The bridge discharged in the following sections)**.** The exact isolated-sphere electrostatic polarizability and finite-band illumination control alone do not imply (288). Three issues must be controlled together: the small-inclusion expansion in a background whose resonant amplification grows like a^{-1}, the source Green response of unselected angular orders, and the absolute flux of all correction fields across the entire plane, including the remote layers. A finite inverse for each separate device would be insufficient unless its dependence on that varying background is controlled.

The sphere volume is $O(a^3)$ and the amplified jet is $O(a^{-1})$. Theorem 17.3 turns the resulting scale $a^3 a^{-2} = a$ into an actual bounded-inverse and whole-plane remainder estimate for an explicit parity reaction kernel. Theorem 18.7 identifies that kernel as the source response of distant finite common stacks in the limit, controlling all angular orders and the remote absolute-flux tails. Its inverse stability step transfers the estimate to actual perturbed devices. These two additional proofs, rather than incident gain or signed power conservation alone, discharge (288). The final fixed-threshold construction is Theorem 19.1.

17 The small-inclusion limit for an explicit parity reaction kernel

We now discharge the small-inclusion and whole-plane error estimates for a specific limiting core Green kernel. This is a theorem about that explicit kernel. Its identification as the limit of physical finite radial backgrounds, together with control of the remote annulus, is proved separately in Theorem 18.7. Neither step is inferred just from finite-band incident amplification; their combination gives Theorem 19.1.

The important point is self-consistency. Once an inclusion is introduced, its induced field feeds back on the other inclusions and on the background; simply adding prescribed dipole fields would omit that interaction. We solve the inclusion equation for the explicit limiting kernel and estimate the difference between the resulting plane flux and the desired edge profile in an integral norm over the whole plane. The separate radial Green limit is what connects this calculation to actual finite stacks.

17.1 The exact kernel and elementary plane estimates

Write $k = k_0$, $\Phi_k(x) = e^{ik|x|}/(4\pi|x|)$, and use the dimensionless electric polarization $P = \chi E$, where $\chi = \varepsilon_r - 1$. The free electric response is

$$\mathcal{K}_0 P = (k^2 I + \nabla\nabla)\Phi_k * P = -\mathcal{P}P + \mathcal{D}P. \tag{289}$$

Here $\mathcal{P}$ is the longitudinal orthogonal projection on $L^2(\mathbb{R}^3;\mathbb{C}^3)$, whose Fourier multiplier is $\xi\xi^T/|\xi|^2$. Thus $\mathcal{P} \geq 0$ and $\|\mathcal{P}\| = 1$. The remainder $\mathcal{D}$ has a kernel bounded by $C/|x|$ on every fixed bounded set. Outside the support of P the static kernel $-\mathcal{P}$ is bounded by $C/|x|^3$. The magnetic response is

$$\mathcal{H}P(x) = \frac{\nabla \times \mathcal{K}_0 P(x)}{i\omega\mu_0} = \frac{k^2}{i\omega\mu_0}\int \nabla\Phi_k(x-y) \times P(y)\, dy. \tag{290}$$

Its kernel is bounded by $C(|x|^{-2} + |x|^{-1})$.

Let $R_z = \mathrm{diag}(1, 1, -1)$ and define the electric-field wall projections

$$\mathcal{W}E(x) = -R_z E(R_z x), \qquad \Pi_{\mathrm{e}} = \tfrac{1}{2}(I + \mathcal{W}), \qquad \Pi_{\mathrm{m}} = \tfrac{1}{2}(I - \mathcal{W}). \tag{291}$$

The first range has electric-wall parity. The entire real kernel

$$J(x) = (k^2 I + \nabla\nabla)\frac{\sin(k|x|)}{4\pi|x|} = \frac{k^3}{16\pi^2}\int_{S^2}(I - \theta\theta^T)e^{ik\theta\cdot x}\, d\theta \tag{292}$$

is the imaginary part of the free electric kernel. Set

$$\mathcal{R}_{\mathrm{e}} P = i\Pi_{\mathrm{e}}(J * P), \qquad \mathcal{R}_{\mathrm{m}} P = i\Pi_{\mathrm{m}}(J * P).$$

For an actual core gain parameter $B > 0$, define

$$\mathcal{K}_B P = \mathcal{K}_0 P + (B^2 - 1)\mathcal{R}_{\mathrm{e}} P + (B^{-2} - 1)\mathcal{R}_{\mathrm{m}} P. \tag{293}$$

All derivatives in these definitions are distributional where necessary. Away from the source support the formulas are classical. Both reaction fields are entire vacuum Maxwell electric fields; their magnetic partners are their curls divided by $i\omega\mu_0$. On $z = 0$ the electric-wall reaction has zero tangential electric field, and the opposite-wall reaction has zero tangential magnetic field.

Lemma 17.1 (Uniform local and far-field kernel bounds)**.** *Fix a ball containing all source supports under consideration. On each fixed observation ball, $\mathcal{R}_{\mathrm{e}}P$, $\mathcal{R}_{\mathrm{m}}P$, and their magnetic partners, with any fixed number of derivatives, are bounded by $C\|P\|_1$. For $|x| = r$ outside a larger fixed ball, each has an expansion*

$$F(x) = \frac{e^{ikr}F_+(\widehat{x}) + e^{-ikr}F_-(\widehat{x})}{r} + O(C\|P\|_1 r^{-2}), \qquad F_\pm(\widehat{x}) \cdot \widehat{x} = 0, \tag{294}$$

with $\|F_\pm\|_\infty \leq C\|P\|_1$. The free electric and magnetic responses have the same statement with $F_- = 0$. For the dynamic electric response $\mathcal{D}P$ the same leading far-field statement holds. These estimates are uniform over all L^1 polarizations in that fixed source ball.

If two such fields have amplitude bounds M_1, M_2 in this statement, then on the measurement plane outside the fixed larger disk

$$|(F_1 \times \overline{F_2}) \cdot \widehat{z}| \leq CM_1M_2r^{-3}, \qquad \int_{r>R}|(F_1 \times \overline{F_2}) \cdot \widehat{z}|\, dA \leq CM_1M_2/R. \tag{295}$$

The same assertions apply to any fixed finite collection of regular vacuum waves, with its coefficient norm replacing $\|P\|_1$.

Proof. The integral in (292) gives all compact derivative bounds directly, including after reflection. The reaction fields are smooth spherical Herglotz fields. Their angular amplitudes and all their derivatives are bounded by $C\|P\|_1$, since y stays in a fixed ball in the factor $e^{-ik\theta\cdot y}$. Stationary phase at the two points $\theta = \pm\widehat{x}$ gives (294), uniformly in direction. The factor $I - \theta\theta^T$ makes the electric leading amplitudes transverse. A curl gives the transverse magnetic leading amplitudes and the same remainder order. Equivalently these statements follow by differentiating the explicit sine kernel.

For the free responses, expand $|x-y| = r - \widehat{x}\cdot y + O(r^{-1})$ and the derivatives of $\Phi_k(x-y)$ uniformly for bounded y. The electric leading matrix is $k^2(I-\widehat{x}\widehat{x}^T)e^{ikr}/(4\pi r)$; the magnetic leading vector is a cross product with $\widehat{x}$. Both are transverse. The static subtraction is $O(\|P\|_1 r^{-3})$, so it does not change the dynamic leading terms. On the plane, $\widehat{x}\cdot\widehat{z} = 0$. The cross product of two vectors transverse to $\widehat{x}$ is parallel to $\widehat{x}$, even with complex coefficients. Consequently every r^{-2} leading contribution to the normal cross product is zero. The remainders give (295), whose radial integral is finite. Finite regular waves have the same transverse incoming and outgoing expansions. □

Lemma 17.2 (Small-source plane estimates)**.** *Let Ω_a be the union of the $2N$ radius-$\rho a\ell_0$ balls from Proposition 16.4, where N is fixed and $a \downarrow 0$. They lie at distances at least $(h-\rho)a\ell_0$ from the plane, and $|\Omega_a| = O(a^3)$. For $P \in L^2(\Omega_a)$, extended by zero, and a fixed plane disk K containing all their projections,*

$$\|\mathcal{P}P\|_{L^1(\mathbb{R}^2)} \le Ca^{-1}\|P\|_1, \tag{296}$$

$$\|\mathcal{P}P\|_{L^2(\mathbb{R}^2)} \le Ca^{-1/2}\|P\|_2, \tag{297}$$

$$\|\mathcal{D}P\|_{L^1(K)} \le C\|P\|_1, \tag{298}$$

$$\|\mathcal{K}_0 P\|_{L^2(K)} \le Ca^{-1/2}\|P\|_2, \qquad \|\mathcal{H}P\|_{L^2(K)} \le Ca^{1/2}\|P\|_2. \tag{299}$$

The constants are independent of a and P.

Proof. For a source point y at height $d \ge ca$,

$$\int_{\mathbb{R}^2} |(x,0)-y|^{-3}\,dx = 2\pi/d, \qquad \int_{\mathbb{R}^2} |(x,0)-y|^{-6}\,dx = \pi/(2d^4).$$

The first proves (296). The second, integrated over Ω_a, bounds the squared Hilbert–Schmidt norm by $Ca^3a^{-4} = Ca^{-1}$, proving (297). The planar integral of $|x-y|^{-1}$ over K is uniformly bounded, which proves (298).

For the magnetic squared kernel, the $|x-y|^{-4}$ planar integral is π/d^2, and the $|x-y|^{-2}$ integral over K is $O(1+|\log d|)$. Its squared Hilbert–Schmidt norm is thus $O(a)+O(a^3|\log a|) = O(a)$. The dynamic electric squared kernel has Hilbert–Schmidt norm squared $O(a^3|\log a|)$. Combine these with the static bound to obtain (299). □

17.2 Self-consistent inclusions and the complete plane remainder

Fix the interpolants v_j, their number λ, the physical incoming basis g_j, and the geometry from Lemmas 16.2–16.3. Let $(E^v(c), H^v(c))$ be the finite regular electric-wall field $\sum_j c_j v_j$. For fixed $t > 0$ put

$$A_a = t/a, \qquad B_a = \sqrt{\lambda}A_a, \qquad (E_a^{\mathrm{bg}}, H_a^{\mathrm{bg}}) = A_a(E^v(c), H^v(c)), \qquad \chi_a = (\varepsilon_p - 1)\mathbf{1}_{\Omega_a}. \tag{300}$$

The distinction between A_a and B_a is necessary: A_a is the jet scale, whereas B_a is the actual common core multiplier on the orthonormal physical inputs g_j.

Theorem 17.3 (Explicit-kernel small-inclusion remainder)**.** *For all sufficiently small a, the equation*

$$P_a = \chi_a\big(E_a^{\mathrm{bg}} + \mathcal{K}_{B_a} P_a\big) \quad \text{in } L^2(\Omega_a) \tag{301}$$

has a unique solution. Define the auxiliary total fields by

$$E_a = E_a^{\mathrm{bg}} + \mathcal{K}_{B_a} P_a, \qquad H_a = \frac{\nabla \times E_a}{i\omega\mu_0}.$$

They solve Maxwell's equations with the actual sphere permittivities locally and outside the spheres, with the feedback condition encoded by (293). If $F_a(c)$ is the explicit cross-profile of Proposition 16.4, then

$$\big\| \tfrac{1}{2}\,\mathrm{Re}(E_a \times \overline{H_a}) \cdot \widehat{z} - F_a(c) \big\|_{L^1(\mathbb{R}^2)} \le Ca\|c\|^2. \tag{302}$$

All constants may depend on the fixed N, points, interpolants, $\lambda, t, k, \rho, h, \varepsilon_p$, but not on a or c. The theorem does not normalize these auxiliary fields by their own free-space incoming amplitude. Their use for physical unit-power scattering requires the separate finite-background limit.

Proof. It suffices to prove estimates for $\|c\| = 1$; linearity of the fields then gives the stated quadratic dependence. Write $s_a = \sqrt{\chi_a}$ and $u_a = s_a E_a$, so $P_a = s_a u_a$. Equation (301) becomes

$$\big(I + s_a \mathcal{P} s_a - s_a \mathcal{D} s_a - (B_a^2 - 1) s_a \mathcal{R}_{\mathrm{e}} s_a - (B_a^{-2} - 1) s_a \mathcal{R}_{\mathrm{m}} s_a\big) u_a = s_a E_a^{\mathrm{bg}}. \tag{303}$$

The first two terms form a self-adjoint operator at least I, so its inverse has norm at most one. A Schur estimate for the $|x-y|^{-1}$ dynamic kernel on Ω_a is $O(a^2)$: within one ball integrate $|x-y|^{-1}$ over a ball of radius $O(a)$, and between distinct balls use their fixed separation. The smooth reaction kernels have operator norms $O(a^3)$. Since $B_a = O(a^{-1})$, the norm of the remaining perturbation in (303) is $O(a^2) + O(B_a^2 a^3) = O(a)$. A Neumann series after the positive inverse proves invertibility, with inverse norm at most two for small a. In particular

$$\|P_a\|_2 \le Ca^{1/2}, \qquad \|P_a\|_1 \le Ca^2. \tag{304}$$

The equation and all its kernels commute with the rotation by π about z; the source and solution are in its invariant sector. No unsupported odd-m extension of a core kernel is used.

Let P_a^0 be constant on each sphere, with the isolated static value

$$P_a^0\big|_{\Omega_{a,j}^{\pm}} = (\varepsilon_p - 1)\frac{3}{\varepsilon_p + 2} E_a^{\mathrm{bg}}(p_j^{\pm}), \qquad p_j^{+} = p_j, p_j^{-} = -p_j. \tag{305}$$

These vectors are normal to the plane. For one isolated sphere they solve the static equation exactly: the interior electric field of its constant polarization is $-P_a^0/3$, so $P_a^0 = \chi(E_a^{\mathrm{bg}} - P_a^0/3)$. The actual background differs from its value at $p_j^{\pm}$ by $O(A_a a) = O(1)$ throughout the corresponding sphere. Its L^2 residual is $O(a^{3/2})$. Static interaction between distinct spheres has operator norm $O(a^3)$, because their mutual distances remain positive. The dynamic and reaction perturbations on P_a^0 have norm $O(a)\|P_a^0\|_2 = O(a^{3/2})$ by the preceding bounds. Applying the uniformly bounded inverse in (303) to this residual proves

$$\|P_a - P_a^0\|_2 \le Ca^{3/2}, \qquad \|P_a - P_a^0\|_1 \le Ca^3. \tag{306}$$

It remains to estimate the whole plane, not merely a compact set. Abbreviate the free response by (E^f, H^f), and the two full reaction responses, including their coefficients in (293), by (E^e, H^e) and (E^m, H^m). On the plane the wall identities give exactly

$$E_{a,t} = E_t^f + E_t^m, \qquad H_{a,t} = H_{a,t}^{\mathrm{bg}} + H_t^f + H_t^e. \tag{307}$$

By Lemma 17.1 and (304), the opposite-wall reaction fields have compact and far-field amplitude $O(a^2)$, while the wall reaction fields have amplitude $O(B_a^2 a^2) = O(1)$. The background fields have amplitude $O(A_a)$.

First take the cross product with H_a^{bg} in (307). Replacing the static free electric response of P_a by that of P_a^0 has plane L^1 error at most $Ca^{-1}\|P_a - P_a^0\|_1 = O(a^2)$ by (296). Since the background is globally bounded by CA_a, its flux error is $O(a)$. The dynamic free electric response has L^1 norm $O(a^2)$ on a fixed disk, by (298); outside that disk the transverse cancellation (295) gives a flux bound $O(A_a\|P_a\|_1) = O(a)$. The same compact bound and tail argument apply to $E^m \times \overline{H_a^{\mathrm{bg}}}$.

The remaining static field of P_a^0 is exactly a sum of normal dipoles, with the polarizabilities from Lemma 16.1. For each individual dipole, its tangential plane trace satisfies

$$\int_{\mathbb{R}^2} |E_t^{0,j}(x)|\, dA \le Ca, \qquad \int_{\mathbb{R}^2} |x - p_j^{\pm}|\, |E_t^{0,j}(x)|\, dA \le Ca^2. \tag{308}$$

These follow directly by scaling (279); the second radial integrand at infinity is $O(r^{-2})$ and is integrable. A finite regular background has global Lipschitz constant CA_a. Replacing its magnetic field in each such cross product by $H_a^{\mathrm{bg}}(p_j^{\pm})$ therefore costs at most $CA_a a^2 = O(a)$. The resulting sum is exactly $F_a(c)$, including the coefficients and signs in (280).

We finally control all cross products with the two correction magnetic fields in (307). On a fixed disk, (299) and (304) give

$$\|E^f\|_2 \le C, \qquad \|H^f\|_2 \le Ca, \qquad \|E^m\|_\infty \le Ca^2, \qquad \|H^e\|_\infty \le C.$$

Thus the free self-cross product and the product $E^m \times \overline{H^f}$ have L^1 norm $O(a)$. For products with H^e, use $\|\mathcal{P}P_a\|_{L^1} \le Ca^{-1}\|P_a\|_1 = O(a)$, $\|\mathcal{D}P_a\|_{L^1(K)} = O(a^2)$, and the bounded opposite-wall reaction, obtaining another $O(a)$ bound. Outside the disk, (295) applies to these products with amplitude pairs (a^2, a^2) or $(a^2, 1)$; both give $O(a)$ or smaller. All normal products are therefore integrable, and their sum proves (302). □

Remark 17.4 (What has been discharged)**.** For the explicit kernel (293), the sufficient plane remainder in Proposition 16.6 is now a conclusion, not an assumption. The proof uses the uniformly positive static block, includes every coherent input, and estimates the full absolute plane flux. Theorem 18.7 supplies the separate physical sequence: its core source Green kernels converge to (293), and its remote-annulus and exterior plane-flux contributions tend to zero at each fixed a. The order is fixed a first, remote radius second, then a diagonal sequence with $a \downarrow 0$. Theorem 19.1 combines these independently proved limits into finite ordinary devices with the original physical incoming normalization.

18 An actual radial Green limit with whole-plane flux convergence

This section proves a source-response and whole-plane convergence theorem for finite ordinary dielectric stacks. The gain is fixed while the stack radius tends to infinity. A later diagonal choice may select that radius after the gain and the inclusion geometry. This order avoids assuming a uniform resolvent bound over unrelated devices.

Earlier transfer estimates control finitely many incident partial waves. Inserted inclusions, however, generate sources whose response contains all angular orders and can affect the plane far from the square. To complete the physical argument we must control that entire source response, including the remote layers, rather than just the selected incident modes. The proof first identifies the limiting source kernel at fixed gain, then bounds the angular tails and the field in the layers, and finally proves convergence of the absolute-flux error over the full measurement plane.

18.1 The common stack and its source coefficient

Fix $1 < q < \sqrt{\varepsilon_+}$ and an integer $M \geq 1$, and put

$$A = q^M, \quad d_A = \frac{M\pi}{2}(1 + q^{-1}), \quad R = 2\pi n, \quad X = R + d_A. \tag{309}$$

Radii in the radial equations below are dimensionless, $x = kr$. Starting at R, place M high–low quarter-wave pairs: index q for length $\pi/(2q)$, followed by index one for length $\pi/2$. The core and exterior are vacuum. Every member has finite support, real scalar permittivity in $[1, q^2]$, and vacuum permeability. The reference transfers, with the angular term removed, are

$$U^0_{\mathrm{TE}} = (-1)^M \operatorname{diag}(A, A^{-1}), \qquad U^0_{\mathrm{TM}} = (-1)^M \operatorname{diag}(A^{-1}, A). \tag{310}$$

For each fixed angular order, the actual transfers tend to these matrices as $n \to \infty$, by the integral equation for their first-order systems: the omitted angular coefficients are $O(l(l+1)/R^2)$ on an interval of fixed length d_A.

Write $\nu = l(l+1)$, $\psi_l(x) = x j_l(x)$, $\chi_l(x) = x y_l(x)$, and

$$F_l(x) = \begin{pmatrix} \psi_l & \chi_l \\ \psi_l' & \chi_l' \end{pmatrix}, \qquad \det F_l(x) = 1. \tag{311}$$

Use the continuous state (u, u') for TE and $(u, \varepsilon_r^{-1} u')$ for TM. They agree in the vacuum regions. If U_l is the actual transfer from R to X, set

$$M_l = F_l(X)^{-1} U_l F_l(R) = \begin{pmatrix} a & b \\ c & d \end{pmatrix}.$$

All these matrices are real with determinant one.

Lemma 18.1 (Exact source coefficient)**.** *The outgoing radial solution normalized to $\psi_l + i\chi_l$ in the exterior has core continuation $z_l = \alpha_l \psi_l + \beta_l \chi_l$, where*

$$\begin{aligned} \alpha_l &= d - ib, & \beta_l &= -c + ia, \\ \gamma_l := \alpha_l/\beta_l &= \frac{-cd - ab - i}{a^2 + c^2}, & \operatorname{Im} \gamma_l &= -\frac{1}{a^2 + c^2}. \end{aligned} \tag{312}$$

In particular $\beta_l \neq 0$ and

$$|\gamma_l| \leq \|M_l\|^2, \qquad |1/\beta_l|^2 = -\operatorname{Im} \gamma_l = |g_l|^2, \tag{313}$$

where g_l is the physical incoming-to-core multiplier. The reduced core Green function with derivative jump $+1$ is

$$G_l(x, y) = \psi_l(x_<) \chi_l(x_>) + \gamma_l \psi_l(x) \psi_l(y). \tag{314}$$

For free outgoing vacuum $\gamma_l = -i$.

Proof. The exterior coefficient vector is $(1, i)^T$, hence the core coefficient vector is $M_l^{-1}(1, i)^T = (d - ib, -c + ia)^T$. Division and $ad - bc = 1$ give (312). The row norm giving $|\alpha_l|$ is at most $\|M_l^{-1}\|$, which equals $\|M_l\|$ for a real determinant-one 2 by 2 matrix. Also $|\beta_l| = |M_l e_1| \geq \|M_l\|^{-1}$. The exterior incoming coefficient of the origin-normalized regular solution is $(a + ic)/2$, giving the physical multiplier $g_l = 1/(a + ic)$ and (313). Finally $W(\psi_l, z_l) = \beta_l$, so the Green function $\psi_l(x_<) z_l(x_>)/\beta_l$ has the asserted jump. The weighted TM derivative equals the ordinary derivative in the core. The real part of γ_l is not controlled by incoming gain alone; the full transfer is used here. □

18.2 Uniform angular tails at fixed gain

Lemma 18.2 (Low and intermediate orders)**.** *Fix $0 < c_0 < 1$. Uniformly in the low range $\nu \le c_0^2 R^2$,*

$$|\gamma_l| \le B_A := \frac{16}{(1-c_0^2)^2}\exp(2C_0 d_A), \qquad C_0 = q^2 + c_0^2 + 1. \tag{315}$$

Every partial stack transfer in that range has norm at most $\exp(C_0 d_A)$. For sufficiently large R, in the intermediate range $c_0^2 R^2 < \nu \le q^2 X^2$,

$$|\gamma_l| \le C_F^4 \exp(4h_q R + 8q^2 d_A), \quad C_F = 4(1+2q), \quad h_q = 2 + 2q\log(4q). \tag{316}$$

Partial transfers in this range have norm at most $\exp(4q^2 d_A)$.

Proof. For $\xi_l = \psi_l + i\chi_l$ the outgoing energy

$$\mathcal{E}(x) = |\xi_l'|^2 + (1 - \nu/x^2)|\xi_l|^2$$

satisfies $\mathcal{E}' = 2\nu x^{-3}|\xi_l|^2 \ge 0$ and $\mathcal{E}(\infty) = 2$. Thus, for $x \ge R$ in the low range, $\|F_l(x)\|, \|F_l(x)^{-1}\| \le 2/\sqrt{1-c_0^2}$. The TE generator is $\left(\begin{smallmatrix} 0 & 1 \\ \nu/x^2 - \varepsilon_r & 0 \end{smallmatrix}\right)$; the TM generator is $\left(\begin{smallmatrix} 0 & \varepsilon_r \\ \nu/(\varepsilon_r x^2) - 1 & 0 \end{smallmatrix}\right)$. Their norms are at most C_0. The transfer estimate and (313) prove (315).

For the intermediate estimate use the finite Hankel polynomial

$$\xi_l(x) = (-i)^{l+1} e^{ix} \sum_{s=0}^{l} i^s \frac{(l+s)!}{s!(l-s)!2^s} x^{-s}.$$

If $a_l = (2l-1)!!$, reversal of its coefficients gives

$$\frac{a_{l-t}^{\mathrm{coeff}}}{a_l} = \frac{2^t}{t!}\prod_{j=0}^{t-1}\frac{l-j}{2l-j} \le \frac{1}{t!}.$$

Consequently

$$|\xi_l(x)| \le a_l x^{-l} e^x, \qquad |\xi_l'(x)| \le (1 + l/x) a_l x^{-l} e^x.$$

For large R, $X \le 2R$ and $l \le 2qR$. At R and X these inequalities, and $a_l \le (2l)^l$, give $\|F_l\|, \|F_l^{-1}\| \le C_F e^{h_q R}$. Both generators have norm at most $4q^2$ on the stack. Combining these bounds proves (316). □

Lemma 18.3 (Barrier-order source estimate)**.** *For $\nu > q^2 X^2$ let*

$$\gamma_* = \frac{1 + \sqrt{1 + 4(\nu - R^2)}}{2}, \qquad \theta_q = \sqrt{1 - q^{-2}}.$$

Then the outgoing core load $h = z_l'(R)/z_l(R)$ has $\operatorname{Re} h \le 0$, and

$$|\gamma_l| \le \frac{|\chi_l'(R)|}{\psi_l'(R)} + \frac{|\chi_l(R)|}{\psi_l(R)}, \tag{317}$$

$$\psi_l(R) \ge \frac{R^{l+1}}{(2l+1)!!}\exp\left[-\frac{R^2}{2(l+\gamma_*+2)}\right]. \tag{318}$$

For fixed $s < R$, and sufficiently large R,

$$|\gamma_l|\psi_l(s)^2 \le C_q \exp\left[\left(1 + \frac{1}{q(1+\theta_q)}\right)R\right]\frac{s^{2l+2}}{(2l+1)R^{2l+1}}, \qquad C_q = 1 + \frac{1+2/q}{\theta_q}. \tag{319}$$

Every fixed polynomial angular weight may be included in the sum of the right side over this range, and that sum tends to zero faster than every inverse power of R.

Proof. The exact positive-coefficient identity

$$|\xi_l(x)|^2 = \sum_{s=0}^{l} \frac{(l+s)!}{(l-s)!} \frac{\binom{2s}{s}}{4^s} x^{-2s} \tag{320}$$

implies $\operatorname{Re}(\xi_l' \overline{\xi_l}) \le 0$. For completeness, if $f = |\xi_l|^2$, the radial equation gives $f''' + 4(1-\nu/x^2)f' + 4\nu x^{-3} f = 0$. Substitution of the finite even inverse-power polynomial yields $c_0 = 1$ and $c_{s+1} = (2s+1)[\nu - s(s+1)]c_s/[2(s+1)]$, which proves (320).

In the barrier stack the derivative of $\operatorname{Re}(p\overline{u})$ is $|p|^2 + (\nu/x^2 - \varepsilon_r)|u|^2 > 0$ for TE, and $\varepsilon_r|p|^2 + (\nu/(\varepsilon_r x^2) - 1)|u|^2 > 0$ for TM. At X its value is nonpositive by (320). Its value at every inner point is therefore nonpositive. The conserved nonzero imaginary Wronskian excludes $u = 0$, so $\operatorname{Re} h \le 0$.

The regular solution is positive and increasing up to R. For $y = x\psi_l'/\psi_l$, the Riccati equation is $xy' = \nu - x^2 + y - y^2$. Comparison with its constant lower barrier γ_* gives $y \ge \gamma_*$ on $(0, R]$; comparison with $l+1$ gives $y \le l+1$. Solving the load equation gives

$$\gamma_l = \frac{\chi_l' - h\chi_l}{h\psi_l - \psi_l'}.$$

Since $\psi_l, \psi_l' > 0$ and $\operatorname{Re} h \le 0$, $|h\psi_l - \psi_l'|^2 \ge |h|^2\psi_l^2 + (\psi_l')^2$. This proves (317).

Put $v = \psi_l/x^{l+1}$. Then $(x^{2l+2}v')' = -x^{2l+2}v$. The Riccati bound gives $v(t)/v(x) \le (x/t)^{l+1-\gamma_*}$ for $0 < t < x \le R$. Integration yields $-v'(x)/v(x) \le x/(l+\gamma_*+2)$. Its integral, using $v(0) = 1/(2l+1)!!$, proves (318). Also $\psi_l(s) \le s^{l+1}/(2l+1)!!$ in this interval. Combine these estimates with the Hankel bounds in the preceding proof, $\gamma_* \ge \theta_q l$, and $R/l \le 2/q$. The factor from the derivative term is at most $(1+2/q)/\theta_q$, and the exponential from (318) is at most $\exp[R/(q(1+\theta_q))]$. This gives (319). Here $l \ge qR + O(1)$, so the factor $(s/R)^{2l}$ dominates that exponential and every fixed polynomial weight. □

18.3 The limiting Maxwell source kernel

Let $\mathcal{K}_R$ be the actual electric response to polarization $P = \chi E$ in the radial background, with the convention $e^{-i\omega t}$. The free kernel is $\mathcal{K}_0(x,y) = (k^2 I + \nabla\nabla)\Phi_k(x-y)$, where $\Phi_k(x) = e^{ik|x|}/(4\pi|x|)$. Define

$$\mathcal{J}(x,y) = \operatorname{Im}\mathcal{K}_0(x,y) = \frac{k^3}{16\pi^2}\int_{S^2} (I - dd^T) e^{ikd\cdot(x-y)}\, dS(d), \tag{321}$$

$$\mathcal{J}_\pm(x,y) = \tfrac{1}{2}[\mathcal{J}(x,y) \pm \mathcal{J}(x,-y)]. \tag{322}$$

These are the projections onto componentwise even and odd electric fields under $x \mapsto -x$.

Theorem 18.4 (Compact smooth source-kernel limit)**.** *For each fixed $A = q^M$, on every fixed compact core product,*

$$\mathcal{K}_R - \mathcal{K}_0 \longrightarrow i\big[(A^2-1)\mathcal{J}_+ + (A^{-2}-1)\mathcal{J}_-\big] \tag{323}$$

with every fixed number of derivatives. The limiting reaction kernel derivative of total order s has operator norm at most $(A^2-1)k^{3+s}/(4\pi)$. On fields invariant under rotation by π about z, $\mathcal{J}_+$ is electric-wall and $\mathcal{J}_-$ is magnetic-wall. Thus (323) equals the reaction part of (293), with $B = A$, on that invariant sector.

Proof. For fixed l, at $R = 2\pi n$ the two columns of $F_l(R)$ converge to the regular sine–cosine parity basis. The exterior outgoing state has a common factor $e^{iX}(-i)^{l+1}$, which cancels in α_l/β_l. Substitution of (310) gives

$$\gamma_l^{\mathrm{TE}} \to \begin{cases} -iA^2 & l \text{ even}, \\ -iA^{-2} & l \text{ odd}, \end{cases} \qquad \gamma_l^{\mathrm{TM}} \to \begin{cases} -iA^{-2} & l \text{ even}, \\ -iA^2 & l \text{ odd}. \end{cases}$$

No exterior phase padding is needed.

On a fixed compact ball the regular TE and TM vector waves and their derivatives are bounded by a fixed polynomial in l times $s^{l+1}/(2l+1)!!$, after harmless enlargement of s. This follows directly from the power series for j_l; the addition theorem and its differentiated form bound the angular factors by fixed powers of l. Low orders are finite. The uniform bound (315), the factorial decay against (316) for $l \geq cR$, and (319) justify termwise limits with every fixed number of derivatives in the reaction series.

To check normalization, the free electric dyadic multipole coefficients are ik^3 on the regular–outgoing TE and TM products. Dividing the actual outgoing continuation by its Wronskian changes its regular–regular coefficient to $-k^3\gamma_l$. The reaction coefficient is therefore $-k^3(\gamma_l + i)$. The regular-wave completeness identity is $\mathcal{J} = k^3 \sum (M_{lm}\overline{M_{lm}} + N_{lm}\overline{N_{lm}})$, equivalently obtained by expanding the Herglotz integral (321). TE electric parity is $(-1)^l$ and TM electric parity is $(-1)^{l+1}$, which gives (323).

Each derivative of (321) is bounded by $k^{3+s}/(4\pi)$. When expressed in $\mathcal{J}(x, y)$ and $\mathcal{J}(x, -y)$, the absolute values of the two coefficients in (323) sum to $A^2 - 1$, proving the bound. Finally let $R_z = \mathrm{diag}(1, 1, -1)$. Rotation invariance gives $E(-x) = -R_z E(R_z x)$, so componentwise inversion equals the wall involution (291) on this sector. □

18.4 Source-normalized bounds throughout the remote layers

Lemma 18.5 (Uniform radial-state sums)**.** *Fix a compact source ball and a gain A. For polarizations in that ball with bounded L^2 norm, the outgoing source response has uniformly bounded sums of its radial-state magnitudes, with every fixed polynomial angular weight, throughout $R \leq x < \infty$. The constants may depend on the gain and source ball, but not on sufficiently large R.*

Proof. Choose a fixed dimensionless $S \geq 1$ slightly beyond the source support. Cauchy–Schwarz and the regular-wave power series bound each source moment by

$$|f_{lm}| \leq C\|P\|_2 (l+1)^b \frac{S^{l+1}}{(2l+1)!!}. \tag{324}$$

Here a fixed b, for example $b = 4$, suffices before adding the desired angular weights. For all sufficiently large l the right side can instead be bounded by $C'\|P\|_2(l+1)^b\psi_l(S)$, by the positive regular-series lower bound. This intermediate bound is used only at large orders; it is not asserted at possible low-order zeros of $\psi_l(S)$. Finitely many exceptions in (324) are absorbed into its constant.

Outside the source the normalized radial factor is $w_l = \chi_l + \gamma_l\psi_l$ in the core, continued by its actual layer equation. In the barrier range the exact Wronskian cancellation gives

$$w_l(R) = \frac{1}{h\psi_l(R) - \psi_l'(R)}, \qquad p_l(R) = \frac{h}{h\psi_l(R) - \psi_l'(R)}. \tag{325}$$

Therefore $|w_l(R)| \leq 1/\psi_l'(R)$ and $|p_l(R)| \leq 1/\psi_l(R)$. Write $u' = \varepsilon_r p$, $p' = Vu$ in the TM barrier, where $V = \nu/(\varepsilon_r x^2) - 1 > 0$; for TE the first coefficient is one and $V = \nu/x^2 - \varepsilon_r > 0$. The proof of

Lemma 18.3 gave $\operatorname{Re}(p\overline{u}) \le 0$ throughout this stack. Consequently

$$(|u|^2)' = 2\varepsilon_r \operatorname{Re}(p\overline{u}) \le 0, \qquad (|p|^2)' = 2V \operatorname{Re}(u\overline{p}) \le 0$$

for TM, with coefficient one in the first equation for TE. Both states are continuous across every interface. Together with (318) this proves, on the entire annulus,

$$|f_{lm}|(|u_l| + |p_l|) \le C\|P\|_2 (l+1)^b e^{C_q' R} (S/R)^{l+1}. \tag{326}$$

The sum over $l \ge qR + O(1)$ decays faster than every inverse power of R, including arbitrary fixed polynomial weights. No large-order transfer estimate of the form $\exp(Cl^2/R^2)$ is being used.

For low orders, (315) and the bounded partial transfers give $|f_{lm}|(|u_l| + |p_l|) \le C_A |f_{lm}|$. For intermediate orders the analogous bound is $e^{C_A R}|f_{lm}|$ by (316). The latter weighted sum is $O(e^{-cR\log R})$ by (324), since $l \ge c_0 R + O(1)$. This proves the uniform annulus assertion.

It also proves the exterior assertion, including all turning points. By (320), $|\xi_l(x)|$ decreases to one. Moreover

$$(|\xi_l'|^2)' = 2(\nu/x^2 - 1)\operatorname{Re}(\xi_l \overline{\xi_l'}),$$

so $|\xi_l'|$ decreases up to $\sqrt{\nu}$ and then increases to one. Thus, for all $x \ge X$,

$$|\xi_l(x)| \le |\xi_l(X)|, \qquad |\xi_l'(x)| \le \max\{|\xi_l'(X)|, 1\} \le \max\{|\xi_l'(X)|, |\xi_l(X)|\}.$$

Multiply by the actual exterior outgoing coefficient. The exterior states are bounded by the annular endpoint states. This proves the lemma without requiring a far-field expansion uniform in uncontrolled angular order. □

Corollary 18.6 (Absolute annulus and exterior flux)**.** *Add a fixed finite-band incident family and its radial-background scattering field, with bounded physical incident coefficients. For its sum with the source response of Lemma 18.5,*

$$|E_{\tan}| + |H_{\tan}| \le C/r, \qquad |E_{\rm rad}| + |H_{\rm rad}| \le C/r^2, \qquad r \ge R/k. \tag{327}$$

The labels refer to spheres centered at the origin. The absolute normal plane flux over the stack annulus is $O(d_A/R^2)$ and over the exterior is $O(1/R)$.

Proof. Tangential vector-wave components are constants times u/r or p/r, and radial components are constants times $\sqrt{\nu}\,u/r^2$, with a bounded ε_r^{-1} factor where appropriate. The angular factors have polynomial sup-norm bounds. Lemma 18.5 gives (327). The finitely many background orders satisfy the same bounds by the fixed-order transfer limit in the annulus and bounded incoming and outgoing coefficients in the exterior. On $z = 0$ the spherical radial direction lies in the plane. Two sphere-tangential vectors have a radial cross product, whose normal component is zero. Thus only radial–tangential products contribute and $|S_z| \le C/r^3$. Integrate over the annulus and exterior. Interface circles have plane measure zero. □

18.5 The whole-plane physical limit

Theorem 18.7 (Source and dielectric whole-plane limit)**.** *Fix $A = q^M$, a compact region K at positive distance from $z = 0$, and a finite-dimensional finite-band incident family. Use a common phase adjustment so that its radial-background fields converge on compact sets to their limiting core fields. Suppose $P_R \to P$ in $L^2(K)$, uniformly on that finite input family. Form the total fields by*

adding the actual radial-background response to P_R. Define their limiting fields using (323) and P. Then the normal plane fluxes are integrable and

$$\sup_{\|c\|=1} \|S_{z,R}(c) - S_{z,\infty}(c)\|_{L^1(\mathbb{R}^2)} \longrightarrow 0. \tag{328}$$

Furthermore, let χ be a fixed bounded contrast supported in K. If the limiting volume equation

$$P = \chi(E_\infty^{\mathrm{bg}} + \mathcal{K}_\infty P) \tag{329}$$

has a bounded inverse on $L^2(K)$ (or on its invariant rotation sector), then for all sufficiently large R the actual radial-background volume equation has a bounded inverse, its solutions converge to P, and (328) holds for the actual scattering fields of the radial layers plus that dielectric perturbation. Their original physical incoming normalization is retained.

Proof. The positive source–plane distance and Theorem 18.4 give uniform field convergence on every fixed plane disk, including the magnetic fields obtained by curl. It remains to control the growing vacuum-core part of the plane.

Split its reaction series at $\nu = c_0^2 R^2$. Low-order coefficients $(\gamma_l + i) f_{lm}$ have uniformly bounded factorial tails by (315) and (324). The associated Herglotz densities are therefore uniformly bounded in every fixed smooth angular norm, although their cutoff depends on R. Their tangential fields are $O(1/r)$ and their radial fields $O(1/r^2)$ uniformly in R. For an elementary verification, express the angular integral in polar coordinates about the observation direction and integrate once in $t = \cos\theta$. This gives the first bound. The radial amplitude vanishes at both endpoints by transversality, so a second integration gives the second. The azimuthally averaged smooth amplitude has bounded endpoint derivatives, as follows from its even local Taylor expansion in $\sin\theta$; uniform C^4 control suffices. The magnetic angular density is the direction crossed with the electric density, divided by Z_0, and has the same properties. The free compact-source response and the fixed finite-band background satisfy these bounds outside a fixed source ball as well. Their combined absolute plane-flux tail beyond radius B is $O(1/B)$, uniformly in R.

The remaining reaction field is negligible uniformly on $B \le r \le R/k$, where B is fixed beyond twice the source ball. In the intermediate range, (316) contributes at most e^{CR}, the source moments have factorial decay with $l \ge cR$, and the observation factors and first derivatives have polynomial bounds. For example the integral representation of j_l gives $|j_l|, |j_l'| \le 1$; inverse-radius factors are harmless on $r \ge B$. Thus this weighted field sum is $O(e^{-cR\log R})$. For barrier orders, combine (317) and (318) with the regular upper bounds at S and at any $0 < x \le R$ to obtain

$$|\gamma_l| \psi_l(S) \psi_l(x) \le C e^{C_q' R} \frac{R}{2l+1} (S/R)^{l+1}.$$

The bound $0 < x\psi_l'/\psi_l \le l+1$ supplies the corresponding derivative estimates. The angular factors add fixed polynomial weights, so these sums too are $O(e^{-cR\log R})$. The free regular coefficient i in $\gamma_l + i$ is smaller. The high-order electric and magnetic reaction fields are therefore $o(R^{-m})$ for every fixed m on the growing core annulus. Their self-flux and their cross-flux with the bounded low-order fields have integral $o(1)$ even after multiplication by its $O(R^2)$ area.

Corollary 18.6 handles the remaining plane. Consequently

$$\limsup_{R\to\infty} \int_{r>B} |S_{z,R}|\, dA \le C/B.$$

The limiting free-plus-Herglotz field has the same tail. Compact convergence, followed by $B \to \infty$, proves (328). The field estimates are linear and uniform on bounded source sets; the quadratic

flux inequality then makes the conclusion uniform on every coherent unit input in the fixed finite-dimensional family.

For the final assertion, the singular free-volume kernel is identical for all R; only its smooth reaction part varies. Theorem 18.4 therefore implies

$$\|\chi(\mathcal{K}_R - \mathcal{K}_\infty)\|_{L^2(K)\to L^2(K)} \longrightarrow 0.$$

The inverse perturbation identity applied to $I - \chi\mathcal{K}_\infty$ gives invertibility for large R and convergence of the actual source solutions in $L^2(K)$. The source version of the theorem applies to these solutions. Uniqueness of outgoing scattering for each finite positive lossless dielectric identifies the volume solution with the physical scattering field. □

Remark 18.8 (Quantifiers for the small-inclusion construction)**.** For every fixed inclusion size a and fixed gain B_a, the preceding theorem is applied first. The radius can then be chosen large enough for any prescribed plane-flux error. There is no claim of a radius bound uniform in a. To realize the actual gain $B_a = \sqrt{\lambda}\,t/a$ in (300) using one fixed index q, take $a_M = t\sqrt{\lambda}/q^M$. Then $B_{a_M} = q^M$ exactly and $a_M \downarrow 0$. The inverse and remainder theorem 17.3 applies along this sequence. All finite devices still have scalar permittivity between one and ε_+, finite support, and a positive vacuum gap at the section plane for each member.

19 Disproof of the unrestricted fixed-section channel bound

The construction in this section exploits the distinction between power crossing a chosen square and power delivered to a receiver on its far side. Near an edge, a circulating field can cross into the square and return outside it. The positive contribution inside the square counts as passage; the return flow contributes to absolute bypass. The definition permits this provided both are within their prescribed thresholds. Selecting the complete outgoing scattering map also counts reflected radiation in the output power.

The construction makes this picture work simultaneously for any prescribed finite number of coherent input directions. Small dielectric spheres near paired edges produce localized circulation. A distant radial stack amplifies the incident fields that drive them, compensating for their shrinking size. The stack and spheres are ordinary finite dielectrics; their size and number of layers may depend on the requested dimension. A uniform estimate for all superpositions, including interference terms and the whole measurement plane, connects this picture to the actual Maxwell fields.

The unrestricted target quantifies over all fixed passage and bypass thresholds in Definition 1.3. The following counterexample uses a permitted range of those thresholds. It does not address the different question obtained by requiring $\delta \le \eta$, or by restricting the selected outputs to a specified receiving hemisphere.

Theorem 19.1 (Arbitrarily large counted subspaces at fixed thresholds)**.** *Fix $k_0 > 0$, $\varepsilon_+ > 1$, $L > 0$, $0 < \tau < 1$, and $0 < \eta < \delta$. For every positive integer N there is a finite, piecewise smooth, real scalar dielectric with $1 \le \varepsilon_r \le \varepsilon_+$, vacuum exterior, and no interior sources, whose physical incoming space contains an N-dimensional counted subspace through the same square $D = (-L/2, L/2)^2 \times \{0\}$. The selected outgoing map is its complete scattering map. In particular, every vector in this subspace has unit power throughput relative to its incident power, passage at least η times that power, and absolute bypass at most δ times that power. All plane fluxes are integrable.*

Consequently the unrestricted finiteness assertion in Conjecture 1.4, and hence its stronger area bound, is false. The frequency, material interval, square and thresholds are common to the whole sequence of devices.

The strict inequality $\eta < \delta$ leaves room to choose an intermediate power p_0: in the limiting construction the passage and absolute bypass both approach p_0 for every unit input in the counted subspace. The proof then chooses a finite device close enough to this limit to satisfy both inequalities. Since the complete lossless scattering map preserves incident power, the throughput condition holds for every $\tau < 1$. This does not require that power leaving on a particular side be collected by a receiver.

The order of limits matters. For each requested dimension, first choose the independent incident data; then increase the stack gain while shrinking the spheres; finally take the stack radius large enough to approximate the limiting Green kernel for that particular choice. No single device or uniform radius is claimed to work for all dimensions at once.

Proof. Choose once and for all an index $1 < q < \sqrt{\varepsilon_+}$, a sphere permittivity $1 < \varepsilon_p \le \varepsilon_+$, and constants $h > \rho > 0$. Choose $p_0 \in (\eta, \delta)$ and then $t > 0$ so that $\alpha t^2/(2\pi h) = p_0$, where $\alpha = 4\pi\rho^3(\varepsilon_p - 1)/(\varepsilon_p + 2) > 0$. These choices do not depend on N.

Fix N. Lemmas 16.2–16.3 supply N distinct right-edge points and their left-edge partners, a finite band of regular electric-wall TE interpolants v_j, and $\lambda > 0$ such that $g_j = v_j/\sqrt{\lambda}$ are orthonormal physical incoming data with the prescribed independent jets. Let

$$B_M = q^M, \qquad a_M = t\sqrt{\lambda}/B_M, \qquad \ell_0 = k_0^{-1}.$$

Thus $a_M \to 0$ and the actual common core gain B_M produces the jet multiplier $A_M = B_M/\sqrt{\lambda} = t/a_M$. Place the $2N$ radius-$\rho a_M \ell_0$ spheres at height $h a_M \ell_0$ above the chosen edge points. For large M they are disjoint, lie strictly above the plane, and remain inside a fixed ball. Their arrangement is invariant under rotation by π about the z axis.

For each such M, Theorem 17.3 proves invertibility of the actual inclusion volume equation for the explicit limiting background kernel with gain B_M. It gives, uniformly for $c \in \mathbb{C}^N$ with $\|c\| = 1$,

$$\|S^{\infty}_{z,M}(c) - F_{a_M}(c)\|_{L^1(\mathbb{R}^2)} \le C_N a_M.$$

The constant is independent of M once N and its interpolants are fixed. This estimate includes the self-consistent polarization, all source angular orders, all coherent cross terms, and the entire measurement plane.

Now hold M fixed. Take a common radial stack of M high-low quarter-wave pairs, with indices q and one, starting at dimensionless radius $R = 2\pi n$. The physical radius is R/k_0. Theorem 18.7 proves both convergence of its source Green kernel to that used above and convergence in whole-plane L^1 of the resulting *actual perturbed-device* fluxes, uniformly on this finite input space. Inverse stability supplies the actual dielectric polarizations, not arbitrary imposed dipole sources. Choose a sufficiently large finite integer $n = n(M, N)$ so that

$$\sup_{\|c\|=1} \|S^{\mathrm{phys}}_{z,M}(c) - S^{\infty}_{z,M}(c)\|_1 < a_M.$$

One harmless common phase in the incident normalization does not affect flux or orthonormality. This order of choices requires no radius estimate uniform in M or N.

Combining the last two estimates with Proposition 16.4 gives uniformly on the unit sphere of $\mathbb{C}^N$

$$P^{\mathrm{phys}}_D(c) \longrightarrow p_0, \qquad \int_{\mathbb{R}^2 \setminus D} |S^{\mathrm{phys}}_{z,M}(c)|\, dA \longrightarrow p_0.$$

Here the absolute-value conclusion uses $\big||f| - |g|\big| \le |f - g|$, so cancellation between distinct inputs or between distant parts of the plane is not substituted for the bypass condition. Choose a finite M large enough that both errors are less than $\frac{1}{2}\min\{p_0 - \eta, \delta - p_0\}$.

The resulting medium consists only of finitely many concentric ordinary dielectric shells and the separated ordinary dielectric spheres. It is compactly supported and piecewise smooth. The volume-equation inverse just proved gives its well-posed response for the prescribed illumination. Equivalently, outgoing uniqueness for this finite positive dielectric follows from the imaginary Green identity, outgoing Rellich theorem and interface unique continuation; the exterior zero field propagates through the finite smooth interfaces. The volume solution defines a bounded physical scattering map on transverse angular L^2 inputs. Choose as $\mathcal{H}_{\mathrm{in}}$ the closed subspace generated by the finite regular TE inputs used here, and keep the complete angular outgoing space. On every finite TE input, the exact lossless power identity is $\|Sa\|^2 = \|a\|^2$. Continuity extends it to the closed input space. That space is a Hilbert space, since transversality and the chosen subspace are closed in angular L^2. Thus the actual restricted scattering map $T = S|_{\mathcal{H}_{\mathrm{in}}}$ satisfies $T^*T = I$ and includes every outgoing radiation channel. No surjectivity assertion is needed.

Set $W = \mathrm{span}\{g_1, \dots, g_N\}$. Its dimension is N and input power is $\|c\|^2$. For unit c the preceding strict margins prove the passage and bypass inequalities, while $\|Tc\|^2 = 1 \geq \tau$ proves throughput. Quadratic homogeneity extends them to every c, including zero. The spheres leave a positive vacuum gap around $\overline{D}$ for each individual device; the remote shells lie outside that neighborhood. The proved plane-tail bounds give legitimate integrable fluxes even where the plane intersects remote interfaces, whose circles have zero plane measure. All admissibility conditions are satisfied. Since N was arbitrary with the displayed fixed parameters, no finite device-independent count can hold there. □

Remark 19.2 (Scope and physical mechanism)**.** The flux near each sphere circulates across a sharp edge of the measurement square: its positive interior contribution is paired with an exterior return of the same limiting magnitude. This is allowed by the frozen definition, which does not require the square to be a sole connection or the selected output to lie above it. The construction uses the strict allowance $\delta > \eta$; it does not refute a reformulated claim with smaller bypass or additional output restrictions. In particular the resource-controlled theorems requiring $\delta < \eta\tau$ retain their stated scope. The total support, common core amplification, interface count and inverse minimum feature size grow along the construction. None is a bounded resource in Conjecture 1.4. The proof is analytic. Its complete physical construction and the same-device passivity identity are formalized in the endpoint listed in Section A.2; no finite-element simulation is claimed.

A Verification, scope, and separate verdicts

A.1 What was checked

The hotspot, channel, and counterexample tracks used disjoint source-file ownership. A different research agent reviewed each track's key arguments, and the coordinator checked their equations and scope. The review found and corrected the direction of the bound on the real parts of the outgoing Dirichlet-to-Neumann multipliers, and made explicit the derivative asymptotic used in the radial angular-momentum obstruction. These are recorded in the review files and Git history. This is independent checking within an AI-assisted investigation, not independent human peer review or a substitute for the separate Lean checks described below.

The proofs use standard Hilbert-space spectral theory, Lax–Milgram, Fredholm theory, Sobolev compactness and local elliptic estimates. The scalar scattering proof supplies its own outgoing uniqueness and material-Runge argument. Its elementary Bessel/Hankel facts can be checked against the Wronskian identities and large-order formulas in [14]. None of these background facts is a substitute for a Maxwell-to-operator bridge in the channel problem.

The reproducible script `scripts/verify.py` checks the exact pair model, passive reciprocal perturbations, the angular monodromy, radial Bragg matching, the conical projection identities, and local evanescent flux. Its fifteen diagnostic groups use fixed seed 140014 where random perturbations are needed. The additional modal groups check the exact sphere determinant against its rational exponential form, the first asymptotic coefficient and nine high-Q dipole poles, and the constant-lifting cancellation through exponent one. The newest groups integrate the actual TE/TM radial systems for the growing-stack construction with step refinement, check the exact real-frequency dynamic-kernel bound, and independently integrate the conjugated angular generator through each layer of the identity loop. The last calculation includes both actual TE and TM interaction matrices. Another group computes source reaction coefficients from the actual regular/irregular transfer matrices of a common finite stack and checks their paired large-radius limit. They do not certify global channel synthesis or the continuous error bounds used in the proofs. All matrix tests use singular values or Hermitian eigenvalues, not tests of randomly selected coherent inputs. Random numbers choose one fully specified perturbation matrix; its full norm and all-subspace certificate are then evaluated. Floating-point residuals support consistency of the analytic proofs; they are not interval-certified error estimates.

Table 2: Exact resonator-model diagnostic family, $J_j = 10^{-j}$ and $\gamma_j = J_j$. This is not a Maxwell device simulation.

N	$\min J_j$	$\sigma_{\min}(T)$	maximum model energy	narrowest FWHM
2	10^{-2}	1	10^{2}	$2.82843\,10^{-2}$
4	10^{-4}	1	10^{4}	$2.82843\,10^{-4}$
8	10^{-8}	1	10^{8}	$2.82843\,10^{-8}$

The ideal model's energy Gram matrix is $\mathrm{diag}(J_j^{-1})$ and its internal exchange-current Gram matrix is I; common detuning is zero. For weighted, purely Hamiltonian perturbations of norm $\rho = 0.01$, Theorem 7.9 bounds transmission-operator error by 0.0100713. This is below $1 - \sqrt{0.9}$, so it certifies transmission above 90% in the perturbed model for every coherent vector. The reproduced smallest powers are approximately 0.999961, 0.999959, and 0.999949. Model power-balance and full-unitarity residuals are below 10^{-14} in the reported run.

The local evanescent example has an analytically exact section Gram matrix I_8. Direct integration

of its explicit trigonometric fields with 33, 65 and 129 transverse quadrature points gives operator errors below 10^{-14}. This refines quadrature of a local analytic formula; it is not a domain, port, or material-mesh convergence study. The Bragg diagnostic uses $q = 2$, $k_0 = 1$, $x_0 \simeq 2.74370727$ and material upper bound below 4.266. For $M = 0, 2, 4, 8$ its core amplitude squared is approximately 8, 115.292, 1824.323, 464888.834, while reflection power remains one. These tests check normalization and exact matching, not an increasing transmission count.

No numerical simulation of the analytic physical N-channel family in Theorem 19.1 was performed. Therefore numerical Maxwell transmission singular values, section-flux matrices, absolute bypass, weakest physical coupling, and relative model-reduction errors for $N = 2, 4, 8$ are *unavailable*, not zero. Their fields in the machine-readable record are null. No rounded-hotspot scattering mesh was computed; that theorem rests on the analytic existence and convergence proof, which is nonconstructive in its illumination cost and rounding scale. The supplied notes' claims about earlier finite-dimensional Lean checks were not rerun. A new formalization is described below, with its own source, pinned dependencies, successful compilation, and axiom audit.

A.2 Lean verification and its precise boundary

The formalization uses Lean 4.19.0 with mathlib pinned to

`c44e0c8ee63ca166450922a373c7409c5d26b00b`.

The source tree contains actual Lebesgue spaces, weak derivatives, compact test functions, distributional Maxwell equations, outgoing Green kernels and physical incoming and outgoing amplitudes. The existence theorems below construct these objects; their missing analytic assertions are not supplied as project axioms.

Unrestricted power channels

The endpoint in `FullChannelExactPassiveWitness.lean`, `unrestricted_exact_passive`, takes only the fixed positive frequency, ordinary dielectric ceiling, square side, $0 < \eta < \delta$, $0 < \tau < 1$, and finite dimension N. It constructs the actual finite shell-and-sphere material and an orthonormal physical incoming family. The counted space has dimension N. Its complete outgoing field, signed passage and whole-plane absolute bypass satisfy the stated inequalities for every coherent input, with the required flux integrability. The volume operator is proved invertible, and an actual bounded scattering map on transverse angular inputs is identified with the counted fields. Its restriction to the closed physical TE incoming Hilbert space satisfies $T^*T = I$, with complete outgoing radiation selected. This adjoint identity is attached to the same material and scattering map inside the exact physical witness. The corollary that no uniform finite count exists uses this constructed witness. No result for $\delta \leq \eta$ or for receiving-only output is asserted.

Normalized modal hotspots

The endpoint `Packet06FinalAffineModal.lean`, `exists_physical_modal_hotspots`, has no sharp-mode, excitation, regularity, collar or peak hypothesis. Its device certificate retains the literal nested material law and smooth interfaces, compact support, the actual complex volume kernel, reciprocal normalization one, the outgoing Maxwell field, and a genuine simple pole observed in the transported selected sector. All finite observation balls are disjoint, their projections lie in the requested patch, and actual continuous one-sided maxima lie on the prescribed affine plane. The same selected index retains open low collars and compact connected full half-amplitude components inside the balls. The material ceiling is the literal $\varepsilon_+ > 1$, and the observation balls have strict

diameter below ℓ. The construction uses an exact proper spatial frame and translation for every unit plane normal. Its spectral and physical transports are explicitly identified: the observed pole belongs to the same final material, support radius and actual normalized mode as the hotspots. The pole is simple in the transported selected sector; ambient rank-one simplicity is not asserted. The general electric-field identification theorem equates the potential representative used for the hotspots with the global outgoing field almost everywhere.

Physical modal volumes

The endpoint `Packet06StrongAffineVolumePaper.lean`, `exists_strong_affine_volume_family`, constructs one common actual family for arbitrary finite N in a prescribed affine-plane patch. It retains the literal dielectric ceiling, smooth three-value material, exact target real frequency, quality, normalization, outgoing behavior and the same selected-sector observed pole. Its closed observation balls are disjoint, project into the patch and have strict diameter below the requested length. The actual open collars are retained. The public wrapper instantiates the complete core construction at $K = \sqrt{\varepsilon_+}$; the separately checked scalar identity $K^2 = \varepsilon_+$ gives the literal pointwise permittivity ceiling.

For each weighted maximum, the same continuous phase representatives are certified against the actual field on a strictly larger closed ball before any maximum is chosen. These certificates survive dilation and the full spatial frame. The intrinsicness theorem proves that replacing them with any other such actual representatives leaves every smaller-ball trace value and the maximum unchanged, including at tangential interface contact. This strengthens the earlier small-ball-only predicates, which did not themselves justify that physical interpretation. The maximum uses the permittivity of the same material side at interfaces, and its reciprocal tends to zero. At these same selected weighted maxima, each tip has a fixed Cartesian component along a strictly increasing subsequence whose complex directional volume tends to zero. The exact normalized dilation factor is included in the proof.

Driven finite-device hotspots

The endpoint `Packet07DrivenPlaneFinal.lean`, `plane_final`, constructs a prescribed-frequency family in an arbitrary affine-plane patch, with one smooth transverse Herglotz illumination of physical incoming power one. The same actual electric and magnetic fields satisfy weak Maxwell and outgoing scattered-field limits. The material is binary, obeys the prescribed positive permittivity ceiling, has bounded support and vacuum exterior, and has smooth boundary and exactly $2N$ nonempty disjoint connected lobes. Disjoint closed observation balls have the prescribed strict diameter, and their projections and the support projection lie in the planar patch. For every finite list of thresholds, all sufficiently late members have simultaneous attained maxima and compact connected half-amplitude regions inside the balls. The maximizers themselves are not required to lie in the plane, in agreement with Theorem 3.1. The exported Maxwell identity also yields actual $H(\mathrm{curl})$ fields on every bounded open region, with almost-everywhere equality to those same electric and magnetic fields; local square integrability of E, H and εE is proved through the physical placement.

Proof and build audit

These endpoints are assembled from the actual global representation, source-response identification, sphere spectral branch, nonzero conical excitation, normalized continuation, regional scalar transmission estimates and finite physical collar covers. The angular coefficient step uses a quantitative

annular pairing; it does not assert analytic continuation of the intrinsic coefficient. The collar proof derives its mixed derivatives from the regional weak equation before using them in the localized forcing. It does not assume the unknown second derivatives on an outer cutoff annulus.

Independent source review and separate direct-compiler builds accompany each accepted batch. The public entry point `OQ14Closure.lean` imports the channel, modal, volume and driven endpoints and prints their axiom dependencies. Exact ordered module lists, source and object hashes, compiler logs and reviews are retained under `checkpoints/`. Stage 116 contains 1586 incremental modules and 6001 standard-only reports beyond the earlier release. These are audit counts, not a measure of mathematical completeness.

The aggregate project build passed 2171 modules and 10946 inline axiom reports. It excludes cached project objects, retaining earlier fresh objects only after source, log and object hash authentication. It records 14 historical linter warnings in four old modules; all new accepted batches have no diagnostics. A separate matching-stage audit checks every kernel-safe declaration owned by these project modules, including private and unprinted declarations: 23697 declarations passed. Unsafe executable compiler implementations are listed separately; the axiom collector does not filter dependencies of any checked declaration. This audit therefore covers more than the explicitly printed theorem reports.

Lean and package objects remain trusted dependencies. Compiler executable hashes, the pinned mathlib revision and the audit tools are recorded, but this is not a from-source rebuild of Lean or mathlib. These checks establish the formal statements under that trusted environment; the manuscript-to- theorem correspondence is a separate source review.

The only permitted logical axioms are `propext`, `Classical.choice` and `Quot.sound`. No admitted proof, project-specific mathematical axiom or numerical experiment replaces any step of the formal endpoint chains. The frozen earlier 5238-report release and its detailed batch history remain available as historical evidence; their earlier coverage limitations are superseded only where the new explicit endpoints discharge them.

A.3 Stricter questions outside the quantified targets

The unrestricted assertion has been disproved in Theorem 19.1 for every $\delta > \eta > 0$ with full scattering output. The following resource estimates describe stronger restricted finiteness questions and the routes leading to that disproof. For a restricted channel proof, Theorem 6.13 controls the complete physical output error after all feedback. What is missing is a uniform estimate of the effective transmission directions with no uncontrolled field-resource factor. A bound on B_* on the counted subspaces would suffice for finiteness in the stated collar class, but the Bragg construction shows why external passivity cannot supply a general input-to-field bound. It does not rule out a sharper global argument using radiative accessibility, through-power and bypass together. Theorem 8.3 proves that local Maxwell equations and whole-plane coherent bypass control alone cannot supply the required restriction. The minimal abstract target is the uniform finite-rank approximation in Remark 6.18; its area scaling is an additional requirement. Corollary 15.5 supplies a physical uniform resource bound when total dielectric volume is sufficiently small, without a support-diameter bound. That additional volume restriction is absent from the primary target. Theorem 10.3 separately gives an area bound in any prescribed finite angular band for the growing radial-stack construction: opposite-parity gains cancel in signed passage, even while local field energy diverges on large physical subspaces. Modes above the prescribed band remain outside that bound. Theorem 9.5 now excludes arbitrary high angular degeneracy in a centered homogeneous core, even with unlimited exterior resonant amplification and both polarizations. It leaves mixed angular orders and structured cores outside its scope.

The earlier disproof criterion in Remark 7.15 specifies a quantitative alternative: a power-normalized Maxwell compression close to a unitary at one common frequency, plus the full physical flux inequality and absolute-bypass certificate on every coherent vector. Resonant algebra proves that weak coupling alone is not an obstruction, but it gives neither simultaneous bounded-index synthesis nor a relative error estimate for finite dielectric structures. Theorem 9.8 does provide actual bounded-index radial controls for small independent changes of finitely many complex core amplitudes. Its explicitly retained local range is not a global reachability or absolute-bypass theorem. Theorem 11.6 now supplies approximate global reachability for every fixed finite set of TE orders, using amplified angular perturbations in distant positive-index layers. The complex core gains can be independently prescribed up to common phase. Theorem 12.2 also controls the paired TM transfers, and Theorem 12.4 amplifies one reflection sector while suppressing its opposite in a fixed C_2-even band. It does not estimate the response to a newly added inclusion or unselected angular orders. Separately, Theorem 14.3 bounds counted dimension for any entire propagating Herglotz family using only its absolute bypass, without a gain bound. Corollary 14.6 transfers this obstruction to actual devices with a sufficiently large vacuum core at each fixed finite angular band. Its radius threshold may depend on the band. Thus neither result controls nearby material or arbitrary simultaneous growth of angular band and radius. Nearby material is essential to the subsequent counterexample. Theorem 13.2 demonstrates why it is essential: actual finite positive dielectrics can have arbitrary coherent passage rank and unit total throughput when bypass is omitted. Section 16 constructs a local edge-circulation profile with equal passage and return, and exact finite-band jets with orthonormal physical inputs. Its Proposition 16.6 states the sufficient whole-plane L^1 Maxwell remainder. Theorem 17.3 proves the self-consistent small-inclusion estimate for the explicit limiting kernel, and Theorem 18.7 proves the all-order physical Green limit and whole-plane convergence for finite radial backgrounds. Theorem 19.1 combines them in the required order to disprove unrestricted finiteness for every fixed $\delta > \eta > 0$. The selected output is the full scattering map; no claim is made here for stronger bypass thresholds or a prescribed receiving hemisphere.

For hotspots, Theorem 3.1 supplies the finite-device driven construction directly, using conical points rather than an extrusion approximation. Its neighborhood projections lie in the prescribed planar patch; it does not require the rounded maxima to lie exactly in that plane. The separate modal construction now closes the modal bridge: Theorem 5.6 produces one high-Q resonance with a finite nonzero reciprocal residue norm, all singular coefficients nonzero, and smooth rounded peaks with actual maxima in the plane patch. The insertion contrast may depend on N, within the same fixed material bounds. The surrounding resonator's support is unrestricted.

A.4 Separate scientific verdicts

Target	Status	Exact conclusion
Driven, invariant 2D electric hotspots	PROVED	Theorem 2.2: any finite number in any open patch, one physical unit-power-per-length illumination, fixed ordinary contrast and frequency, smooth rounded binary interfaces.
Driven finite 3D point hotspots	PROVED	Theorem 3.1: one finite-power illumination, fixed small positive contrast, $2N$ smooth finite inclusions, disjoint 3D peak neighborhoods projecting into the prescribed patch.

Target	Status	Exact conclusion
Modal hotspot packing	PROVED	Theorem 5.6: one genuine normalized QNM, arbitrary finite peak count and quality factor, fixed real frequency and common ordinary bounds, actual maxima in the plane patch. Reciprocal residue normalization is explicit.
Scalar electric Helmholtz waves	OPEN here	The hotspot construction uses $u = H_z$ and in-plane vector E; it is not a singular scalar-electric-field example. Restricted scalar slab results do not settle OQ14.
Full vector, unrestricted fixed-section finiteness and area law	DISPROVED	Theorem 19.1: arbitrary counted dimension at every fixed $\delta > \eta > 0$, with the complete scattering map selected as output and common ordinary bounds. Stricter regimes remain separate.
Resource-controlled vector channels	PROVED / CONDITIONAL	Explicit finite-rank, count, average-resource and essential-norm results hold under the listed hypotheses. Uniform area scaling requires uniform additional resources.
Ordinary dielectrics	PROVED scoped results	Driven and modal hotspot constructions and Bragg/local-flux obstructions use common positive ordinary bounds. None uses ENZ.
Common positive lower bound below one	DISPROVED unrestricted count	Any such class admitting the scalar interval $[1, \varepsilon_+]$ contains the counterexample of Theorem 19.1. No ENZ limit is needed.
Shape-varying, ENZ, ideal guides	Excluded from primary target	The prior report supplies a qualified broader counterexample. Its varying lower bound and section shape are retained; this manuscript does not promote it or independently certify its entire construction.
Real symmetric positive anisotropy	PROVED local extension	Corollary 6.17 extends the local resource theorem. Tensor classes admitting the scalar examples inherit both hotspot constructions and the unrestricted channel counterexample; stricter channel regimes are not settled.
Fixed total support	OPEN here	The growing-support Bragg sequence does not refute this more restricted problem.
Operator and Maxwell formalization	LEAN VERIFIED endpoints	Section A.2 identifies the actual unrestricted-channel, arbitrary-plane modal and driven hotspot, and common arbitrary-plane modal-volume existence chains, with matching aggregate and all-safe-declaration audits.

A.5 Build and provenance

The canonical source is `manuscript/main.tex` and its included sections. The documented build is `python scripts/build.py` with Tectonic 0.17.0, followed or preceded by `python`

`scripts/verify.py`. Tectonic runs the required bibliography and reference passes. The build script rejects unresolved final-pass citations, references and overfull boxes. Rendered pages are inspected separately; compilation never counts as mathematical verification. The build manifest records the source revision, working-tree state, engine, source hashes and PDF hash. The saved manuscript snapshot and its provenance are described in `paper/README.md`. The historical release record separately identifies its clean-checkout build and formal audit. These records do not establish independent human review.

References

[1] Jean-Paul Bézivin and Philippe Robba. A new p-adic method for proving irrationality and transcendence results. *Annals of Mathematics*, 129(1):151–160, 1989. doi:10.2307/1971488.

[2] Valdemar Bille-Lauridsen and Jesper Mørk. The dielectric bowtie effect: classical electromagnetic edge singularities in subwavelength cavities. arXiv:2607.11613v1, 2026. Preprint.

[3] Martin Costabel, Monique Dauge, and Serge Nicaise. Singularities of Maxwell interface problems. *ESAIM: Mathematical Modelling and Numerical Analysis*, 33(3):627–649, 1999. doi:10.1051/m2an:1999155.

[4] Martin Costabel and Alan McIntosh. On Bogovskiĭ and regularized Poincaré integral operators for de Rham complexes on Lipschitz domains. *Mathematische Zeitschrift*, 265(2):297–320, 2010. doi:10.1007/s00209-009-0517-8.

[5] Vinicius S. de Angelis, Maximilian Jeindl, Leonardo A. Ambrosio, David A. B. Miller, Federico Capasso, and Ahmed H. Dorrah. Multi-plane spatially resolved phase structuring using optical communication modes. *Journal of Optics*, 28(6):065603, 2026. doi:10.1088/2040-8986/ae709d.

[6] Shanhui Fan, Wonjoo Suh, and J. D. Joannopoulos. Temporal coupled-mode theory for the Fano resonance in optical resonators. *Journal of the Optical Society of America A*, 20:569–572, 2003. doi:10.1364/JOSAA.20.000569.

[7] Saddam Gafsi and Judson D. Ryckman. All-dielectric metawaveguide ring resonators with deeply sub-diffractive mode volumes. *Laser & Photonics Reviews*, 19:2401579, 2025. doi:10.1002/lpor.202401579.

[8] Bastian Harrach, Yi-Hsuan Lin, and Hongyu Liu. On localizing and concentrating electromagnetic fields. *SIAM Journal on Applied Mathematics*, 78(5):2558–2574, 2018. doi:10.1137/18M1173605.

[9] Zeyu Kuang, David A. B. Miller, and Owen D. Miller. Bounds on the coupling strengths of communication channels and their information capacities. *IEEE Transactions on Antennas and Propagation*, 73(6):3959–3974, 2025. doi:10.1109/TAP.2025.3533263.

[10] Wen-Zhi Mao, Hong-Yi Luan, and Ren-Min Ma. Singulonics: narwhal-shaped wavefunctions for sub-diffraction-limited nanophotonics and imaging. *eLight*, 5:27, 2025. doi:10.1186/s43593-025-00104-x.

[11] David A. B. Miller. Why optics needs thickness. *Science*, 379:41–45, 2023. Including Supplements S2 and S12; doi:10.1126/science.ade3395.

[12] Owen D. Miller and Francesco Monticone. Fundamental limits in photonics and electromagnetics: a tutorial. arXiv:2605.24738v1, 2026. Version 1, Sections 3.4, 3.5 and 5.6.

[13] E. A. Muljarov and W. Langbein. Exact mode volume and Purcell factor of open optical systems. *Physical Review B*, 94:235438, 2016. doi:10.1103/PhysRevB.94.235438.

[14] NIST. Digital Library of Mathematical Functions, chapter 10. Bessel and Hankel Wronskians and large-order asymptotics; consulted 17 October 2026; `https://dlmf.nist.gov/10`.

[15] NIST. Digital Library of Mathematical Functions, section 10.49. Exact finite spherical-Hankel expansions, equations 10.49.1, 10.49.6 and 10.49.7; consulted 18 October 2026; https://dlmf.nist.gov/10.49.

[16] R. L. Ochs, Jr. A version of Runge's theorem for the Helmholtz equation with applications to scattering theory. *Proceedings of the Edinburgh Mathematical Society*, 32(1):107–119, 1989. doi:10.1017/S0013091500006957.

[17] A. Douglas Stone, William R. Sweeney, Chia Wei Hsu, Kabish Wisal, and Zeyu Wang. Reflectionless excitation of arbitrary photonic structures: a general theory. *Nanophotonics*, 10(1):343–360, 2021. doi:10.1515/nanoph-2020-0403.

[18] Wonjoo Suh, Zheng Wang, and Shanhui Fan. Temporal coupled-mode theory and the presence of non-orthogonal modes in lossless multimode cavities. *IEEE Journal of Quantum Electronics*, 40(10):1511–1518, 2004. doi:10.1109/JQE.2004.834773.

[19] OQ14 channel bounds, version 2, 2026. User-supplied unpublished HTML research notes; author not identified. Input hash recorded in evidence/input-manifest.json.

[20] Structured Maxwell bottlenecks: A quantitative flux–energy bound, exact proof obstructions, and the scope of an ENZ counterexample, 2026. User-supplied unpublished research report, dated 8 October 2026; 33 PDF pages. Author not identified. Input hash recorded in evidence/input-manifest.json.

[21] Qingqing Zhao, Lang Zhang, and Owen D. Miller. Minimum dielectric-resonator mode volumes. arXiv:2008.13241, 2020.